GEORG-AUGUST-UNIVERSITÄT
GÖTTINGEN

Fakultät für
Physik

$[q,p]=i\hbar$

Masterarbeit

Interferenzeffekte im MSSM in einer verallgemeinerten Näherung schmaler Breiten

Interference Effects in the MSSM in a Generalised Narrow-Width Approximation

angefertigt am DESY Hamburg/
II. Physikalisches Institut, Georg-August-Universität Göttingen
von Elina Fuchs (20677732) aus Hannover

DESY

Bearbeitungszeit: 21. September 2011 bis 21. März 2012

Thesis number: II.Physik-UniGö-MSc-2012/03

Betreuer: Prof. Dr. Georg Weiglein

Erstgutachter: Prof. Dr. Arnulf Quadt

Zweitgutachter: Prof. Dr. Georg Weiglein

Abstract

A generalised narrow-width approximation (NWA) that takes interference terms into account is investigated. The factorisation of a more complicated process into the on-shell production of an intermediate particle times the branching ratio of its subsequent decay is not valid within the framework of the usual NWA if nearly mass-degenerate particles interfere. Large interference effects between the contributions of the two neutral $\mathcal{CP}$-even Higgs bosons of the Minimal Supersymmetric Standard Model are encountered for the studied example of the decay of a heavy neutralino. While the usual NWA deviates strongly from the full result, the inclusion of the interference term in the generalised NWA predicts the decay width to an accuracy of few percent. One-loop corrections to the neutralino-Higgs vertex in an on-shell renormalisation of the neutralino sector and a mixed on-shell and $\overline{\text{DR}}$-scheme for the Higgs sector are incorporated into the generalised NWA. Using the convenient simplification of factorising the full process into production and decay, this method facilitates the inclusion of higher-order corrections of sub-processes in combination with a consistent prediction for the interference term.

Zusammenfassung

Eine verallgemeinerte Näherung schmaler Breiten (NWA, *narrow-width approximation*) wird untersucht, die die Berücksichtigung eines Interferenzterms in einer Näherung auf der Massenschale ermöglicht. Denn im Fall von Interferenzen zwischen quasi massenentarteten Teilchen verliert die gewöhnliche NWA ihre Gültigkeit, einen komplizierteren Prozesses in die Produktion eines instabilen Teilchens auf seiner Massenschale und den anschließenden Zerfall mittels Multiplikation mit dem entsprechenden Verzweigungsverhältinis zu faktorisieren. Beispielsweise treten große Interferenzeffekte zwischen den Beiträgen der beiden $\mathcal{CP}$-geraden Higgs-Bosonen des Minimal Supersymmetrischen Standardmodells auf, die im Zerfall eines schweren Neutralinos entstehen. Während die gewöhnliche NWA stark von der exakten Zerfallsbreite abweicht, gelingt es, mit Hilfe der verallgemeinerten NWA inklusive Interferenzterm das volle Ergebnis mit einer Genauigkeit von wenigen Prozent anzunähern. Zusätzlich werden in der NWA Ein-Schleifen-Korrekturen zum Neutralino-Higgs-Vertex berücksichtigt, wobei der Neutralino-Sektor in einem Schema auf der Massenschale und der Higgs-Sektor in einem kombinierten Massenschalen- und $\overline{\text{DR}}$-Schema renormiert werden. Diese Methode erlaubt unter Ausnutzung der Vereinfachung durch Faktorisierung in Produktion und Zerfall, Korrekturen höherer Ordung in Teilprozessen mit einer konsistenten Vorhersage für den Interferenzterm zu verbinden.

Contents

1. Introduction

The smallest components of matter and their interactions have been an issue of strong interest from ancient philosophy up to modern particle physics, which is equipped with powerful accelerators and detectors to precisely probe established theories and to look for evidence of new physics.

The Standard Model of particle physics (SM) describes electroweak and strong interactions in impressive agreement with the experiments of the last decades. However, theoretical considerations, such as the stability of the Higgs boson mass with respect to quantum corrections and a consistent description of all forces including gravity, as well as experimental evidence, such as dark matter and the baryon asymmetry of the universe, indicate that the SM cannot be a complete theory, but it must be extended to a more fundamental level at higher energies.

Theories beyond the SM and in particular supersymmetry (SUSY) have been discussed for a long time, but no signal of the additional states predicted in those models has been observed yet. Now particle physics has entered a new era with the start of the Large Hadron Collider (LHC) at so far unexplored energies. Two of its main goals are the discovery of the mechanism responsible for electroweak symmetry breaking and the detection of or limits on supersymmetric new particles. The Minimal Supersymmetric Standard Model (MSSM) features an extended Higgs sector, leading to the interesting combination of these two topics.

The discovery of supersymmetry or limits on the parameter space require both reliable experimental analyses and accurate theoretical predictions. However, the aim for high precision needs to be balanced with the feasibility of the calculation. In SUSY one typically faces long decay chains with many particles in the final state (see Fig. 1.1), which make an exact calculation of higher-order corrections complicated or sometimes even impossible with today's methods.
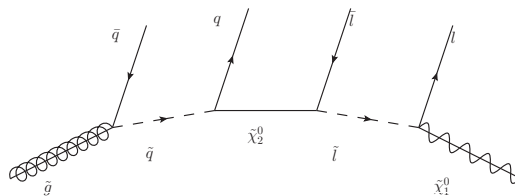
Figure 1.1.: Example of a SUSY cascade decay which might be decomposed in several steps by means of the narrow-width approximation.

1

The idea is to factorise the whole process into the on-shell production of an intermediate particle with a narrow width and its subsequent decay. This procedure can be applied iteratively until the long cascade is decomposed into smaller sub-processes, which are taken into account by multiplication with their branching ratios.

However, this so-called narrow-width approximation (NWA) neglects the fact that diagrams with the same initial and final states, but different intermediate particles, can interfere. These interference effects can be large if the mass difference between the intermediate particles is less than their total widths such that the Breit-Wigner shapes of their propagators overlap significantly. In these cases an extension of the usual NWA is necessary in order to accommodate the possibly large interference term which would be discarded otherwise.

These effects might become important especially - but not exclusively - in supersymmetric models. The reason is that the enlarged particle spectrum allows for more combinations of almost degenerate masses.

In the literature, some processes with sizable interference effects in several MSSM scenarios have been encountered [1–4]. The authors suggest not to work in the NWA in these cases, but to perform a full calculation. In this thesis, we study as an example process the production of interfering MSSM Higgs bosons in a decay of a heavier neutralino, and their subsequent decay. The exact calculation of the full process is compared to the usual NWA and an interference-improved NWA. Considering cost and benefit of an approximation, in other words confronting technical simplification versus achieved accuracy, we evaluate the interference term in different ways and include also loop corrections.

Outline After motivating a generalised narrow-width approximation (NWA) in the context of the Minimal Supersymmetric Standard Model (MSSM) in Chap. 1, this master's thesis starts with the basics of the Standard Model (SM) in Chap. 2, followed by an introduction to the MSSM with complex parameters in Chap. 3. After these considerations at tree-level, the procedure of regularisation and renormalisation is presented in Chap. 4 with a focus on the Higgs and neutralino sectors of the MSSM. Algebraic and numerical programs that are used in our calculations are described in Chap. 5. Subsequently, Chap. 6 contains useful kinematic relations for decay processes. The usual NWA and its generalisation for interference effects are discussed in Chap. 7. As an example process, a neutralino decay with an interference of Higgs bosons is calculated analytically in Chap. 8. Numerical results are shown and the accuracy of the approximation is evaluated in Chap. 9. Extending the previous tree-level computations, vertex corrections are discussed in Chap. 10. Finally, after summing up, an outlook for future work is given in Chap. 11.

2. The Standard Model

In this chapter, we give a short introduction to the Standard Model of particle physics (SM), following primarily Refs. [5, 6]. The content of matter fields and their interactions as well as the Higgs mechanism are discussed before pointing out some limitations of the precisely tested and so far remarkably successful SM.

2.1. Fields and interactions

The SM [7–10] describes all elementary particles discovered so far (and the yet undiscovered Higgs boson) and their interactions as a Lorentz invariant quantum field theory. Non-abelian gauge symmetries lead to the fundamental interactions known as the electromagnetic, weak and strong forces. It is comprised of twelve fermions (spin $s = 1/2$), namely six quarks and six leptons together with their antiparticles. The interactions are mediated by gauge bosons ($s = 1$).

The particles acquire mass by the so-called Higgs mechanism. However, the discovery of the Higgs boson is still eagerly awaited. The Higgs mass is not predicted by theory, but experimental input is needed. LEP excluded the SM Higgs boson with a mass below 114.4 GeV [11]. The current status of LHC Higgs searches is an exclusion at 95% confidence level in the range of $m_H \in [112.9\,\mathrm{GeV}, 115.5\,\mathrm{GeV}]$ and $m_H \in [127.5\,\mathrm{GeV}, 600\,\mathrm{GeV}]$ by ATLAS and CMS. But in the unexcluded region an excess around 124-126 GeV is observed by both experiments with a global statistical significance in the entire mass range of $2.2\,\sigma$ and $0.8\,\sigma$ in an integrated luminosity of $4.9\,\mathrm{fb}^{-1}$ or $4.7\,\mathrm{fb}^{-1}$, respectively [12–15]. The combination [16] of the Tevatron experiments DØ and CDF with $10\,\mathrm{fb}^{-1}$ yields an excess for $m_H \in [115\,\mathrm{GeV}, 135\,\mathrm{GeV}]$ with a global significance of $2.2\,\sigma$.

2.1.1. Particle content

The fermions are arranged in three families, forming left-handed weak isospin (I_3) doublets and right-handed singlets. While each lepton doublet contains one neutrino (ν_e, ν_μ, ν_τ) with electric charge $Q = 0$ and one lepton with the elementary charge $Q = -1$ (e, μ, τ), both quarks in a quark doublet are electrically charged. Those quarks with positive electric charge $Q = +\frac{2}{3}$ (u, c, t) are called up-type, those ones with negative charge $Q = -\frac{1}{3}$ (d, s, b) are called down-type. The masses of the particles range from the nearly massless neutrinos to $m_e \approx 0.511$ MeV to the top mass of

$m_t = 173.2 \pm 0.6 \pm 0.8\,\text{GeV}\,[17]^1$ (with the statistical and systematic uncertainty, respectively), which is a crucial parameter for precision analyses. The antiparticles have the same mass as their corresponding particles due to $\mathcal{CPT}$-invariance, but opposite values of the quantum numbers. The following table 2.1 summarises the particles' properties like the spin s, the third component of the isospin I_3, the electromagnetic charge Q, the weak hypercharge Y and the colour charge C.

Table 2.1.: Fermions and the Higgs boson of the Standard Model [5, 20] and their spin s, weak isospin I_3, electric charge Q, weak hypercharge Y and colour charge C. Weak eigenstates are denoted by q'. The gauge bosons are described in the text.

Particles			s	I_3	$Q[e]$	Y	C
Fermions							
$\begin{pmatrix} \nu_e \\ e^- \end{pmatrix}_L$	$\begin{pmatrix} \nu_\mu \\ \mu^- \end{pmatrix}_L$	$\begin{pmatrix} \nu_\tau \\ \tau^- \end{pmatrix}_L$	$\frac{1}{2}$	$\begin{pmatrix} +\frac{1}{2} \\ -\frac{1}{2} \end{pmatrix}$	$\begin{pmatrix} 0 \\ -1 \end{pmatrix}$	-1	0
$\begin{pmatrix} u \\ d' \end{pmatrix}_L$	$\begin{pmatrix} c \\ s' \end{pmatrix}_L$	$\begin{pmatrix} t \\ b' \end{pmatrix}_L$	$\frac{1}{2}$	$\begin{pmatrix} +\frac{1}{2} \\ -\frac{1}{2} \end{pmatrix}$	$\begin{pmatrix} +\frac{2}{3} \\ -\frac{1}{3} \end{pmatrix}$	$+\frac{1}{3}$	r, g, b
e_R	μ_R	τ_R	$\frac{1}{2}$	0	-1	-2	0
u_R	c_R	t_R	$\frac{1}{2}$	0	$+\frac{2}{3}$	$+\frac{4}{3}$	r, g, b
d'_R	s'_R	b'_R	$\frac{1}{2}$	0	$-\frac{1}{3}$	$-\frac{2}{3}$	r, g, b
Higgs Boson							
H			0	$-\frac{1}{2}$	0	+1	0

The weak and the mass eigenstates, q', q respectively, are not equal, but linear combinations of each other, $q_i^{'L/R} = U_{ij}^{u/d,L/R} q_j^{L/R}$, mixed by the unitary 3×3 CABIBBO-KOBAYASHI-MASKAWA (CKM) matrix $V_{ij} = U_{il}^{u,L} U_{lj}^{d,L\dagger}$ [21, 22]. A unitary $n \times n$ matrix contains n^2 real parameters. Regarding the quarks, $2n - 1$ of these parameters represent the choice of quark phases which can be absorbed into the fields. Hence, they are not physically meaningful. Exploiting this freedom, $(n-1)^2$ parameters are left out of which $\frac{1}{2}n(n-1)$ are quark mixing angles and the remaining $\frac{1}{2}(n-1)(n-2)$ parameters are complex phases. Thus, $n = 2$ quark generations would have only one mixing angle whereas in $n = 3$ generations 3 mixing angles and one complex phase are present, which can lead to $\mathcal{CP}$-violation. Unitarity of V prevents flavour changing neutral currents at lowest order.

In this thesis, though, we neglect flavour mixing by setting $V = \mathbb{1}_3$.

---

[1] The LHC experiments measured $m_t = 175.9 \pm 0.9 \pm 2.7\,\text{GeV}$ at ATLAS [18] and $m_t = 173.4 \pm 1.9 \pm 2.7\,\text{GeV}$ at CMS [19]. The systematic uncertainty is dominated by the jet energy scale.

2.1.2. Interactions

The theory of the electromagnetic, weak, and strong interactions is mathematically expressed by local gauge symmetries, i.e. the invariance of the Lagrangian under the local action of a certain Lie-group G. In the SM, relevant Lie-groups are the special unitary groups $SU(N)$. The dimension of any $SU(N)$ group is $|G| = N^2 - 1$ which equals the number of generators T^a, $a = 1, ..., |G|$ of the group or number of gauge fields A_μ^a belonging to the interaction with a coupling g. Gauge invariance is achieved by replacing the derivative ∂_μ by the covariant derivative

$$D_\mu := \partial_\mu - ig \sum_{a \in G} T^a A_\mu^a. \tag{2.1}$$

The abelian Lie-group $U(1)_Y$ of the weak hypercharge $Y = 2(Q - I_3)$ consists of phase transformations $\Psi(x) \to \Psi'(x) = e^{i\alpha}\Psi(x)$. It is connected to the gauge field B_μ and the coupling constant is denoted as g'. In contrast, the non-abelian group $SU(2)$ is generated by the three Pauli matrices σ^i with $i \in 1, 2, 3$, which do not commute. There are three gauge fields W_μ^i and the coupling strength is g. With the covariant derivative

$$D_\mu = \partial_\mu - ig\sigma^i W_\mu^i - i\frac{g'}{2}Y B_\mu, \tag{2.2}$$

the two interactions are unified to the symmetry group $SU(2)_L \otimes U(1)_Y$ which contains the $U(1)_{em}$ of electromagnetism as a subgroup. The subscript L indicates the exclusive coupling of the gauge bosons W_μ^i, $i = 1, 2, 3$ associated with the $SU(2)_L$ to left-handed particles. The vector bosons of the mass eigenstates, A_μ and Z_μ, are obtained from linear combinations of the gauge fields B_μ and W_μ^3.

$$W_\mu^\pm = \frac{1}{\sqrt{2}} \left(W_\mu^1 \mp iW_\mu^2 \right) \qquad\qquad \leftrightarrow W^\pm \tag{2.3}$$

$$A_\mu = +B_\mu \cos(\theta_W) - W_\mu^3 \sin(\theta_W) \qquad\qquad \leftrightarrow \gamma \tag{2.4}$$

$$Z_\mu = +B_\mu \sin(\theta_W) + W_\mu^3 \cos(\theta_W) \qquad\qquad \leftrightarrow Z^0. \tag{2.5}$$

The electroweak mixing angle θ_W is given by

$$s_W := \sin(\theta_W) = \frac{g'}{\sqrt{g^2 + g'^2}}, \ c_W := \cos(\theta_W). \tag{2.6}$$

The symmetry group $SU(3)_C$ of quantum chromodynamics is generated by the eight Gell-Mann matrices λ^a. Here, the index C indicates the colour charge red, green, blue. There are eight gluon fields $G_{\mu\nu}^a$, with $a \in 1, ..., 8$, which carry colour themselves. Combining the electroweak and strong interaction results in the symmetry

group of the Standard Model:

$$SU(3)_C \otimes SU(2)_L \otimes U(1)_Y$$

Except the gluon and right-handed states, all particles participate in the weak interaction, whereas only charged particles can interact electromagnetically. Gluons only couple to colour-charged particles, i.e., to quarks and to themselves. While the weak gauge bosons can couple to themselves, too, the photon, however, is electrically neutral so that a self-interaction is not possible. Mathematically, this is due to the abelian nature of the group $U(1)_{em}$. From the renormalisation of the charge it follows that the coupling strengths are not constant, but run with the energy scale. In the renormalisation group equation (RGE), the change of the coupling is expressed as the so-called β-function. The coupling increases for higher energies in the electromagnetic case. The strong coupling, on the contrary, diverges at low and decreases at high energies which is known as *confinement* and *asymptotic freedom*, respectively. As a consequence of confinement, no free quarks have been observed so far. The masses, total decay widths and other properties of the SM particles are listed in Ref. [20].

2.1.3. Electroweak symmetry breaking

The SM in its form described above predicts massless fermions and gauge bosons, which is in contradiction to the experimental results. Explicit mass terms in the Lagrangian would violate gauge invariance and spoil renormalisability, but with spontaneous breaking of the electroweak symmetry, the gauge boson masses can be incorporated in a consistent way. In this case, only the symmetry of the vacuum is broken while keeping the Lagrangian invariant. This is the so-called Higgs mechanism [23–27]. The breaking is due to a complex scalar doublet, $\phi = \begin{pmatrix} \phi_+(x) \\ \phi_0(x) \end{pmatrix}$, in the fundamental representation of $SU(2)$ with $Y = 1$, giving rise to a scalar term in the Lagrangian,

$$\mathscr{L} = (D_\mu \phi)^\dagger (D_\mu \phi) - V(|\phi|^2). \tag{2.7}$$

The Higgs potential as a function of the scalar field depends only on the combination $\phi^\dagger \phi$,

$$V(\phi) \equiv V(\phi^\dagger \phi) = -\mu^2 \phi^\dagger \phi + \frac{\lambda}{4}(\phi^\dagger \phi)^4. \tag{2.8}$$

In order to respect renormalisability, no higher powers than $(\phi^\dagger \phi)^4$ are allowed. At large $(\phi^\dagger \phi)^4$ the quartic term dominates so that λ must be positive in order for the potential to be bounded from below. If $\mu^2 < 0$, then the potential is minimised at $\phi = 0$ so that no symmetry breaking is present. On the other hand, a positive μ^2 results in the so-called 'Mexican hat' potential which exhibits infinitely many

degenerate minima on a circle of radius

$$|\phi| = \sqrt{\phi_+^\dagger \phi_+ + \phi_0^\dagger \phi_0} = \sqrt{\frac{2\mu^2}{\lambda}} \equiv \frac{v}{\sqrt{2}} \neq 0 \tag{2.9}$$

with the non-vanishing vacuum expectation value v. The set of degenerate minima is still invariant under rotations, but the choice of one particular ground state, $\langle \phi \rangle = \begin{pmatrix} 0 \\ \frac{v}{\sqrt{2}} \end{pmatrix}$, breaks the symmetry of the underlying Lagrangian. So the original $SU(2)_L \otimes U(1)_Y$ is broken down to the $U(1)_{em}$ of electromagnetism. Then, $\phi(x)$ is expanded about the vacuum in terms of $\eta = \phi_+$ and $\frac{1}{\sqrt{2}}(H + i\chi) = \phi_0 - \frac{v}{\sqrt{2}}$,

$$\phi(x) = \begin{pmatrix} \eta(x) \\ \frac{1}{\sqrt{2}}(v + H + i\chi) \end{pmatrix}. \tag{2.10}$$

Two degrees of freedom (dof), η, χ, are massless scalar would-be Nambu-Goldstone bosons [28, 29]. They are 'eaten up' by the longitudinal modes of the gauge bosons which acquire a mass of

$$M_W = g\frac{v}{2} \quad \text{and} \quad M_Z = \sqrt{g^2 + g'^2}. \tag{2.11}$$

The current experimental world averages are $M_W = 80.385 \pm 0.015\,\text{GeV}$ (including [30, 31]) and $M_Z = 91.1876 \pm 0.0021\,\text{GeV}$ [20] while the photon remains massless, $M_A = 0$. Prior to symmetry breaking, the number of dof amounts to 12 ($4 \cdot 2$ for the four massless gauge bosons plus 4 of the complex doublet). Thereafter, the three massive and one massless gauge bosons sum up to only 11 dof. Consequently, the residual dof must be carried by a physical Higgs boson H. By expressing the potential in terms of the Higgs field, its mass, which arises from Higgs self-interaction λ, can be identified as

$$m_H^2 = \frac{\partial^2 V(H)}{\partial H^2} = 2\mu^2 = \lambda\frac{v^2}{2}. \tag{2.12}$$

Fermions acquire their mass through YUKAWA couplings, y_f, to the Higgs field:

$$m_f = y_f\frac{v}{\sqrt{2}}. \tag{2.13}$$

2.2. Shortcomings of the Standard Model

Although the Standard Model of particle physics (SM) turns out to be very successful at the energy scales probed so far, it can only be regarded as an effective theory. Several issues indicate that new physics might enter above a cut-off scale Λ.

The validity of the SM is limited at the latest by the Planck scale $M_P \sim \mathcal{O}(10^{19})\,\text{GeV}$ beyond which gravity becomes relevant. However, the implementation of the algebra of general relativity cannot be accomplished within the framework of the SM. A consistent description of all four fundamental forces is still missing.

This raises the question of naturalness of the huge hierarchy between the electroweak scale M_W and M_P, which differ by 17 orders of magnitude. In case that no new physics is present between these two scales, the cut-off scale is set to $\Lambda \simeq M_P$. But then the problem arises that loop corrections to scalar mass squares, which diverge quadratically with the cut-off, shift the Higgs mass from the tree-level value around the electroweak scale to the Planck scale by

$$\delta M_H^2 \sim \Lambda^2 \sim M_P^2. \tag{2.14}$$

Fermion masses, on the other hand, are protected by chiral symmetry so that their quantum corrections grow only as $\delta m_f \sim m_f \ln \Lambda$. But in order to compensate the large radiative corrections to the Higgs mass, an unnatural fine tuning becomes necessary to keep M_H at the electroweak scale since unitarity demands a Higgs boson mass below $1\,\text{TeV}$.

Moreover, there are further indications that the SM cannot be a complete theory, for example if a unification of all gauge couplings is required. The three running SM gauge couplings cannot coincide at one high energy scale if no new physics enters below the scale M_{GUT} of a Grand Unified Theory (GUT).

Furthermore, astrophysical observations imply that, besides the 5% of ordinary matter, 23% of the energy content of the universe should be made of dark matter (DM). The SM does not provide a viable candidate for DM which ought to be stable on cosmological time scales and can interact only weakly with ordinary matter. In addition, the baryon asymmetry in the universe makes new sources of $\mathcal{CP}$-violation, besides the one complex phase in the CKM-matrix, indispensable.

Several ideas exist for how to embed the SM in a more fundamental theory, such as supersymmetry (SUSY), extra dimensions or string theory. We will focus on SUSY and its elegant solutions to the shortcomings of the SM mentioned in this section - keeping in mind that more limitations of the SM exist which cannot be resolved immediately by SUSY, for example the demand for a consistent quantum field theory of gravitation.

The description in this section and in the following chapter is mostly based on references [32–34].

3. The Minimal Supersymmetric Standard Model

3.1. Motivation for supersymmetry

Supersymmetry is a symmetry relating bosons and fermions. SM fermions are partnered with bosons and vice versa. These so-called s(uper)particles (indicated by a tilde) share all quantum numbers with their SM partners except the spin. Although not initially designed for these purposes, it is compelling that SUSY possibly provides solutions to all of the issues addressed in Sect. 2.2 at once.

Gravitation can be included at the classical level by making SUSY local. This gauged SUSY is called supergravitation (SUGRA) [35].

Furthermore, if supersymmetry is realised at the TeV-scale, this also solves the hierarchy problem of the scales M_W and M_P. Quadratically divergent self-energy corrections to the bare Higgs mass, $m_H^2 = m_{H,bare}^2 + \Delta m_H^2$, would require order-by-order an unnatural fine tuning which can be avoided with supersymmetry. Fermions in a loop contribute with a negative sign as $-g_f^2 \Lambda^2$, where g_f denotes the coupling of fermions to a Higgs boson, whereas scalars with a coupling g_S yield $+g_S \Lambda^2$. So fermionic and scalar corrections to the Higgs propagator as in Fig. 3.1 cancel exactly if the couplings are related by $g_f^2 = g_S$. This is indeed achieved in a supersymmetric theory. However, in the presence of SUSY breaking (see Sect. 3.3.2), SM particles and their superpartners are not mass-degenerate any more, $m_{\tilde{f}}^2 = m_f^2 + \Delta^2$. But as long as the mass splittings are small enough, i.e. $\Delta \sim \mathcal{O}(\text{TeV})$, no new unnatural quadratic hierarchy in the order of Δ^2 is reintroduced. Instead, logarithmic corrections to the Higgs mass are still acceptable to keep m_H around the electroweak scale. Hence, this stabilisation of the Higgs mass is a motivation for low-energy supersymmetry (i.e. sparticle masses in the range of at most roughly 1-10 TeV).

Furthermore, the aim of Grand Unified Theories is to find a larger simple group of

Figure 3.1.: Fermion and scalar loops in the Higgs propagator.

inner symmetries which is broken down to the SM group $SU(3) \otimes SU(2) \otimes U(1)$ at lower energies. Strikingly, SUSY predicts a natural unification of all gauge couplings at M_{GUT} which is not possible in the SM [36]. The reason is that the additional group theoretical factors of the superparticles enter into the coefficients of the β-function in the RGE which governs the running of the gauge couplings.

Moreover, the SUSY particle spectrum provides candidates for cold dark matter, such as the lightest neutralino (see Section 3.3.1) and in the SUGRA case also the gravitino. SUSY also introduces various new parameters which can in principle be complex and hence contribute to the necessary amount of $\mathcal{CP}$-violation for the matter-antimatter asymmetry in the universe. However, stringent experimental constraints limit the allowed range of the new complex phases [37–39].

3.2. SUSY algebra

Does the SM exploit all symmetries that are consistent with Lorentz invariance?
In their famous no-go theorem, COLEMAN and MANDULA proved in 1967 [40] that the only Lie group containing the Poincaré group for a relativistic quantum field theory in $D = 4$ dimensions is the direct product of the Poincaré spacetime symmetries and inner symmetries. Since in a direct product all generators of the first group commute with all generators of the second group, this is only a trivial extension.
However, in 1975 HAAG, LOPUSZANSKI and SOHNIUS [41] proposed to replace the ordinary Lie algebra by a graded Lie algebra. This bypasses the no-go theorem with supersymmetry as the unique non-trivial extension of the spacetime symmetries of the Poincaré algebra.
The supersymmetry generator Q alters the spin by $1/2$ and thus relates fermions to bosons. With Lorentz index μ, spinor indices $\alpha, \beta, \dot{\alpha}, \dot{\beta}$ and four-momentum P^μ, the SUSY algebra combines commutators and anticommutators:

$$\left\{ Q_\alpha, Q^\dagger_{\dot{\alpha}} \right\} = -2\sigma^\mu_{\alpha\dot{\alpha}} P_\mu \tag{3.1}$$

$$\{ Q_\alpha, Q_\beta \} = \left\{ Q^\dagger_{\dot{\alpha}}, Q^\dagger_{\dot{\beta}} \right\} = 0 \tag{3.2}$$

$$[P^\mu, Q_\alpha] = \left[P^\mu, Q^\dagger_{\dot{\alpha}} \right] = 0. \tag{3.3}$$

The fields are arranged in left-chiral and vector/ gauge supermultiplets which contain an equal number of fermionic and bosonic degrees of freedom and furnish an irreducible representation of supersymmetry [42]. Eq. (3.3) even implies

$$\left[Q_\alpha, P^2 \right] = [Q_\alpha, P_\mu] P^\mu + P_\mu [Q_\alpha, P^\mu] = 0, \tag{3.4}$$

which means that all fields in one supermultiplet are mass degenerate. This implication must be revisited in the context of broken SUSY in Sect. 3.3.2.

3.3. Specification of a SUSY theory

The algebra alone does not fully determine the theory. In addition, the superpotential $\mathcal{W}$ and the Lagrangian of soft SUSY breaking $\mathscr{L}_{soft}$ must be defined. This is explicated in the following two sections.

3.3.1. Superpotential and R-parity

To specify a supersymmetric theory, it is necessary to define the superpotential $\mathcal{W}$ which dictates all couplings allowed in the supersymmetric theory apart from the gauge couplings. The Minimal Supersymmetric Standard Model (MSSM) is the smallest supersymmetric extension of the SM. It is characterised by the choice

$$\mathcal{W}_{MSSM} = \epsilon_{\alpha\beta}[-H_u^\alpha \, Q_i^\beta y_u^{ij} \bar{u}_j + H_d^\alpha \, Q_i^\beta y_d^{ij} \bar{d}_j + H_d^\alpha \, L_i^\beta y_e^{ij} \bar{e}_j - \mu H_d^\alpha H_u^\beta]. \qquad (3.5)$$

Here, i, j are family indices and α, β are $SU(2)$ indices which are contracted by the antisymmetric tensor $\epsilon_{\alpha\beta} = -\epsilon_{\beta\alpha}$ with the convention $\epsilon_{12} = +1$. An unbarred field is the left-handed component of a Dirac spinor, whereas the bar is part of the name of a conjugate of the right-handed part of a Dirac spinor.

In Eq. (3.5), y are the Yukawa coupling matrices. Despite the absence of a conventional mass term, μ is a parameter of mass dimension one and this so-called μ-term is the $SU(2)$-invariant coupling of the two Higgs doublets H_u, H_d. It is the only allowed bilinear combination because Hermitian conjugates of the fields in $\mathcal{W}$ would violate SUSY. The field content of the chiral superfields of the sfermions Q, u, d, L, e, as well as the two Higgs doublets for up- and down-type fermions, are listed in Tab. 3.1 and further explained in the subsequent sections.

In addition to the superpotential given in Eq. (3.5), gauge invariance and renormalisability do not exclude - in contrast to the SM - baryon (B) and lepton (L) number violating terms containing the couplings λ_L, λ_B which may lead to a rapid proton decay. B- and L- violating processes have not been observed experimentally. Nonetheless, due to non-perturbative electroweak effects at very high energy scales [43], B- and L-conservation cannot be assumed to be a fundamental symmetry which would set λ_L and λ_B identically to zero. So instead a new symmetry, called R-symmetry [44], is introduced which forbids the baryon and lepton number violating terms, but allows all interactions in Eq. (3.5). The R-parity $R := (-1)^{3B+L+2s}$, where s denotes the spin, assigns +1 to SM particles and -1 to their SUSY partners. The multiplicative conservation of the R-parity implies that SUSY particles can only be pair-produced and that the lightest supersymmetric particle (LSP) is absolutely stable. As a consequence, the final state in a decay of any sparticle must contain an odd number of LSPs. If the LSP is neutral, it is suited as a candidate for non-baryonic cold dark matter [45, 46]. In the MSSM this role might be played by, e.g., the lightest neutralino $\tilde{\chi}_1^0$.

3.3.2. SUSY breaking

SUSY breaking mechanisms are reviewed comprehensively e.g. in Ref. [34].

If SUSY were an exact symmetry, particles and their superpartners would have exactly the same mass. The non-observation of SUSY particles at energies reached up to now implies that SUSY can only be realised as a broken symmetry. Yet it remains an open question how this SUSY breaking is accomplished. Spontaneous SUSY breaking such as in the models by O'Raifeartaigh [47] or Fayet and Iliopoulos [48] are not viable in the MSSM. Instead, the breaking is assumed to happen in a *hidden sector* which has no direct renormalisable couplings to the *visible* or *observable sector* of the SM fields together with their superpartners. While the phenomenology is largely insensitive to the exact dynamics of the SUSY breaking in the hidden sector, it does indeed strongly depend on the so far unknown way of mediation from the hidden to the visible sector.

The crucial point is that SUSY breaking terms in the Lagrangian must not reintroduce the quadratic divergences whose cancellation were one feature of exact SUSY. The divergences are avoided by allowing only so-called *soft* terms that, by having a positive mass dimension, maintain the relations between dimensionless couplings, namely all gauge and Lorentz invariant terms of dimension two and three. The ignorance of the actual SUSY breaking mechanism is parametrised in the soft Lagrangian, $\mathscr{L}_{soft}$, which comprises trilinear couplings, bilinear couplings, soft scalar mass squares and soft gaugino masses.

Possible messenger interactions to mediate SUSY breaking from the hidden to the visible sector are, for instance,

- *gauge mediation* (GMSB): some new chiral supermultiplets couple as messengers directly to the source of SUSY breaking and indirectly through gauge bosons and their superpartners to MSSM particles so that SUSY breaking is mediated by ordinary gauge interactions, see e.g. [49],

- *gravity mediation* (SUGRA): making SUSY local gives rise to supersymmetric gravity which can mediate SUSY breaking by non-renormalisable, but M_P-suppressed gravitational interaction [35],

- *anomaly mediation* (AMSB): soft terms arise from the violation of superconformal invariance [50].

If universal masses or couplings are assumed at a high scale, the number of free parameters is reduced. This facilitates experimental analyses in a lower dimensional parameter space as discussed in Sect. 3.5.

3.4. Field content of the MSSM

In arranging fermions and bosons in supermultiplets, the question is raised whether the SM bosons might serve as the superpartners of the SM fermions and vice versa. But this is not possible because they reside in different representations of the gauge groups, the fermions in the fundamental and the gauge bosons in the adjoint one. Consequently, distinct superparticles need to be introduced which more than double the spectrum. The scalar partners of the SM fermions are called sleptons and squarks. The gauge bosons get spin-1/2 superpartners, denoted by the suffix '-ino', namely the gauginos called binos, winos and gluinos. A second complex scalar Higgs doublet is added (see below) and both Higgs doublets have higgsino partners with spin-1/2.

Since fields with identical charge and colour, but different weak quantum numbers are allowed to mix, gauge and mass eigenstates are distinguished. The superpartners of the left- and right-handed states of a fermion f mix to $\tilde{f}_1, \tilde{f}_2$. If the mixing is negligible, the mass eigenstates nearly coincide with the gauge eigenstates. But large mixing is expected to occur in the third generation. Eight degrees of freedom from the two complex Higgs doublets form the Higgs bosons $h^0, H^0, A^0, H^\pm$ and three Goldstone bosons. In addition, all neutral gauginos and higgsinos mix to the four neutralinos $\tilde{\chi}_i^0, i = 1, 2, 3, 4$, and all charged gauginos and higgsinos form the charginos $\tilde{\chi}_i^\pm, i = 1, 2$. This is summarised in Tab. 3.1, and the following sections go into more detail for each sector. The enlarged particle spectrum leads to more possibilities for mass degeneracies, depending on the SUSY parameters realised in nature, see Sect. 3.5. This thesis is focussed on scenarios featuring mass splittings of the order of the decay width of one of the particles.

Table 3.1.: Field content of the MSSM, grouped in chiral and gauge supermultiplets, which mix to form the mass eigenstates [32, 33].

Chiral		**spin-0** $(R = -1)$	**spin-1/2** $(R = +1)$	mass eigenstates
(s)quarks	Q	$(\tilde{u}_L, \tilde{d}_L)$	(u_L, d_L)	
	$\bar{u}$	$\tilde{u}_R$	u_R	$\sim$ same or
	$\bar{d}$	$\tilde{d}_R$	d_R	$\tilde{t}_1, \tilde{t}_2, \tilde{b}_1, \tilde{b}_2$
(s)leptons	L	$(\tilde{\nu}, \tilde{l}_L)$	(ν, l_L)	$\sim$ same or
	$\bar{e}$	$\tilde{l}_R$	l_R	$\tilde{\tau}_1, \tilde{\tau}_2$
Higgs/inos	H_d	$\mathcal{H}_1 = \left(h_d^0, h_d^-\right)$	$(\tilde{h}_d^0, \tilde{h}_d^-)$	
	H_u	$\mathcal{H}_2 = \left(h_u^+, h_u^0\right)$	$(\tilde{h}_u^+, \tilde{h}_u^0)$	$h^0, H^0, A^0, H^\pm$
Gauge		**spin-1** $(R = +1)$	**spin-1/2** $(R = -1)$	
B-boson/neutralinos		B	$\tilde{B}^0, \tilde{W}^0$ (mix with $\tilde{h}_u^0, \tilde{h}_d^0$)	$\tilde{\chi}_1^0, \tilde{\chi}_2^0, \tilde{\chi}_3^0, \tilde{\chi}_4^0$
W-boson/charginos		$W^\pm$	$\tilde{W}^\pm$ (mix with $\tilde{h}_u^+, \tilde{h}_d^-$)	$\tilde{\chi}_1^\pm, \tilde{\chi}_2^\pm$
gluon/ino		g	$\tilde{g}$	same
goldstone/ino		G	$\tilde{G}$	(unphysical)

3.4.1. The Higgs sector

In addition to the SM particles and their superpartners, the MSSM contains a second Higgs doublet, which is required to render both up- and down-type quarks massive. In the SM, this is done by the Hermitian conjugate of the Higgs field, but this construction would break SUSY because the superpotential $\mathcal{W}_{MSSM}$ must be holomorphic in the fields. Furthermore, for the cancellation of unphysical degrees of freedom and to preserve gauge invariance, the theory must be anomaly-free. This means that the following traces over all left-handed Weyl fermions must vanish: $Tr[T_3^2 Y] = Tr[Y^3] \overset{!}{=} 0$. So we need two complex scalar Higgs doublets with opposite hypercharge $Y_{\mathcal{H}_{1/2}} = \pm 1$,

$$\mathcal{H}_1 = \begin{pmatrix} h_d^0 \\ h_d^- \end{pmatrix} = \begin{pmatrix} v_d + \frac{1}{2}(\phi_1^0 + i\chi_1^0) \\ \phi_1^- \end{pmatrix} \tag{3.6}$$

$$\mathcal{H}_2 = \begin{pmatrix} h_u^+ \\ h_u^0 \end{pmatrix} = e^{i\xi} \begin{pmatrix} \phi_2^+ \\ v_u + \frac{1}{2}(\phi_2^0 + i\chi_2^0) \end{pmatrix}. \tag{3.7}$$

The Higgs potential is constructed from the so-called F-terms (derived from derivatives of $\mathcal{W}_{MSSM}$ with respect to the Higgs doublets), D-terms (composed of the gauge couplings, gauge group generators and Higgs fields) and soft SUSY breaking terms (b parametrises the only mass-square term allowed in the MSSM),

$$
\begin{aligned}
V_H &= V_F + V_D - \mathcal{L}_{soft} \\
&= (|\mu|^2 + m_{H_u}^2)(|h_u^0|^2 + |h_u^+|^2) + (|\mu|^2 + m_{H_d}^2)(|h_d^0|^2 + |h_u^-|^2) \\
&\quad + [b(h_u^+ h_d^- - h_u^0 h_d^0) + h.c.] + \frac{g^2 + g'^2}{8} \left[|h_u^0|^2 + |h_u^+|^2 - |h_d^0|^2 - |h_u^-|^2\right]^2. \tag{3.8}
\end{aligned}
$$

One component of each Higgs doublet can be chosen to have a vanishing vacuum expectation value, $\langle h_u^+ \rangle = \langle h_d^- \rangle = 0$. But the two neutral components of both doublets acquire a non-zero, real vev,

$$v_1 \equiv \langle h_d^0 \rangle, \qquad v_2 \equiv \langle h_u^0 \rangle, \tag{3.9}$$

and their ratio $\frac{v_2}{v_1} =: \tan\beta$ is a crucial input parameter for the MSSM. Analogously to the SM, the Higgs doublets can then be expanded about these vevs as shown in the second equality of Eqs. (3.6,3.7).

Mixing in the neutral Higgs sector leads to the $\mathcal{CP}$-even Higgs bosons h^0, H^0 with mixing angle α,

$$\tan(2\alpha) = \frac{m_A^2 + M_Z^2}{m_A^2 - M_Z^2} \tan(2\beta), \tag{3.10}$$

and the $\mathcal{CP}$-odd A^0 and the Goldstone boson G^0. Because the complex phase of the soft breaking parameter ϕ_b and the phase between the Higgs doublets ξ can be

rotated away, $\mathcal{CP}$-violation is absent in the Higgs sector at tree-level. So the 4×4 mixing matrix is block-diagonal. Finally, there are two charged Higgs bosons $H^\pm$ along with the Goldstone bosons $G^\pm$. The relation between the fields is parametrised in Eqs. (3.11, 3.12) by the mixing angle α for the $\mathcal{CP}$-even Higgs bosons, β_n for the neutral $\mathcal{CP}$-odd ones and β_c for the charged ones,

$$
\begin{pmatrix} h \\ H \\ A \\ G \end{pmatrix} = \begin{pmatrix} -s_\alpha & c_\alpha & 0 & 0 \\ c_\alpha & s_\alpha & 0 & 0 \\ 0 & 0 & -s_\beta & c_\beta \\ 0 & 0 & c_\beta & s_\beta \end{pmatrix} \begin{pmatrix} \phi_1^0 \\ \phi_2^0 \\ \chi_1^0 \\ \chi_2^0 \end{pmatrix} \tag{3.11}
$$

$$
\begin{pmatrix} G^\pm \\ A^\pm \end{pmatrix} = \begin{pmatrix} c_\beta & s_\beta \\ -s_\beta & c_\beta \end{pmatrix} \begin{pmatrix} \phi_1^\pm \\ \phi_2^\pm \end{pmatrix}, \tag{3.12}
$$

where we introduced the short-hand notation $s_\beta \equiv \sin\beta$, $c_\beta \equiv \cos\beta$, and analogously for α. At tree-level, the relation

$$
m_{h/H}^2 = \frac{1}{2}\left(m_A^2 + M_Z^2 \mp \sqrt{(m_A + M_Z^2)^2 - 4 m_A^2 M_Z^2 \cos^2(2\beta)} \right) \tag{3.13}
$$

$$
= \mp M_Z^2 \cos 2\beta \begin{cases} \frac{\sin(\alpha+\beta)}{\sin(\beta-\alpha)}, & \text{for } h \\ \frac{\cos(\alpha+\beta)}{\cos(\beta-\alpha)}, & \text{for } H \end{cases} \tag{3.14}
$$

sets the limit $m_h \leq M_Z$ which was excluded by LEP for a $\mathcal{CP}$-even Higgs boson [11]. Nevertheless, sizable 1-loop corrections (especially from the third generation quarks and their superpartners due to the largest coupling) shift this upper bound to roughly $140\,\text{GeV}$ [51–55],

$$
M_h^2 \lesssim M_Z^2 + \frac{3 g^2 m_t^4}{8\pi^2 M_W^2}\left[\ln\left(\frac{M_S^2}{m_t^2}\right) + \frac{X_t^2}{M_S^2}\left(1 - \frac{X_t^2}{12 M_S^2}\right) \right] \tag{3.15}
$$

$$
\text{with } X_t \equiv A_t - \mu \cot\beta, \quad M_S^2 = \frac{1}{2}(m_{\tilde{t}_1}^2 + m_{\tilde{t}_2}^2), \tag{3.16}
$$

where A_t is the trilinear top coupling and M_S^2 the average squared stop mass, see Sect. 3.4.4. However, the leading 2-loop corrections [56] lead to a considerable reduction of the upper bound on M_h to $130 - 135\,\text{GeV}$.

At tree level, the masses of the $\mathcal{CP}$-odd and the charged Higgs bosons are related by

$$
m_{H^\pm}^2 = m_A^2 + M_W^2, \tag{3.17}
$$

$$
m_A^2 = \frac{2b}{\sin(2\beta)}. \tag{3.18}
$$

Thus at tree-level, the Higgs sector is fully determined by the two SUSY input parameters (in addition to SM masses and gauge couplings) $\tan\beta$ and $m_{H^\pm}$ (or, for conserved $\mathcal{CP}$, equivalently m_A). However, particles from other sectors can enter in loops so that the Higgs boson masses also depend in particular on parameters from the sfermion sector, such as the trilinear coupling A_f and the higgsino mass parameter μ.

Higgs couplings and the decoupling limit   The couplings of MSSM Higgs bosons to SM fields expressed in terms of the corresponding SM couplings ($V = Z, W^\pm$ and u, d denote the up/down-type quarks and charged leptons) are shown in the following table.

Table 3.2.: The couplings of the MSSM Higgs bosons to SM particles. V denotes the massive vector bosons and u, d the massive fermions.

XY	$g_{hXY}/g_{hXY}^{(SM)}$	$g_{HXY}/g_{HXY}^{(SM)}$	$g_{AXY}/g_{AXY}^{(SM)}$
VV	$\sin(\beta - \alpha)$	$\cos(\beta - \alpha)$	$0,\ g_{hAZ} = \cos(\beta - \alpha)\frac{g}{2c_W}$
uu	c_α/s_β	s_α/s_β	$\gamma_5 \tan\beta$
dd	$-s_\alpha/c_\beta$	c_α/c_β	$\gamma_5 \cot\beta$

Owing to $g_{h_iVV}^{(MSSM)} < h_{HVV}^{(SM)}$, the MSSM Higgs couplings to the gauge bosons are limited by those of the SM. On the other hand, the couplings to fermions can be either suppressed or enhanced, depending on the angles α and β. However, if $M_A \gg M_Z$, the mixing angle α approaches

$$\sin(\alpha) \to -\cos(\beta), \quad \cos(\alpha) \to \sin(\beta), \quad \sin(\beta - \alpha) \to 1, \cos(\beta - \alpha) \to 0, \quad (3.19)$$

so that H and A decouple from VV, and the hAZ-coupling vanishes while h couples like the SM Higgs boson. Hence, in this *decoupling limit* [57] the MSSM Higgs sector appears SM-like.

3.4.2. The chargino-neutralino sector

At tree-level, mixing in the chargino sector is governed by the higgsino and wino mass parameters μ and M_2, respectively. In the neutralino sector it additionally depends on the bino mass parameter M_1.

The charginos $\tilde{\chi}_i^\pm$, $i = 1, 2$, as mass eigenstates are superpositions of the wino $\tilde{W}^\pm$ and higgsino $\tilde{H}^\pm$,

$$\begin{pmatrix} \tilde{\chi}_1^\pm \\ \tilde{\chi}_2^\pm \end{pmatrix} = \underbrace{\begin{pmatrix} M_2 & \sqrt{2}M_W s_\beta \\ \sqrt{2}M_W c_\beta & \mu \end{pmatrix}}_{=:X} \begin{pmatrix} \tilde{W}^\pm \\ \tilde{\chi}_i^\pm \end{pmatrix}. \quad (3.20)$$

To obtain the Dirac chargino masses, the matrix X is diagonalised by the biunitary transformation

$$\text{diag}(m_{\chi_1^\pm}, m_{\chi_2^\pm}) = U^* X V^\dagger. \tag{3.21}$$

The mixing in the neutralino sector is described by the matrix Y,

$$\underbrace{\begin{pmatrix} \tilde{\chi}_1^0 \\ \tilde{\chi}_2^0 \\ \tilde{\chi}_3^0 \\ \tilde{\chi}_4^0 \end{pmatrix}}_{=:\chi^0} = \underbrace{\begin{pmatrix} M_1 & 0 & -M_Z c_\beta s_W & M_Z s_\beta s_W \\ 0 & M_2 & M_Z c_\beta c_W & -M_Z s_\beta c_W \\ -M_Z c_\beta s_W & M_Z c_\beta c_W & 0 & -\mu \\ M_Z s_\beta s_W & -M_Z s_\beta c_W & -\mu & 0 \end{pmatrix}}_{=:Y} \underbrace{\begin{pmatrix} \tilde{B} \\ \tilde{W}^3 \\ \tilde{h}_d^0 \\ \tilde{h}_u^0 \end{pmatrix}}_{=:\psi^0}. \tag{3.22}$$

Since neutralinos are Majorana particles, one unitary matrix $\tilde{N}$ suffices to diagonalise the symmetric mixing matrix Y, which has real, but not necessarily positive eigenvalues,

$$\tilde{N}^* Y \tilde{N}^{-1} =: D' = \text{diag}(m'_{\tilde{\chi}_1^0}, m'_{\tilde{\chi}_2^0}, m'_{\tilde{\chi}_3^0}, m'_{\tilde{\chi}_4^0}). \tag{3.23}$$

In order to render all mass eigenvalues non-negative, the Takagi factorisation [58, 59] can be applied. If $m'_{\tilde{\chi}_j^0}$ happens to be negative, one can rotate this eigenvalue by a unitary transformation T which can be chosen as a 4×4 unit matrix with an i on the jth position instead of the 1.

Then, with $N := T \cdot \tilde{N}$, the diagonalisation

$$\begin{aligned} N^* D' N^{-1} &= T^* (\tilde{N}^* Y \tilde{N}^{-1}) T^{-1} = N^* Y N^{-1} \\ &=: D = \text{diag}(m_{\tilde{\chi}_1^0}, m_{\tilde{\chi}_2^0}, m_{\tilde{\chi}_3^0}, m_{\tilde{\chi}_4^0}) \end{aligned} \tag{3.24}$$

yields $m_{\tilde{\chi}_i^0} \geq 0 \; \forall i = 1, .., 4$. Using $\chi_i^0 = N_{ij}\psi_j^0$, the neutralino part in the Lagrangian can be expressed in the mass eigenbasis:

$$\mathscr{L}_{\chi_0} = \frac{1}{2}\overline{\tilde{\chi}_i^0}[\not{p}\delta_{ij} - \omega_L(N^* Y N^\dagger)_{ij} - \omega_R(N Y^\dagger N^T)_{ij}]\tilde{\chi}_j^0. \tag{3.25}$$

3.4.3. The gluino sector

The 8 coloured gluinos $\tilde{g}$ ($s = \frac{1}{2}$) are the fermionic superpartner of the gluons. Unlike their massless SM partners, they have a mass of $m_{\tilde{g}} = |M_3|$ where $M_3 = |M_3| e^{i\phi_{M_3}}$ is the possibly complex gluino parameter. The gluino mass term in the tree-level Lagrangian is

$$\mathscr{L}_{\tilde{g}} = -\frac{1}{2}\overline{\tilde{g}} M_3 \tilde{g}. \tag{3.26}$$

3.4.4. The sfermion sector

Neglecting flavour mixing, sfermions $\tilde{f}_L, \tilde{f}_R$ with the same $SU(3)_C \otimes U(1)_{em}$ quantum numbers can still mix within one generation to form the mass eigenstates $\tilde{f}_1, \tilde{f}_2$. This is parametrised by the matrix

$$M_{\tilde{f}} = \begin{pmatrix} M_{\tilde{f}_L}^2 + m_f^2 + M_Z^2 \cos 2\beta (I_3^f - Q_f s_W^2) & m_f X_f^* \\ m_f X_f & M_{\tilde{f}_R}^2 + m_f^2 + M_Z^2 \cos 2\beta Q_f s_W^2 \end{pmatrix}, \tag{3.27}$$

$$X_f := A_f - \mu^* \cdot \begin{cases} \cot\beta, & f = u, c, t & \text{(up-type)} \\ \tan\beta, & f = d, s, b; e, \mu, \tau & \text{(down-type)} \end{cases}. \tag{3.28}$$

The trilinear couplings $A_f = |A_f|e^{i\phi_{A_f}}$, as well as $\mu = |\mu|e^{i\phi_\mu}$, can be complex. These phases enter the Higgs sector via sfermion loops.

SUSY is softly broken by the real parameters $M_{\tilde{f}_L}$ and $M_{\tilde{f}_R}$, which respect $M_{\tilde{q}_{u,L}} = M_{\tilde{q}_{d,L}}$. The sfermion masses are obtained by diagonalising $M_{\tilde{f}}$ for all $\tilde{f}$ separately. For the first two generations, the sfermion masses exceed the masses of their SM partners so that the hierarchy of the matrix elements in Eq. (3.27) is approximately diagonal. However, in the case of the stop and, for sufficiently high $\tan\beta$, also sbottom, the mixing can be rather large.

3.5. Discussion of parameters

While the SM contains 'only' 19 free parameters, most of which lie in the flavour sector, the MSSM with complex parameters confronts us with additional 105 parameters, most of which model our lack of knowledge by which mechanism SUSY is broken. $\mathcal{CP}$-violation enters through 14 complex phases, but 2 unphysical ones (ϕ_{M_2}, the phase of the wino parameter M_2, and ϕ_b, the phase of the soft breaking parameter b) can be rotated away. Hence 12 phases remain, although limited by experiment. Assuming minimal flavour violation [60], that is, the only source of mixing between generations comes from the CKM matrix as in the SM, we are left with 41 parameters on top of the SM ones: $\tan\beta$ in the Higgs sector, the masses $|M_1|, |M_2|, |M_3|, |\mu|$ and phases $\phi_{M_1}, \phi_{M_3}, \phi_\mu$ in the neutralino/chargino sector and the masses $M_{\tilde{l}_R}, M_{\tilde{q}_{uR}}, M_{\tilde{q}_{dR}}; M_{\tilde{l}_L}, M_{\tilde{q}_L}$ and trilinear couplings $|A_f|, \phi_{A_f}$ of the fermions. In addition, a Higgs boson mass must be specified. For the general MSSM including complex phases it is convenient to choose $M_{H^\pm}$ as the input mass because even with $\mathcal{CP}$-violation the charged Higgs bosons do not mix. In the $\mathcal{CP}$-conserving case, m_A can be chosen equally well.

In order to enable comparison of experimental searches to theoretical predictions, several benchmark points and parameter lines in the high-dimensional parameter space of the unconstrained MSSM were specified and are referred to as the 'Snow-

mass Points and Slopes (SPS)' [61]. They were chosen according to certain SUSY breaking mechanisms.

One particularly popular model is the constrained MSSM (CMSSM) [62]. It is based on the underlying assumption of universality not only of all gaugino masses $M_i = m_{1/2}$, $i = 1, 2, 3$, but also of the scalar masses m_0, i.e. of all sfermions and Higgs doublets, and of the trilinear couplings $A_i = A_0$. Apart from these three quantities, which are defined at the GUT scale, two additional free parameters are left: $\tan\beta$ and μ at the electroweak scale. All parameters are assumed to be real. They are extrapolated from the scale of their definition to a variable energy scale by means of RGE running.

Limits on sparticle masses are often presented in the $m_0 - m_{1/2}$ plane. Current results from ATLAS and CMS in various search channels and constraints can be found in [63, 64].

4. Higher-order corrections in the MSSM

The Lagrangian contains free parameters which are not predicted by theory, but need to be determined from the experimental measurements of equally many observables. In order to compare theoretical predictions and experimental measurements or to set limits on observables or parameters in the case of the non-observation of a predicted signal, a high precision of the physical quantities is demanded. From the theoretical side, this requires calculations beyond tree level in many processes because the contributions from higher orders in perturbation theory are not necessarily negligible. Higher order effects exist as real corrections by radiation off an external particle or as virtual corrections in a loop. In this thesis only virtual corrections are considered.

However, technical problems arise because the momentum in a loop is not constrained so that it has to be integrated over from $-\infty$ to $+\infty$, potentially leading to divergent integrals. This type of divergence is known as ultraviolet (UV) divergence. In contrast, infrared divergences can arise in real and in virtual corrections.

The two-step procedure of regularisation and renormalisation consistently treats the infinities to render all physical observables finite. This may be performed in various schemes some of which are presented in the following sections [65, 66]. The subsequent sections of this chapter deal with the renormalisation of the Higgs and the neutralino sector in the MSSM in a hybrid on-shell/ $\overline{\text{DR}}$-scheme. Later on, in Chap. 10, this scheme is applied to a process involving Higgs bosons and neutralinos.

4.1. Regularisation and renormalisation

4.1.1. SM: DREG and $\overline{\text{MS}}$ vs. on-shell renormalisation

The general approach is to isolate well-defined divergences from the finite part of bare parameters and fields in the framework of regularisation. The divergences are cancelled by so-called counterterms which are fixed by renormalisation conditions so that the remaining physical parameters and fields become finite.

There exist several regularisation schemes. Broadly applied in the SM is Dimensional Regularisation (DREG) [67] in which momenta and Lorentz covariants are extended from 4 to $D = 4 - 2\epsilon$ dimensions. Yet, there is no well-defined generalisation of γ_5 in

arbitrary D dimensions. The concept of DREG is that divergent integrals in $D = 4$ become finite in $D < 4$ with the replacement $\int \frac{\mathrm{d}^4 q}{(2\pi)^4} \to \mu^{4-D} \int \frac{\mathrm{d}^D q}{(2\pi)^D}$, where the arbitrary mass scale (the renormalisation scale) μ is introduced to preserve the mass dimension of the expression. The UV and IR singularities manifest themselves as $\frac{1}{\epsilon}$-poles. DREG has the benefit of regularising UV and IR divergences simultaneously and preserving both Lorentz and gauge invariance. As mentioned above, we consider only UV divergences here. An alternative regularisation is, for example, a cut-off

$$\int \frac{\mathrm{d}^4 q}{(2\pi)^4} \to \int^\Lambda \frac{\mathrm{d}^4 q}{(2\pi)^4},$$

with a cut-off scale Λ.

Renormalisation removes divergences by a redefinition of the physical meaning of parameters and fields in the Lagrangian order by order in perturbation theory. A counterterm is assigned to each divergent ('bare') parameter a and field ϕ by an additive or multiplicative prescription, where a hat denotes a renormalised, i.e., finite quantity

$$a = Z_a \hat{a} = \hat{a} + \delta a \tag{4.1}$$

$$\phi = \sqrt{Z_\phi} \hat{\phi} = \left(1 + \frac{1}{2} \delta Z_\phi\right) \hat{\phi}. \tag{4.2}$$

Then the Lagrangian can be split into two parts,

$$\mathscr{L} = \mathscr{L}_0 + \delta\mathscr{L}, \tag{4.3}$$

where $\mathscr{L}_0$ has the same functional form as $\mathscr{L}$, but it depends on the bare fields and parameters, and $\delta\mathscr{L}$ contains the counterterms. The set of Feynman rules is extended to the existing rules with renormalised parameters plus new rules for counterterm vertices.

The divergent parts of the bare parameters or fields and their counterterms cancel exactly to render the renormalised quantities and physical observables finite. After the renormalisation has been carried out, the limit of removing the regularisation is taken (e.g. $\epsilon \to 0$ in DREG or $\Lambda \to \infty$ in the cut-off regularisation scheme), yielding infinite bare quantities and renormalisation constants $\delta a, \delta Z_\phi$.

While the coefficients in front of the divergences are unambiguous, the definition of the finite parts of the counterterms is not unique. It depends on the chosen renormalisation scheme. Physical results are independent of the scheme and the renormalisation scale only if all orders of perturbation theory are included. Yet, in a truncated series the remnant dependence on the renormalisation prescription is of the order of the higher uncalculated orders [68].

Among the most commonly used schemes, there are the *(modified) minimal sub-*

traction (MS/$\overline{\text{MS}}$) and the *on-shell scheme*. While the MS scheme, used in connection with DREG, only absorbs the term proportional to the divergence $\frac{1}{\epsilon}$ into the counterterm, the $\overline{\text{MS}}$ scheme subtracts also finite constants for convenience because $\frac{1}{\epsilon} - \gamma_E + \ln(4\pi)$ always appears as a combination, where γ_E is the Euler constant. The on-shell scheme, on the other hand, fixes the mass counterterms through a condition that identifies the renormalised ('physical') mass with the pole of the propagator. So a different physical meaning and a different numerical value is attributed to the mass in the on-shell or $\overline{\text{MS}}$-scheme. When comparing experiment to theory, one has to keep in mind which mass definition is referred to.
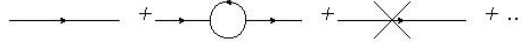
Figure 4.1.: Scalar propagator at one-loop order: the tree-level propagator, a loop whose inverse gives rise to a self-energy, and the counterterm. The ellipsis represents contributions from higher orders.

Masses and width As an example, Fig. 4.1 shows the scalar propagator at one-loop order. It is the inverse of the irreducible vertex function. The tree-level scalar propagator receives corrections from the self-energy loop diagram and the counterterm. The correction of the mass at the loop-level due to self-energy contributions is cancelled by the counterterm so that the position of the physical pole is not altered. The complex pole of the propagator is located at the solution of

$$p^2 - m^2 + \text{Re}\Sigma(p^2) - \delta m^2 = 0. \tag{4.4}$$

The renormalised self-energy $\hat{\Sigma}$ is decomposed in terms of the unrenormalised self-energy Σ and the mass and field counterterms as

$$\hat{\Sigma}(p^2) = \Sigma(p^2) - \delta m^2 + (p^2 - \mathcal{M}^2)\delta Z, \tag{4.5}$$

where δZ is the field renormalisation constant. The mass counterterm δm^2 is fixed by the on-shell renormalisation condition that the renormalised self energy evaluated at the pole mass must vanish, $\hat{\Sigma}(p^2 = \mathcal{M}^2) = 0$. Thus in the on-shell renormalisation scheme, the mass counterterm is obtained from the bare self-energy Σ, evaluated on the complex mass shell $p^2 = \mathcal{M}^2$,

$$\delta m^2 = \text{Re}\Sigma(p^2 = \mathcal{M}^2). \tag{4.6}$$

The physical mass square M^2 is identified as the real part of the complex pole $\mathcal{M}^2 = M^2 - iM\Gamma$. Evaluating Eq. (4.4) at $\mathcal{M}^2$

$$\mathcal{M}^2 - m^2 + \hat{\Sigma}(\mathcal{M}^2) = M^2 - iM\Gamma - m^2 + \text{Re}\hat{\Sigma}(\mathcal{M}^2) + i\text{Im}\hat{\Sigma}(\mathcal{M}^2) = 0, \tag{4.7}$$

one obtains the width Γ, which is a result of the summation of self-energy diagrams from all orders, from the imaginary part of the renormalised self energy at the complex pole,

$$\Gamma = \frac{1}{M}\text{Im}\hat{\Sigma}(\mathcal{M}^2). \tag{4.8}$$

Expanding the renormalised self-energy about the pole and requiring a unity residue of the renormalised propagator fixes the field renormalisation

$$\delta Z = -\frac{\partial \Sigma(p^2)}{\partial p^2}\big|_{p^2=\mathcal{M}^2}. \tag{4.9}$$

In case of fermionic instead of scalar propagators, the self-energy is split into a vector, axial vector, scalar and pseudoscalar part. This is relevant, for example, in the neutralino renormalisation discussed in Sect. 4.3. Gauge boson self-energies have a transverse (T) and longitudinal (L) part.

Renormalisation of the SM   In renormalisable theories, a finite number of counterterms is sufficient to cancel all divergences. In 1972, 't Hooft proved that gauge theories containing spontaneous symmetry breaking - such as the SM - are renormalisable to all orders of perturbation theory [67, 69].
In the on-shell scheme following Ref. [70], the electric charge e is renormalised in the Thomson limit, i.e., the renormalisation constant δZ_e is fixed by the requirement that it coincides with the $ee\gamma$ coupling in the case of on-shell external particles and for vanishing photon momentum in the transverse self-energy $\Sigma^T_{\gamma Z}$ and in the photon vacuum polarisation $\Pi_\gamma(0) = \frac{\partial \Sigma_{\gamma\gamma(k^2)}}{\partial k^2}\big|_{k^2=0}$:

$$\delta Z_e = \frac{1}{2}\Pi_\gamma(0) + \frac{s_W}{c_W}\frac{\text{Re}\Sigma^T_{\gamma Z}(0)}{M_Z^2}. \tag{4.10}$$

From the very precise experimental input of the measured electromagnetic coupling constant α_{em} [20],

$$\alpha_{em}(0) = 1/137.0359895 = \frac{e(0)^2}{4\pi}, \tag{4.11}$$

it can be extrapolated to M_Z by $\alpha(M_Z^2) = \frac{\alpha(0)}{1-\Delta\alpha}$. The shift

$$\Delta\alpha = \Delta\alpha_{lep} + \Delta\alpha^{(5)}_{had} = -\left(\text{Re}\hat{\Pi}^{lep}_\gamma(M_Z^2) + \text{Re}\hat{\Pi}^{had,5}_\gamma(M_Z^2)\right) \tag{4.12}$$

has a leptonic and a hadronic contribution (considering only the five lightest quarks) to the photon vacuum polarisation Π_γ. The renormalised vacuum polarisation eval-

uated at M_Z^2 is related to $\Pi_\gamma(0)$ by the photon self-energy,

$$\mathrm{Re}\hat{\Pi}_\gamma(M_Z^2) = \frac{\mathrm{Re}\Sigma_{\gamma\gamma}(M_Z^2)}{M_Z^2} - \Pi_\gamma(0). \tag{4.13}$$

While $\Delta\alpha_{lep}$ has been calculated in Ref. [71], $\Delta\alpha_{had}^{(5)}$ had to be determined from measurements [72]. The renormalisation constant δZ_e can then be expressed in terms of $\Delta\alpha$ instead of logarithms of the fermion masses in the vacuum polarisation (see Ref. [70]) by defining $\Pi_\gamma(0)^{heavy}$ as the photon vacuum polarisation restricted to exclusively heavy particles in the loops. This means that leptons and the five light quark flavours are not allowed, and by absorbing large logarithms from $\alpha(M_Z^2)$ at 1-loop order into the tree-level expression. The final result

$$\delta Z_e^{(M_Z^2)} = \delta Z_e - \frac{\Delta\alpha_{lep} + \Delta\alpha_{had}^{(5)}}{2} = \frac{1}{2}\Pi_\gamma(0)^{heavy} + \frac{s_W}{c_W}\frac{\mathrm{Re}\Sigma_{\gamma Z}^T(0)}{M_Z^2} + \frac{1}{2}\mathrm{Re}\Pi_\gamma(M_Z^2)^{light}. \tag{4.14}$$

An alternative approach is to define the quark masses as effective parameters in order to achieve an equivalent numerical value of $\Pi_\gamma(0)$. This is the standard in `FormCalc` (see Chap. 5). But we pursued the approach with $\Delta\alpha$ as input according to Ref. [70].

The counterterms of the following SM masses, the electric charge and the CKM-matrix,

$$\begin{aligned}
M_Z^2 &\to M_Z^2 + \delta M_Z^2, & M_W^2 &\to M_W^2 + \delta M_W^2, \\
M_H^2 &\to M_H^2 + \delta M_H^2, & m_{f_i}^2 &\to m_{f_i}^2 + \delta m_{f_i}^2, \\
e &\to (1 + \delta Z_e)e, & V_{ij} &\to V_{ij} + \delta V_{ij},
\end{aligned} \tag{4.15}$$

are sufficient to render all S-matrix elements finite, but for finite Green's functions the field renormalisation constants are also needed,

$$W^\pm \to \left(1 + \frac{1}{2}\delta Z_{WW}\right)W^\pm, \tag{4.16}$$

$$V_i^0 \to \left(\delta_{ij} + \frac{1}{2}\delta Z_{ij}\right)V_j^0, \ V_1^0 \equiv Z, \ V_2^0 \equiv \gamma, \tag{4.17}$$

$$H \to \left(1 + \frac{1}{2}\delta Z_H\right)H, \tag{4.18}$$

$$f_i^{L/R} \to \left(\delta_{ij} + \frac{1}{2}\delta Z_{ij}^{L/R}\right). \tag{4.19}$$

Parameters $P = \prod P_i$, consisting of the product of parameters P_i which have to be renormalised, receive a 1-loop counterterm in the form of $\delta P = \sum \frac{\delta P_i}{P_i} \cdot P$. Thus, the counterterms of parameters that depend on those listed in Eq. (4.15) can be

expressed in terms of the above counterterms, such as the gauge boson mass squares

$$\delta M_W = \frac{\delta M_W^2}{2M_W}, \quad \delta M_Z = \frac{\delta M_Z^2}{2M_Z}. \tag{4.20}$$

With $c_W = \frac{M_W}{M_Z}$, the corresponding counterterm is expressed as

$$\delta c_W = c_W \left(\frac{\delta M_W}{M_W} - \frac{\delta M_Z}{M_Z} \right) = \frac{c_W}{2} \left(\frac{\delta M_W^2}{M_W^2} - \frac{\delta M_Z^2}{M_Z^2} \right). \tag{4.21}$$

Likewise, for $s_W^2 = 1 - c_W^2$, the counterterm reads

$$\delta s_W^2 = -\delta c_W^2 = -2c_W \delta c_W = 2s_W \delta s_W, \tag{4.22}$$

and finally

$$\delta s_W = -\frac{c_W}{s_W} \delta c_W = \frac{c_W^2}{2s_W} \left(\frac{\delta M_Z^2}{M_Z^2} - \frac{\delta M_W^2}{M_W^2} \right). \tag{4.23}$$

As one example, we give the mass and field renormalisation constants of the W-boson and the Z-boson:

$$\delta M_W^2 = \mathrm{Re}\Sigma_T^W(M_W^2), \quad \delta Z_W = -\frac{\partial \Sigma_T^W(p^2)}{\partial p^2}\big|_{p^2=M_W^2}. \tag{4.24}$$

More details on the on-shell renormalisation of SM parameters and fields can be found in Refs. [6, 73].

4.1.2. MSSM: DRED and $\overline{\text{DR}}$ vs. on-shell renormalisation

Despite the appealing benefits of DREG described in Sect. 4.1.1, this regularisation leads to a mismatch of bosonic and fermionic degrees of freedom and breaks supersymmetry [74] so that SUSY restoring counterterms need to be introduced. Instead, it is replaced in the MSSM by the scheme of *dimensional reduction (DRED)* [75–77]. Here, space-time, momenta and momentum integrals are dealt with in $D = 4 - 2\epsilon$ dimensions, whereas fields and γ-matrices remain in 4 dimensions. It has been confirmed to be mathematically well-defined and SUSY preserving [78].

Instead of introducing counterterms, the scheme of *constrained differential renormalisation (CDR)* [79] renders Green functions already finite. Divergent expressions are written as derivatives of finite functions in coordinate space. Finally, they are transformed back to momentum space. This enables a direct identification with the scalar and tensor one-loop integrals (see Sect. 10). At one loop-level, CDR has been shown to be equivalent to DRED [80].

4.2. Renormalisation of the Higgs sector

Radiative corrections in the Higgs sector turn out to be substantial. The tree-level mass of the lightest MSSM Higgs boson in Eq. (3.13) is bounded from above by M_Z, which was excluded by LEP, albeit only for $\mathcal{CP}$-conserving MSSM benchmark scenarios. Yet, large loop corrections shift this bound by roughly $40\,\text{GeV}$ [51–55]. The other Higgs masses are also subject to loop corrections. Even in the case of $\mathcal{CP}$-conservation, mixing self-energy diagrams contribute, but there are more combinations if $\mathcal{CP}$-violating mixings allowed in the MSSM with complex parameters. While we renormalise the gauge and (s)fermion sector based on the masses in an on-shell scheme, the renormalisation of the Higgs sector for the parameter $\tan\beta$ and the fields is done separately in a hybrid on-shell/ $\overline{\text{DR}}$-scheme, following Ref. [81].

4.2.1. Field renormalisation

Finite Higgs self-energies for the general case of the full momentum-dependence require a renormalisation of the Higgs fields. Each of the two Higgs doublets is given a field renormalisation constant, $\delta Z_{\mathcal{H}_i}$, with the renormalisation transformation

$$\mathcal{H}_i \to (1 + \frac{1}{2}\delta Z_{\mathcal{H}_i})\mathcal{H}_i, \quad i = 1, 2. \tag{4.25}$$

The renormalisation constants of the first and the second doublet are related to the divergent parts of the derivatives of the diagonal self-energies of H and h, respectively,

$$\delta Z_{\mathcal{H}_1}^{\overline{DR}} = -\text{Re}\left[\Sigma_{HH}^{'(div)}(m_H^2)\right]_{\alpha=0} \tag{4.26}$$

$$\delta Z_{\mathcal{H}_2}^{\overline{DR}} = -\text{Re}\left[\Sigma_{hh}^{'(div)}(m_h^2)\right]_{\alpha=0}. \tag{4.27}$$

The self-energies depend on the mixing angle α. However, for a separate renormalisation of the two Higgs doublets the mixing is switched off by setting α to zero in the evaluation of the derivatives of the self-energies. Explicit expressions for the restriction that only (s)quarks of the third generation contribute in loops to the self-energies are given in Chap. 10. The neutral fields in the mass eigenstate basis $\{h_i\} = \{h, H, A, G\}$ are renormalised as

$$h_j \to h_j + \delta Z_{h_j} = h_j + \frac{1}{2}\sum_{h_i} \delta Z_{h_j h_i} h_i. \tag{4.28}$$

Since the Higgs potential is $\mathcal{CP}$-conserving at lowest order, the $\mathcal{CP}$-violating self-energies vanish,

$$\delta Z_{hA} = \delta Z_{hG} = \delta Z_{HA} = \delta Z_{HG} = 0. \tag{4.29}$$

This results in the following relation between the renormalisation constants of the doublets and the mass eigenstates:

$$\frac{1}{2}\begin{pmatrix} -s_\alpha & c_\alpha \\ c_\alpha & s_\alpha \end{pmatrix}\begin{pmatrix} \phi_1\,\delta Z_{\mathcal{H}_1} \\ \phi_2\,\delta Z_{\mathcal{H}_2} \end{pmatrix} = \begin{pmatrix} \delta Z_h \\ \delta Z_H \end{pmatrix} \overset{(4.28)}{=} \begin{pmatrix} \frac{1}{2}(\delta Z_{hh}h + \delta Z_{hH}H) \\ \frac{1}{2}(\delta Z_{Hh}h + \delta Z_{HH}H) \end{pmatrix}, \qquad (4.30)$$

$$\frac{1}{2}\begin{pmatrix} -s_\beta & c_\beta \\ c_\beta & s_\beta \end{pmatrix}\begin{pmatrix} \chi_1\,\delta Z_{\mathcal{H}_1} \\ \chi_2\,\delta Z_{\mathcal{H}_2} \end{pmatrix} = \begin{pmatrix} \delta Z_A \\ \delta Z_G \end{pmatrix} \overset{(4.28)}{=} \begin{pmatrix} \frac{1}{2}(\delta Z_{AA}A + \delta Z_{AG}G) \\ \frac{1}{2}(\delta Z_{GA}A + \delta Z_{GG}G) \end{pmatrix}. \qquad (4.31)$$

From Eq. (4.30) we can derive the renormalisation constants of the neutral $\mathcal{CP}$-even fields,

$$\delta Z_h = \frac{1}{2}[-s_\alpha(-s_\alpha h + c_\alpha H)\delta Z_{\mathcal{H}_1} + c_\alpha(c_\alpha h + s_\alpha H)\delta Z_{\mathcal{H}_2}]$$
$$= \frac{1}{2}[\underbrace{(s_\alpha^2 \delta Z_{\mathcal{H}_1} + c_\alpha^2 \delta Z_{\mathcal{H}_2})}_{=\delta Z_{hH}} h + \underbrace{s_\alpha c_\alpha(\delta Z_{\mathcal{H}_2} - \delta Z_{\mathcal{H}_1})}_{=\delta Z_{hH}} H]. \qquad (4.32)$$

Proceeding analogously for $\delta Z_H, \delta Z_A$ and δZ_G and for the charged Higgs bosons $H^\pm, G^\pm$ we obtain

$$\delta Z_{hh} = s_\alpha^2 \delta Z_{\mathcal{H}_1} + c_\alpha^2 \delta Z_{\mathcal{H}_2}, \qquad \delta Z_{AA} \;=\; \delta Z_{H^-H^+} = s_\beta^2 \delta Z_{\mathcal{H}_1} + c_\beta^2 \delta Z_{\mathcal{H}_2} \qquad (4.33)$$

$$\delta Z_{hH} = s_\alpha c_\alpha(\delta Z_{\mathcal{H}_2} - \delta Z_{\mathcal{H}_1}), \qquad \delta Z_{AG} \;=\; \delta Z_{H^\pm G^\mp} = s_\beta c_\beta(\delta Z_{\mathcal{H}_2} - \delta Z_{\mathcal{H}_1}) \qquad (4.34)$$

$$\delta Z_{HH} = c_\alpha^2 \delta Z_{\mathcal{H}_1} + s_\alpha^2 \delta Z_{\mathcal{H}_2}, \qquad \delta Z_{GG} \;=\; \delta Z_{G^-G^+} = c_\beta^2 \delta Z_{\mathcal{H}_1} + s_\beta^2 \delta Z_{\mathcal{H}_2}. \qquad (4.35)$$

4.2.2. Renormalisation of $\tan\beta$

The $\overline{\text{DR}}$-scheme is adopted for the renormalisation of $t_\beta \equiv \tan\beta$ because this parameter - although it is an important input for most scenarios, theoretical predictions and experimental searches - is not directly related to an observable like a mass which could be defined on-shell. In choosing a renormalisation scheme, one has to balance gauge invariance, process independence and numerical stability [82]. Although the $\overline{\text{DR}}$-scheme is not fully gauge independent, gauge independence holds for the class of R_ξ-gauges at the one-loop level. Furthermore, it does not refer to any specific process, is technically convenient and numerically stable [83]. Other schemes may feature instabilities at thresholds where a kink in the self-energy leads to a discontinuity of its derivative.

As in Ref. [81], the parameter $\tan\beta$ receives a counterterm according to the transformation

$$\tan\beta \rightarrow \tan\beta(1 + \delta\tan\beta). \qquad (4.36)$$

In the $\overline{\text{DR}}$-scheme, which is applied in the Higgs sector, the counterterm for $\tan\beta$ reads

$$\delta\tan\beta^{\overline{DR}} = \frac{1}{2}(\delta Z_{\mathcal{H}_2}^{\overline{DR}} - \delta Z_{\mathcal{H}_1}^{\overline{DR}}). \qquad (4.37)$$

Treating $\tan\beta$ as one of the two independent input parameters of the Higgs sector, we express the counterterms of $\sin\beta$ and $\cos\beta$ in terms of $\delta\tan\beta$:

$$\delta s_\beta = s_\beta c_\beta^2 \delta t_\beta, \qquad\qquad \delta c_\beta = -c_\beta s_\beta^2 \delta t_\beta. \qquad (4.38)$$

The parameters β_n, β_c and α from Eqs. (3.11, 3.12), however, are simply mixing angles and hence not renormalised. The mixing angles β_n, β_c coincide with the β from the ratio of Higgs vevs only at tree level.

4.2.3. Higgs masses and mixing at higher order

Masses   For the self-energies and mass counterterms we refer to Ref. [81]. They are fixed by the on-shell condition for $M_{H^\pm}^2$,

$$\mathrm{Re}\hat{\Sigma}_{H^+H^-}(M_{H^\pm}^2) = 0. \qquad (4.39)$$

The program `FeynHiggs` [56, 81, 84–86] (see Sect. 5.2) calculates, among others, the Higgs masses at full one-loop order and incorporates leading two-loop terms. Dominant contributions are the loops containing (s)tops and (s)bottoms. One example of the impact of two-loop corrections and the M_{H^+}-dependence of M_h, M_H and M_A is shown in Fig. 4.2. While m_h is constant and much lower than m_H and m_A at tree-level, it increases if loop-corrections are included, and it reaches its maximum for higher $M_{H^\pm}$.
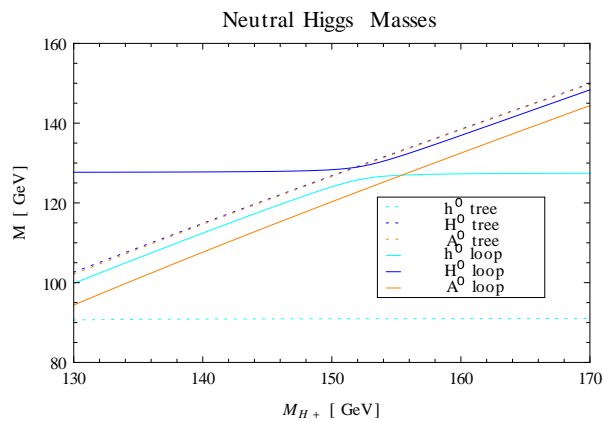
Figure 4.2.: Higgs masses at tree-level and at 2-loop order with $\tan\beta = 40$ and variable M_{H^+} in a m_h^{max}-like scenario, calculated with `FeynHiggs`.

For lower values of the input mass $M_{H^\pm}$, the loop-corrected masses M_h and M_A are similar and the lightest Higgs boson couples SM-like, whereas at higher $M_{H^\pm}$ the heavier Higgs bosons H, A are nearly mass-degenerate and H is the SM-like Higgs boson. This cross-over effect is induced by a strong change in the Higgs boson mixing matrix parametrised by α (see Eq. (3.11)) and in the $\hat{\mathbf{Z}}$-factors (see Eq. (4.48)). The

higher $\tan\beta$ is, the smaller is the mass difference $M_H - M_h$ at the cross-over point. This is relevant for the numerical analysis in Chaps. 9 and 10.

Mixing In principle, all neutral bosons h, H, A, G, Z and γ mix, which is accounted for by a propagator mixing matrix, albeit here in a 3×3 approximation for the neutral Higgs bosons h, H, A. However, the mixing of the neutral Higgs bosons with $G, Z\,\gamma$ only has a sub-leading two-loop impact on the calculation of the Higgs masses. So it is not inconsistent to neglect that mixing because other two-loop effects are not yet contained in `FeynHiggs` either. Tree level masses are denoted by m and loop-corrected ones by M. The propagator matrix is expressed in terms of the inverse irreducible vertex function,

$$\Delta_{hHA}(p^2) = -\left(\hat{\Gamma}_{hHA}(p^2)\right)^{-1},\tag{4.40}$$

with

$$\left[\hat{\Gamma}_{hHA}(p^2)\right]_{ij} = i[(p^2 - m_{h_i}^2)\delta_{ij} + \hat{\Sigma}_{h_i h_j}(p^2)] = i[p^2\mathbb{1} - M_0(p^2)]_{ij}.\tag{4.41}$$

The mass matrix of the three neutral Higgs bosons, $\mathbf{M}_n(p^2)$, is constructed from tree-level masses, diagonal and mixing self-energies,

$$\mathbf{M}_n(p^2) = \begin{pmatrix} m_h^2 - \hat{\Sigma}_{hh}(p^2) & -\hat{\Sigma}_{hH}(p^2) & -\hat{\Sigma}_{hA}(p^2) \\ -\hat{\Sigma}_{hH}(p^2) & m_H^2 - \hat{\Sigma}_{HH}(p^2) & -\hat{\Sigma}_{HA}(p^2) \\ -\hat{\Sigma}_{hA}(p^2) & -\hat{\Sigma}_{HA}(p^2) & m_A^2 - \hat{\Sigma}_{HA}(p^2) \end{pmatrix}.\tag{4.42}$$

Mixing contributions, in addition to the usual diagonal self-energy, are absorbed into the effective self-energy $\hat{\Sigma}_{ii}^{eff}(p^2)$ which replaces the usual self-energy in the denominator of the propagator. The physical masses are obtained as the real part of the complex pole $\mathcal{M}_i^2$ solving

$$\mathcal{M}_i^2 - m_i^2 + \hat{\Sigma}_{ii}^{eff}(\mathcal{M}_i^2) = 0 \ \text{ with } \mathcal{M}_i^2 = M_i^2 - iM_i\Gamma_i.\tag{4.43}$$

Z-factors Mixing does not only occur in propagators, but also between external Higgs bosons. In an on-shell scheme, all external particles do not mix on their mass shell by definition. On account of the hybrid on-shell/ $\overline{\text{DR}}$-scheme, though, finite normalisation factors $\hat{\mathbf{Z}}_{ij}$ come along for the sake of correct on-shell properties and

a properly normalised S-matrix. They are given in [81] by

$$\hat{Z}_{ij} = -\frac{\hat{\Sigma}_{ij}(M_i^2)}{M_i^2 - m_j^2 + \hat{\Sigma}_{jj}(M_i^2)} \tag{4.44}$$

$$\hat{Z}_i = \frac{1}{1 + \left(\hat{\Sigma}_{ii}^{eff}\right)'(M_i^2)}. \tag{4.45}$$

This helps to approximate the effective self-energy and the diagonal propagator close to the complex pole, $p^2 \approx \mathcal{M}_i^2$,

$$\hat{\Sigma}_{ii}^{eff}(p^2) = \hat{\Sigma}_{ii}^{eff}(\mathcal{M}_i^2) + \frac{\partial \hat{\Sigma}_{ii}^{eff}(p^2)}{\partial p^2}|_{p^2=\mathcal{M}_i^2}(p^2 - \mathcal{M}_i^2) + \mathcal{O}\{(p^2 - \mathcal{M}_i^2)^2\}. \tag{4.46}$$

This expansion and the definition of the Z_i-factor is used to obtain for the diagonal propagator near the complex pole

$$\Delta_{ii}(p^2) = \frac{i}{p^2 - m_i^2 + \hat{\Sigma}_{ii}^{eff}(p^2)} \stackrel{(4.43)}{=} \frac{i}{(p^2 - \mathcal{M}_i^2) \cdot \left[1 + \left(\hat{\Sigma}_{ii}^{eff}\right)'(\mathcal{M}_i^2)\right]}$$

$$\stackrel{(4.43, 4.45)}{=} \frac{i}{p^2 - M_i^2 + iM_i\Gamma_i}\hat{Z}_i = \Delta_i^{BW}(p^2)\hat{Z}_i. \tag{4.47}$$

So the propagator can be approximated around the pole by a Breit-Wigner propagator times a normalisation factor [70]. Furthermore, vertices involving external Higgs bosons are correctly normalised by a combination of Z-factors,

$$\hat{\Gamma}_{h_i} = \sum_{\alpha=h,H,A} \sqrt{\hat{Z}_i}\,\hat{Z}_{i\alpha}\,\hat{\Gamma}_{h_\alpha} = \sum_{\alpha=h,H,A} \hat{\mathbf{Z}}_{i\alpha}\,\hat{\Gamma}_{h_\alpha}, \tag{4.48}$$

$$\hat{\mathbf{Z}}_{i\alpha} := \sqrt{\hat{Z}_i}\,\hat{Z}_{i\alpha} \text{ and } \hat{Z}_{ii} = 1, \tag{4.49}$$

where $\alpha = 1, 2, 3$ labels the unmixed and $i = 1, 2, 3$ the mixed states of h, H, A. In a $\mathcal{CP}$-conserving scenario, however, this mixing is reduced to a 2×2 mixing between h and H.

Internal Higgs bosons mix via a unitary matrix U which diagonalises the matrix $\text{Re}[\mathbf{M}_n(p^2 \text{ on-shell})]$ [81]. U can even be chosen real and it can quantify the amount of $\mathcal{CP}$-violation in the Higgs mixing. In contrast, Z is not unitary and in general complex. Strictly speaking, it can therefore not be considered a rotation matrix. But in the approximation of $p^2 = 0$, the matrix $\hat{\mathbf{Z}}_{i\alpha}$ from Eq. (4.49) becomes a unitary rotation matrix.

4.3. Renormalisation of the neutralino sector

The renormalisation of the neutralino-chargino sector at the 1-loop level has been studied in the literature for real parameters, for instance in Refs. [87–90]. The general case of complex parameters with on-shell renormalisation conditions was developed in Refs. [70, 91, 92].

We have re-derived those formulae in this thesis and found agreement with the final results. In this section and in Appendix A, we calculate the neutralino field renormalisation constants in detail and give the counterterms of the parameters of the chargino-neutralino sector and the loop-corrected neutralino masses.

We implemented this on-shell scheme into the MSSM model file of `FeynArts` (see Chap. 5) which contains only MSSM tree-level vertices and SM counterterms in the distributed version. Although we apply the general complex scheme only to a special case of real parameters in this thesis (see Chap. 10), we have already derived and coded the counterterms of the complex neutralino sector for future applications involving complex parameters to allow for $\mathcal{CP}$-violation.

4.3.1. Counterterms for the parameters in the neutralino and chargino mixing matrices and for the neutralino fields

Parameter renormalisation Each element of the chargino and neutralino mixing matrices X and Y as defined in Eqs. (3.20, 3.22), containing the parameters M_1, M_2, μ, β, is renormalised upon the parameter renormalisation. The renormalisation of $\tan\beta$ is discussed in Sect. 4.2.2. Besides, renormalisation in the neutralino and chargino sector requires the counterterms

$$M_i \rightarrow M_i + \delta M_i, \quad i = 1, 2 \tag{4.50}$$

$$\mu \rightarrow \mu + \delta\mu. \tag{4.51}$$

The counterterms of the following matrix elements coincide with these parameters:

$$\delta Y_{11} = \delta M_1 \tag{4.52}$$

$$\delta X_{11} = \delta Y_{22} = \delta M_2 \tag{4.53}$$

$$\delta X_{22} = -\delta Y_{34} = -\delta Y_{43} = \delta\mu. \tag{4.54}$$

For example, in the renormalisation of the product $X_{12} = \sqrt{2}M_W \sin\beta$ we use $\delta s_\beta = s_\beta c_\beta^2 \delta t_\beta$, and we express $\delta M_W = \frac{\delta M_W^2}{2M_W}$ in terms of δM_W^2,

$$\delta X_{12} = \left(\frac{\delta M_W}{M_W} + \frac{\delta s_\beta}{s_\beta}\right) \cdot X_{12} = \left(\frac{\delta M_W^2}{2M_W^2} + \frac{s_\beta c_\beta^2 \delta t_\beta}{s_\beta}\right) \cdot \sqrt{2}M_W s_\beta$$
$$= \frac{s_\beta \delta M_W^2}{\sqrt{2}M_W} + \sqrt{2}s_\beta c_\beta^2 M_W \delta t_\beta. \tag{4.55}$$

Likewise, the other matrix elements of the chargino mixing matrix are renormalised via

$$\delta X_{21} = \delta(\sqrt{2}M_W c_\beta) = \left(\frac{\delta M_W}{M_W} + \frac{\delta c_\beta}{c_\beta}\right)\sqrt{2}M_W c_\beta = \frac{\delta M_W^2}{M_W}\frac{c_\beta}{\sqrt{2}} - \sqrt{2}M_W c_\beta s_\beta^2 \delta t_\beta. \tag{4.56}$$

We calculate the counterterms of the elements in the neutralino mixing matrix in the same manner,

$$\delta Y_{14} = \delta Y_{41} = \left(\frac{\delta M_Z^2}{2M_Z^2} + \frac{s_\beta c_\beta^2 \delta t_\beta}{s_\beta} + \frac{\delta s_W}{s_W}\right) M_Z s_\beta s_W$$
$$= \frac{s_\beta s_W}{2M_Z}\delta M_Z^2 + M_Z s_W s_\beta c_\beta^2 \delta t_\beta + M_Z s_\beta \delta s_W,$$
$$\delta Y_{23} = \delta Y_{32} = \left(\frac{\delta M_Z^2}{2M_Z^2} + \frac{c_\beta s_\beta^2 \delta t_\beta}{c_\beta} + \frac{\delta c_W}{c_W}\right) M_Z c_\beta c_W$$
$$= \frac{c_\beta c_W}{2M_Z}\delta M_Z^2 + M_Z c_W c_\beta s_\beta^2 \delta t_\beta - M_Z c_\beta \delta c_W,$$
$$\delta Y_{24} = \delta Y_{42} = -\left(\frac{\delta M_Z^2}{2M_Z^2} + \frac{s_\beta c_\beta^2 \delta t_\beta}{s_\beta} + \frac{\delta c_W}{c_W}\right) M_Z s_\beta c_W$$
$$= -\frac{s_\beta c_W}{2M_Z}\delta M_Z^2 - M_Z c_W s_\beta c_\beta^2 \delta t_\beta - M_Z s_\beta \delta c_W,$$
$$\delta Y_{13} = \delta Y_{31} = -\left(\frac{\delta M_Z^2}{2M_Z^2} - \frac{c_\beta s_\beta^2 \delta t_\beta}{c_\beta} + \frac{\delta s_W}{s_W}\right) M_Z c_\beta s_W$$
$$= -\frac{c_\beta s_W}{2M_Z}\delta M_Z^2 + M_Z s_W c_\beta s_\beta^2 \delta t_\beta - M_Z c_\beta \delta s_W. \tag{4.57}$$

Field renormalisation We now introduce the neutralino field renormalisation constants, distinguishing between left- and right-handed components and treating the renormalisation constants of incoming (unbarred) and outgoing (barred) fields independently in order to allow for the most general case. The four renormalisation

transformations are the following:

$$
\begin{aligned}
\omega_L \tilde{\chi}_i^0 &\rightarrow (1 + \frac{1}{2}\delta Z_0^L)_{ij}\omega_L\tilde{\chi}_j^0, \quad \overline{\tilde{\chi}_i^0}\omega_R \rightarrow \overline{\tilde{\chi}_i^0}(1 + \frac{1}{2}\delta\bar{Z}_0^L)_{ij}\omega_R \\
\omega_R \tilde{\chi}_i^0 &\rightarrow (1 + \frac{1}{2}\delta Z_0^R)_{ij}\omega_R\tilde{\chi}_j^0, \quad \overline{\tilde{\chi}_i^0}\omega_L \rightarrow \overline{\tilde{\chi}_i^0}(1 + \frac{1}{2}\delta\bar{Z}_0^R)_{ij}\omega_L.
\end{aligned}
\tag{4.58}
$$

As a first step, we want to derive the counterterms of the fermion self-energies, decomposed into left- and right-handed contributions as well as vector and scalar parts,

$$
\Sigma_{ij}(p^2) = \not{p}\left(\omega_L\Sigma_{ij}^L(p^2) + \omega_R\Sigma_{ij}^R(p^2)\right) + \omega_L\Sigma_{ij}^{SL}(p^2) + \omega_R\Sigma_{ij}^{SR}(p^2),
\tag{4.59}
$$

The renormalised self-energies are defined as

$$
\hat{\Sigma}_{ij}^{(S)R/L}(p^2) = \Sigma_{ij}^{(S)R/L}(p^2) + \Delta\Sigma_{ij}^{(S)R/L}.
\tag{4.60}
$$

Inserting the parameter renormalisation transformations from Eq. (4.57) and the field renormalisation transformations from Eq. (4.58) into the Lagrangian of the neutralino sector at tree-level from Eq. (3.25) and taking the orthogonality of the projection operators into account,

$$
\omega_{L/R}\cdot\omega_{R/L} = 0 \text{ and } (\omega_{L/R})^2 = \omega_{L/R},
$$

we obtain the renormalised Lagrangian

$$
\begin{aligned}
\mathscr{L}_{\chi 0} \rightarrow \frac{1}{2}\overline{\tilde{\chi}_i^0} &\left[(1 + \frac{1}{2}\delta\bar{Z}_0^L)_{ik}\omega_R + (1 + \frac{1}{2}\delta\bar{Z}_0^R)_{ik}\omega_L\right] \\
&\cdot\left[\not{p}\delta_{kl} - \omega_L(N^*\{Y + \delta Y\}N^\dagger)_{kl} - \omega_R(N\{Y^\dagger + \delta Y^\dagger\}N^T)_{kl}\right] \\
&\cdot\left[(1 + \frac{1}{2}\delta Z_0^L)_{lj}\omega_L + (1 + \frac{1}{2}\delta Z_0^R)_{lj}\omega_R\right]\tilde{\chi}_j^0 \\
= \mathscr{L}_{\chi 0}^{Born} + \frac{1}{2}\overline{\tilde{\chi}_i^0}\not{p}&[\underbrace{\frac{1}{2}(\delta\bar{Z}_0^R + \delta Z_0^R)}_{\Delta\Sigma_{ij}^R}\omega_R + \underbrace{\frac{1}{2}(\delta\bar{Z}_0^L + \delta Z_0^L)}_{\Delta\Sigma_{ij}^L}\omega_L]_{ij}\tilde{\chi}_j^0 \\
& - \frac{1}{2}\overline{\tilde{\chi}_i^0}\omega_R\underbrace{[N\delta Y^\dagger N^T + \frac{1}{2}(NY^\dagger N^T\delta Z_0^R + \delta\bar{Z}_0^L NY^\dagger N^T)]_{ij}}_{-\Delta\Sigma_{ij}^{SR}}\tilde{\chi}_j^0 \\
& - \frac{1}{2}\overline{\tilde{\chi}_i^0}\omega_L\underbrace{[N^*\delta Y N^\dagger + \frac{1}{2}(N^*YN^\dagger\delta Z_0^L + \delta\bar{Z}_0^R N^*YN^\dagger)]_{ij}}_{-\Delta\Sigma_{ij}^{SL}}\tilde{\chi}_j^0 + \mathcal{O}(\delta^2).
\end{aligned}
\tag{4.61}
$$

According to Eq. (4.3), the Lagrangian of the neutralino sector, $\mathscr{L}_{\chi 0}$, is separated into two pieces, the Born part $\mathscr{L}_{\chi 0}^{Born}$ and the part $\delta\mathscr{L}_{\chi 0}$ containing the counterterms. Comparing Eqs. (4.59) and (4.60), we determine the counterterms of the scalar and vector coeffcients of the left- and right-handed self-energies. They can be expressed in terms of the field renormalisation constants:

$$\Delta\Sigma_{ij}^{R/L} = \frac{1}{2}(\delta\bar{Z}_0^{R/L} + \delta Z_0^{R/L}) \tag{4.62}$$

$$\Delta\Sigma_{ij}^{SR} = [-N\delta Y^\dagger N^T - \frac{1}{2}(NY^\dagger N^T \delta Z_0^R + \delta\bar{Z}_0^L NY^\dagger N^T)]_{ij} \tag{4.63}$$

$$\Delta\Sigma_{ij}^{SL} = [-N^*\delta Y N^\dagger - \frac{1}{2}(N^*YN^\dagger \delta Z_0^L + \delta\bar{Z}_0^R N^*YN^\dagger)]_{ij}. \tag{4.64}$$

The renormalised propagators $\hat{S}_{ij}$ and two-point vertex functions $\hat{\Gamma}_{ij} = i\hat{S}_{ij}^{-1}$ are expressed as follows [91]:

$$\hat{S}_{ij}(p) = i[\hat{\Gamma}_{ij}(p)]^{-1} = [(\not{p} - m_{\tilde{\chi}_i^0})\delta_{ij} + \hat{\Sigma}_{ij}(p)]^{-1}. \tag{4.65}$$

4.3.2. On-shell field renormalisation in the neutralino sector

We renormalise the neutralino sector in an on-shell scheme, fixing the renormalisation constants by imposing on-shell renormalisation conditions. A detailed calculation of the on-shell field renormalisation constants in the neutralino sector, $\delta Z_{ij}^{R/L}$ and $\delta\bar{Z}_{ij}^{R/L}$, can be found in Appendix A. In this section, we just present a summary of the results that are directly needed.

The off-diagonal field renormalisation constants for $\tilde{\chi}_i^0, \tilde{\chi}_j^0$ with $i \neq j$ are obtained from the condition (A.8) that $\tilde{\chi}_i^0$ and $\tilde{\chi}_j^0$ do not mix in the on-shell limit:

$$\delta Z_{ij}^{L/R} = \frac{2}{m_{\tilde{\chi}_i^0}^2 - m_{\tilde{\chi}_j^0}^2} \cdot [m_{\tilde{\chi}_j^0}^2\Sigma_{ij}^{L/R}(m_{\tilde{\chi}_j^0}^2) + m_{\tilde{\chi}_i^0}m_{\tilde{\chi}_j^0}\Sigma_{ij}^{R/L}(m_{\tilde{\chi}_j^0}^2) + m_{\tilde{\chi}_i^0}\Sigma_{ij}^{SL/SR}(m_{\tilde{\chi}_j^0}^2)$$

$$+ m_{\tilde{\chi}_j^0}\Sigma_{ij}^{SR/SL}(m_{\tilde{\chi}_j^0}^2) - m_{\tilde{\chi}_{j/i}}(N^*\delta Y N^\dagger)_{ij} - m_{\tilde{\chi}_{j/i}}(N\delta Y^\dagger N^T)_{ij}] \tag{4.66}$$

$$\delta\bar{Z}_{ij}^{L/R} = \frac{2}{m_{\tilde{\chi}_j^0}^2 - m_{\tilde{\chi}_i^0}^2} \cdot [m_{\tilde{\chi}_i^0}^2\Sigma_{ij}^{L/R}(m_{\tilde{\chi}_i^0}^2) + m_{\tilde{\chi}_i^0}m_{\tilde{\chi}_j^0}\Sigma_{ij}^{R/L}(m_{\tilde{\chi}_i^0}^2) + m_{\tilde{\chi}_i^0}\Sigma_{ij}^{SL/SR}(m_{\tilde{\chi}_i^0}^2)$$

$$+ m_{\tilde{\chi}_j^0}\Sigma_{ij}^{SR/SL}(m_{\tilde{\chi}_i^0}^2) - m_{\tilde{\chi}_{i/j}}(N^*\delta Y N^\dagger)_{ij} - m_{\tilde{\chi}_{j/i}}(N\delta Y^\dagger N^T)_{ij}]. \tag{4.67}$$

In the diagonal case, $i = j$, the field renormalisation constants read

$$\delta Z_{ii}^{L/R}$$
$$= -\Sigma_{ii}^{L/R}(m_{\tilde{\chi}_i^0}^2) - m_{\tilde{\chi}_i^0}^2 \left[\hat{\Sigma}_{ii}^{'L}(m_{\tilde{\chi}_i^0}^2) + \hat{\Sigma}_{ii}^{'R}(m_{\tilde{\chi}_i^0}^2) \right] - m_{\tilde{\chi}_i^0} \left[\hat{\Sigma}_{ii}^{'SL}(m_{\tilde{\chi}_i^0}^2) + \hat{\Sigma}_{ii}^{'SR}(m_{\tilde{\chi}_i^0}^2) \right]$$
$$\mp \frac{1}{2m_{\tilde{\chi}_i^0}} \left[\Sigma_{ii}^{SR}(m_{\tilde{\chi}_i^0}^2) - \Sigma_{ii}^{SL}(m_{\tilde{\chi}_i^0}^2) + (N^* \delta Y N^\dagger)_{ii} - (N \delta Y^\dagger N^T)_{ii} \right] \qquad (4.68)$$

$$\delta \bar{Z}_{ii}^{L/R}$$
$$= -\Sigma_{ii}^{L/R}(m_{\tilde{\chi}_i^0}^2) - m_{\tilde{\chi}_i^0}^2 \left[\hat{\Sigma}_{ii}^{'L}(m_{\tilde{\chi}_i^0}^2) + \hat{\Sigma}_{ii}^{'R}(m_{\tilde{\chi}_i^0}^2) \right] - m_{\tilde{\chi}_i^0} \left[\hat{\Sigma}_{ii}^{'SL}(m_{\tilde{\chi}_i^0}^2) + \hat{\Sigma}_{ii}^{'SR}(m_{\tilde{\chi}_i^0}^2) \right]$$
$$\pm \frac{1}{2m_{\tilde{\chi}_i^0}} \left[\Sigma_{ii}^{SR}(m_{\tilde{\chi}_i^0}^2) - \Sigma_{ii}^{SL}(m_{\tilde{\chi}_i^0}^2) + (N^* \delta Y N^\dagger)_{ii} - (N \delta Y^\dagger N^T)_{ii} \right]. \qquad (4.69)$$

Symmetry relations between the neutralino field renormalisation constants
Owing to the Majorana nature of neutralinos, they are invariant under charge conjugation so that the following $\mathcal{C}$-invariance relations hold for their self-energies:

$$\Sigma_{ij}^L(p^2) = \Sigma_{ji}^R(p^2) \qquad (4.70)$$
$$\Sigma_{ij}^{SL/SR}(p^2) = \Sigma_{ji}^{SL/SR}(p^2). \qquad (4.71)$$

Moreover, Y is a symmetric matrix, $Y = Y^T$, and hence matrix of counterterms is also symmetric,

$$\delta Y_{ij} = \delta Y_{ji}. \qquad (4.72)$$

This further implies that the following expression in the field renormalisation constants is symmetric:

$$[N^* \delta Y N^\dagger]_{ji} = [(N^* \delta Y N^\dagger)^T]_{ij} = [N^* \delta Y N^\dagger]_{ij}. \qquad (4.73)$$

Although we introduced the barred and unbarred field renormalisation constants as independent quantities, they are related for Majorana particles due to (4.70-4.73):

$$\delta Z_{ij}^{L/R} = \delta \bar{Z}_{ji}^{R/L}. \qquad (4.74)$$

4.3.3. Loop-corrections to the masses

Imposing on-shell conditions for the masses, tree-level masses m_i coincide with loop-corrected masses M_i. However, the number of independent parameters determines the number of renormalisation conditions, in this case $|\mu|, |M_1|$ and $|M_2|$. The neutralino-chargino sector contains in total six masses, the neutralino masses $m_{\tilde{\chi}_i^0}, i = 1, ..., 4$ as well as the chargino masses $m_{\tilde{\chi}_i^\pm}, i = 1, 2$.
Moreover, the renormalisation conditions for the fields ensure correct on-shell properties, i.e. fields do not mix on the mass shell. Consequently, only the complex poles,

denoted by $\mathcal{M}_i^2 := M_{\tilde{\chi}i}^2 - iM_{\tilde{\chi}i}\Gamma_{\tilde{\chi}i}$, of the diagonal propagators S_{ii} are considered. They solve

$$\mathcal{M}_i^2 \left[1 + \hat{\Sigma}_{ii}^L(\mathcal{M}_i^2)\right]\left[1 + \hat{\Sigma}_{ii}^R(\mathcal{M}_i^2)\right] - \left[m_{\tilde{\chi}i} - \hat{\Sigma}_{ii}^{SL}(\mathcal{M}_i^2)\right]\left[m_{\tilde{\chi}i} - \hat{\Sigma}_{ii}^{SR}(\mathcal{M}_i^2)\right] = 0.$$
(4.75)

So the real part of the renormalised, diagonal self-energies gives rise to corrections to the tree-level masses.

$$
\begin{aligned}
M_{\tilde{\chi}i} &= m_{\tilde{\chi}i} + \Delta m_{\tilde{\chi}i} \quad \text{with} \\
\Delta m_{\tilde{\chi}i} &= -\frac{m_{\tilde{\chi}i}}{2}\text{Re}\{\hat{\Sigma}_{ii}^L(m_{\tilde{\chi}i}^2) + \hat{\Sigma}_{ii}^R(m_{\tilde{\chi}i}^2)\} - \frac{1}{2}\text{Re}\{\hat{\Sigma}_{ii}^{SL}(m_{\tilde{\chi}i}^2) + \hat{\Sigma}_{ii}^{SR}(m_{\tilde{\chi}i}^2)\} \\
&\overset{(A.5,A.6)}{=} -m_{\tilde{\chi}i}\text{Re}\hat{\Sigma}_{ii}^L(m_{\tilde{\chi}i}^2) - \text{Re}\hat{\Sigma}_{ii}^{SL}(m_{\tilde{\chi}i}^2)
\end{aligned}
$$
(4.76)

Explicit neutralino self-energies can be found, for instance, in Refs. [93, 94].

4.3.4. Parameter renormalisation

The neutralino-chargino sector is governed by the - possibly complex - parameters μ, M_1 and M_2. While the phase ϕ_{M_2} can be rotated away, the other phases, in principle, have to be renormalised in addition to the absolute values of the parameters.

$$|\mu| \to |\mu| + \delta|\mu|, \qquad\qquad \phi_\mu \to \phi_\mu + \delta\phi_\mu \qquad (4.77)$$
$$|M_1| \to |M_1| + \delta|M_1|, \qquad\qquad \phi_{M_1} \to \phi_{M_1} + \delta\phi_{M_1} \qquad (4.78)$$
$$|M_2| \to |M_2| + \delta|M_2| \qquad\qquad\qquad (4.79)$$

However, the phase counterterms, $\delta\phi_\mu$ and $\delta\phi_{M_1}$ turn out to be UV-finite at the 1-loop level [70] so that the phases ϕ_μ and ϕ_{M_1} can be kept unrenormalised.
The ith neutralino is on-shell if $\Delta m_{\tilde{\chi}_i^0} = 0$ in Eq. (4.76). This condition on the self energies can be translated into a condition on the parameter counterterms [70]. The exact structure of the counterterms depends on the chosen mass scheme, i.e., which three out of the six neutralino and chargino masses to impose on-shell conditions on. All masses are renormalised and receive a counterterm according to Eq. (4.76). For the three chosen masses, the physical meaning of the masses changes, but the numerical value stays the same when going from the tree-level to the one-loop level. The application to an example process in Chaps. 8, 9 and 10 does not involve any external charginos, but only external neutralinos, in particular $\tilde{\chi}_1^0$ and $\tilde{\chi}_4^0$. Consequently, a scheme is chosen which sets three neutralino masses on-shell[1].
In any case, the three on-shell masses must be chosen carefully [70, 95, 96]. If all three on-shell masses depend only weakly on one of the bino-, wino- or higgsino mass parameters (M_1, M_2 or μ, respectively), this could give rise to unphysically

---

[1]In Ref. [70] this scheme is called "NNN".

large loop contributions. But very large counterterms are problematic for perturbativity and numerical stability. In a general scheme with $\tilde{\chi}_i^0$, $\tilde{\chi}_j^0$ and $\tilde{\chi}_k^0$ on-shell, the solution of Eq. (4.76) implies [70]

$$\delta|M_1| = [(\text{Re}\{e^{-i\phi_\mu}N_{i3}N_{i4}\}\text{Re}\{N_{j2}^2\} - \text{Re}\{e^{-i\phi_\mu}N_{j3}N_{j4}\}\text{Re}\{N_{i2}^2\})N_k$$
$$+ (\text{Re}\{e^{-i\phi_\mu}N_{j3}N_{j4}\}\text{Re}\{e^{-i\phi_{M_1}}N_{k2}^2\} - \text{Re}\{e^{-i\phi_\mu}N_{k3}N_{k4}\}\text{Re}\{N_{j2}^2\})N_i$$
$$+ (\text{Re}\{e^{-i\phi_\mu}N_{k3}N_{k4}\}\text{Re}\{N_{i2}^2\} - \text{Re}\{e^{-i\phi_\mu}N_{i3}N_{i4}\}\text{Re}\{N_{k2}^2\})N_j]/L \qquad (4.80)$$

$$\delta|M_2| = [(\text{Re}\{e^{-i\phi_\mu}N_{j3}N_{j4}\}\text{Re}\{e^{-i\phi_{M_1}}N_{i1}^2\} - \text{Re}\{e^{-i\phi_\mu}N_{i3}N_{i4}\}\text{Re}\{e^{-i\phi_{M_1}}N_{j1}^2\})N_k$$
$$+ (\text{Re}\{e^{-i\phi_\mu}N_{k3}N_{k4}\}\text{Re}\{e^{-i\phi_{M_1}}N_{j1}^2\} - \text{Re}\{e^{-i\phi_\mu}N_{j3}N_{j4}\}\text{Re}\{e^{-i\phi_{M_1}}N_{k1}^2\})N_i$$
$$+ (\text{Re}\{e^{-i\phi_\mu}N_{i3}N_{i4}\}\text{Re}\{e^{-i\phi_{M_1}}N_{k1}^2\} - \text{Re}\{e^{-i\phi_\mu}N_{k3}N_{k4}\}\text{Re}\{e^{-i\phi_{M_1}}N_{i1}^2\})N_j]/L$$
$$(4.81)$$

$$\delta|\mu| = -[(\text{Re}\{N_{i2}^2\}\text{Re}\{e^{-i\phi_{M_1}}N_{j1}^2\} - \text{Re}\{e^{-i\phi_{M_1}}N_{i1}^2\}\text{Re}\{N_{j2}^2\})N_k$$
$$+ (\text{Re}\{N_{j2}^2\}\text{Re}\{e^{-i\phi_{M_1}}N_{k1}^2\} - \text{Re}\{e^{-i\phi_{M_1}}N_{j1}^2\}\text{Re}\{N_{k2}^2\})N_i$$
$$+ (\text{Re}\{N_{j2}^2\}\text{Re}\{e^{-i\phi_{M_1}}N_{k1}^2\} - \text{Re}\{e^{-i\phi_{M_1}}N_{k1}^2\}\text{Re}\{N_{k2}^2\})N_j]/(2L), \qquad (4.82)$$

where we defined the following shorthand notations:

$$N_i := \text{Re}\{m_{\tilde{\chi}_i^0}\left[\Sigma_{ii}^L(m_{\tilde{\chi}_i^0}^2) + \Sigma_{ii}^R(m_{\tilde{\chi}_i^0}^2)\right] + \left[\Sigma_{ii}^{SL}(m_{\tilde{\chi}_i^0}^2) + \Sigma_{ii}^{SR}(m_{\tilde{\chi}_i^0}^2)\right]\}$$
$$- 4\sum_{k=1}^{2}\sum_{l=3}^{4}\delta Y_{lk}\text{Re}\{N_{ik}N_{il}\} \qquad (4.83)$$

$$L := 2(\text{Re}\{e^{-i\phi_{M_1}}N_{k1}^2\}\left[\text{Re}\{e^{-i\phi_\mu}N_{i3}N_{i4}\}\text{Re}\{N_{j2}^2\} - \text{Re}\{e^{-i\phi_\mu}N_{j3}N_{j4}\}\text{Re}\{N_{i2}^2\}\right]$$
$$+ \text{Re}\{N_{k2}^2\}\left[\text{Re}\{e^{-i\phi_\mu}N_{j3}N_{j4}\}\text{Re}\{e^{-i\phi_{M_1}}N_{i1}^2\} - \text{Re}\{e^{-i\phi_\mu}N_{i3}N_{i4}\}\text{Re}\{e^{-i\phi_{M_1}}N_{j1}^2\}\right]$$
$$+ \text{Re}\{e^{-i\phi_\mu}N_{k3}N_{k4}\}\left[\text{Re}\{N_{i2}^2\}\text{Re}\{e^{-i\phi_{M_1}}N_{j1}^2\} - \text{Re}\{N_{j2}^2\}\text{Re}\{e^{-i\phi_{M_1}}N_{i1}^2\}\right])$$
$$(4.84)$$

We have implemented these counterterms into the `FeynArts` MSSM model file allowing to choose three of the four neutralino masses on-shell. In our later application, we have $\tilde{\chi}_1^0$ and $\tilde{\chi}_4^0$ as external particles. Setting them on-shell renders the dependence of the mass renormalisation condition in Eq. (4.76) on M_1 and μ strong enough in a scenario where $\tilde{\chi}_1^0$ is mostly bino-like and $\tilde{\chi}_4^0$ higgsino-like. In addition, for an appropriate M_2-dependence $\tilde{\chi}_2^0$ should be set on-shell. So we choose $i, j, k = 1, 2, 4$.

5. Algebraic and numerical tools

Depending on the complexity of the studied process, calculations of cross sections or decay widths by hand might be laborious or even impracticable. Especially internal loops or the presence of several contributing diagrams complicate the computation. Hence it is convenient to automatise the calculation starting from the generation of Feynman diagrams, ranging over the algebraic simplifications and encompassing also the numerical evaluation. Among the available programme packages, there is the combination of `FeynArts` [97–101], `FormCalc` [80, 102–105] and `LoopTools` [80, 106] for carrying out such tasks in the calculation.

`FeynArts` can create amplitudes and paint diagrams with up to three loops.

`FormCalc` performs the algebraic simplification, converts `Mathematica` output to `Fortran` code and supplies driver programs for the numerical evaluation. It can handle up to $2 \to 4$ kinematics and tree-level or one-loop processes. `LoopTools` provides a library of one-loop integrals.

In contrast, `FeynHiggs` [56, 81, 84–86] contains results for observables in the MSSM Higgs sector including full one-loop and leading two-loop corrections. They can be used to supplement the calculations carried out in `FeynArts, FormCalc` and `LoopTools`.

All these packages are based on `Mathematica`, `Form` [107] and `Fortran`.

5.1. FeynArts, Form, FormCalc, LoopTools

General procedure First of all, `FeynArts` can be used to generate the topologies for $n \to m$ processes with k loops. Then the allowed fields and vertices are inserted according to the model specified by the user. Particles on internal lines can be restricted manually. Subsequently, the contributing diagrams are drawn and an amplitude is created from the Feynman rules as a symbolic expression.

The calculation of the amplitude is performed by `FormCalc`. Next, the function `SquaredME` computes the squared matrix element and takes thereby care of the contraction of indices, the evaluation of fermion traces and the calculation of the algebra in `Form`. Fermion chains, which can be defined in the DIRAC or WEYL representation, are simplified by making use of the Dirac equation. Abbreviations and invariants can be introduced.

By `WriteSquaredME`, `FormCalc` automatically writes Fortran code for a faster numerical evaluation into a process-specific directory. The user can adjust for example

parameter values and integration options. Either all parameters are defined explicitly or a scan over a parameter range can be performed. After building up the m-particle phase space iteratively, the squared matrix element is integrated numerically with the `Cuba` library [108], resulting in cross sections or partial decay widths. An executable file is produced in the Fortran or Mathematica interface provided by `FormCalc` which can be run at the desired centre of mass energy or over an energy range.

Calculations at one-loop level If $k = 1$ loops are selected in `FeynArts`, the topology categories besides Born are split into vertex, box and self-energy diagrams. Undesired topology shapes can be excluded. It is possible to create the amplitudes separately for each category.

For radiative corrections in the SM, Dimensional Regularisation can be chosen in `FormCalc`. For SUSY, the scheme of Constrained Differential Renormalisation (see Sect. 4.1.2) is used which was proven to be equivalent at one-loop level to dimensional reduction. Tensor integrals are decomposed into Lorentz covariant coefficients in a basis spanned by the metric $g_{\mu\nu}$ and sums of external momenta $k_\mu^{(i)}$ according to PASSARINO-VELTMAN reduction, see Sect. 10.1.2.

The amplitudes contain finite parts and coefficients of divergent one-loop integrals which are implemented in `LoopTools` in the convention by Ref. [6] to return numerical results.

In the distributed version, counterterms are only available for the SM. Beyond, they must be calculated in the considered renormalisation scheme and they have to be implemented into the `FeynArts` model file by the user himself. Then `FeynArts` is able to generate the counterterm diagrams and to apply the definitions from the extended model file. This is done in Chap. 4 for the Higgs and neutralino sector of the MSSM.

The UV-finiteness of an amplitude can be checked by making sure that the coefficients in front of the divergence $\Delta := \frac{2}{4-D}$ (in D dimensions) cancel analytically or within the numerical precision. An alternative is to vary Δ and check numerically whether the final (integrated) result is independent of Δ.

5.2. FeynHiggs

Besides, `FeynHiggs` can be invoked by `FormCalc` or directly to obtain precise values of the Higgs masses, widths, branching fractions, mixing matrices, couplings and Z-factors and other results from the specified SM and (real or complex) SUSY input parameters. Full one-loop results, allowing for the complete MSSM particle spectrum in loops, and leading two-loop contributions of order $\alpha_s\alpha_t, \alpha_s\alpha_b, \alpha_t^2, \alpha_t\alpha_b$ are included.

An algorithm in `FeynHiggs` solves for the complex roots of the mass matrix $\mathcal{M}^2(q^2)$

in Eq. (4.42) whose real parts, i.e. the real parts of the complex poles of the propagator, are identified as the masses.

Options can be chosen regarding the loop-level of the computation, restrictions to certain subsets of particles in loops, schemes for the field and $\tan\beta$ renormalisation, approximations for the mixing of self-energies and specifications for running masses. We use the $\overline{\text{DR}}$ scheme for the renormalisation of fields and $\tan\beta$ and the full MSSM spectrum as the scope of the one-loop part.

The versions used in this thesis are `FeynArts 3.6, FormCalc 7.1, LoopTools 2.7` and `FeynHiggs 2.8.6`.

6. Kinematic relations in decay processes

6.1. The phase space

The phase space Φ is a Lorentz invariant quantity. Its differential is denoted as *dlips* (differential Lorentz invariant phase space) or $d\Phi_n$. It is characterised by the number n of particles in the final state[1]

$$d\Phi_n \equiv dlips\,(P; p_1, ..., p_f) = (2\pi)^4 \delta^{(4)}(P - \sum_{f=1}^{n} p_f) \prod_{f=1}^{n} \frac{d^3 p_f}{(2\pi)^3 2E_f}. \qquad (6.1)$$

The 2-body phase space For later use in Sects. 6.2 and 8.1.2, we need an explicit expression for the 2-body phase space $d\Phi_2$. Consider a particle a with m_a, p_a, decaying into b, c with m_b, p_b, m_c, p_c: $p_a = p_b + p_c$. In the rest frame of the decaying particle, the centre of mass energy is $\sqrt{s} = m_a$. So we get

$$p_a = (m_a, \vec{0}) \Rightarrow m_a = E_b + E_c = \sqrt{s}, \quad \vec{p_b} = -\vec{p_c} \equiv \vec{p}. \qquad (6.2)$$

We will apply the following property of the Dirac δ-distribution:

$$\delta(x - x_0) = \sum_i \frac{x - x_i}{|g'(x_i)|} \ \text{ with } g(x_i) = 0. \qquad (6.3)$$

Furthermore, we will use the energy-momentum relation

$$E(|p|) = \sqrt{|p|^2 + m^2} \ \Rightarrow \ E'(|p|) = \frac{|p|}{E},$$

$$\text{with } g(|\vec{p}|) := \sqrt{s} - E_b(|\vec{p}|) - E_c(|\vec{p}|)$$

$$\Rightarrow \int \delta(g(|\vec{p}|)) d|\vec{p}| = \frac{1}{|g'(|\vec{p}|)|_{E_b + E_c = \sqrt{s}}} = \frac{1}{\frac{|\vec{p}|}{E_b} + \frac{|\vec{p}|}{E_c}}. \qquad (6.4)$$

We start by splitting the $\delta^{(4)}$-distribution in the time and spacial components and transforming the momentum differential in spherical coordinates introducing the

---

[1] Our notation agrees with the convention in References [4, 70], but differs from [20] by a factor of $(4\pi)^4$.

solid angle $d\Omega \equiv d\phi\, d\cos\theta$. The calculation is done in the rest frame of the decaying particle, $\vec{p}_a = 0$ so that $\vec{p}_b = -\vec{p}_c =: \vec{p}$ and $M = E_b + E_c$.

$$d\Phi_2 \equiv dlips(p_a; p_b, p_c) = (2\pi)^4 \delta^{(4)}(p_a - p_b - p_c) \frac{d^3\vec{p}_b}{(2\pi)^3 2E_b} \frac{d^3\vec{p}_c}{(2\pi)^3 2E_c}$$

$$= 2\pi\delta(\sqrt{s} - E_b - E_c) \underbrace{(2\pi)^3 \delta^{(3)}(\vec{p}_a)}_{\int \frac{d^3\vec{p}_c}{(2\pi)^3}(2\pi)^3\delta^{(3)}(\vec{p}_a)=1} \frac{d^3\vec{p}_b}{(2\pi)^3 2E_b} \frac{d^3\vec{p}_c}{(2\pi)^3 2E_c}$$

$$= 2\pi\delta(\underbrace{\sqrt{s} - E_b(|\vec{p}|) - E_c(|\vec{p}|)}_{=g(|\vec{p}|)}) \frac{d^3\vec{p}}{(2\pi)^3 4E_b E_c}$$

$$= \frac{1}{(2\pi)^2} \delta(g(|\vec{p}|)) \frac{|\vec{p}|^2 d|\vec{p}| d\Omega}{4E_b E_c} \cdot \frac{4\pi}{4\pi}$$

$$\overset{(6.4)}{=} \frac{1}{4\pi^2} \frac{4\pi|\vec{p}|^2}{4E_b E_c} \frac{d\Omega}{4\pi} \frac{1}{\frac{|\vec{p}|}{E_b} + \frac{|\vec{p}|}{E_c}} \quad = \frac{1}{4\pi} \frac{|\vec{p}|}{E_b + E_c} \frac{d\Omega}{4\pi}$$

$$= \frac{1}{4\pi} \frac{|\vec{p}|}{m_a} \frac{d\Omega}{4\pi} \tag{6.5}$$

Before the calculation of a specific process, we will review kinematic properties of generic 2- and 3- body decays [20].

6.2. 2-body decay

Labelling the involved particles as in Eq. (6.2), the momenta and energies in the final state are determined by the following mass relations.

$$|\vec{p}| \equiv |\vec{p}_b| \equiv |\vec{p}_c| = \frac{\sqrt{\left(m_a^2 - (m_b + m_c)^2\right)\left(m_a^2 - (m_b - m_c)^2\right)}}{2m_a} \tag{6.6}$$

$$|\vec{p}|^2 = \frac{(m_a^2 - m_b^2 + m_c^2)^2}{4m_a^2} - m_c^2 = \frac{(m_a^2 + m_b^2 - m_c^2)^2}{4m_a^2} - m_b^2 \tag{6.7}$$

$$E_b = \frac{m_a^2 + m_b^2 - m_c^2}{2m_a} \tag{6.8}$$

$$E_c = \frac{m_a^2 - m_b^2 + m_c^2}{2m_a} \tag{6.9}$$

Special case of equal masses   In the case of particles with the same mass $m_b = m_c$ in the final state, Eqs. (6.6)-(6.9) are reduced to

$$E_b = E_c = \frac{m_a}{2}, \qquad\qquad |\vec{p}_b|^2 = |\vec{p}_c|^2 = \frac{m_a^2}{4} - m_b^2.$$

Width   With the 2-body phase space in Eq. (6.5) and the flux factor

$$F = 2\sqrt{s} = 2m_a, \tag{6.10}$$

we can calculate the differential width

$$d\Gamma = \frac{1}{F}|\mathcal{M}|^2 dlips(a; b, c) = \frac{1}{32\pi^2}|\mathcal{M}|^2\frac{|\vec{p_b}|}{m_a^2}d\phi d\cos\theta. \tag{6.11}$$

If the process is isotropic the angular integral yields $\int d\Omega = 4\pi$, thus the decay width reads

$$\Gamma = \frac{1}{8\pi}|\mathcal{M}|^2\frac{|\vec{p_b}|}{m_a^2}. \tag{6.12}$$

Since $|\vec{p_b}|$ is fixed by Eq. (6.6), the 2-body decay width is determined by the squared matrix element and the involved masses. This result will be used in Chap. 8 for the factorisation of a 3-body decay.

6.3. 3-body decay

The phase space is more complicated for 3 particles in the final state: $a \to b, c, d$ Constructing invariants by defining $p_{ij} := p_i + p_j$ and $m_{ij}^2 = p_{ij}^2$, we get the relations

$$m_{bc}^2 + m_{cd}^2 + m_{bd}^2 = \sum_{i=a}^{d} m_i^2. \tag{6.13}$$

It is convenient to choose a frame in which a pair of particles is produced at rest. According to the three possible pairs within the three-body final state, there exist three equivalent, so-called Gottfried-Jackson frames [109]. With the choice of the bc-rest frame $\vec{p_b} + \vec{p_c} = 0$, the phase space can be parametrised in the following way [110]:

$$d\Gamma = \frac{1}{(2\pi)^3}\frac{1}{8m_a}|\mathcal{M}|^2 dE_b dE_c = \frac{1}{(2\pi)^3}\frac{1}{32m_a^3}|\mathcal{M}|^2 dm_{bc}dm_{cd} \tag{6.14}$$

The energies

$$E_c^* := \frac{m_{bc}^2 - m_b^2 + m_c^2}{2m_{bc}} \qquad\qquad E_d^* := \frac{-m_{bc}^2 + m_a^2 - m_d^2}{2m_{bc}} \tag{6.15}$$

are the boosted energies of c and d in the m_{bc} rest frame. The integration limits of m_{cd} are functions of m_{bc} which itself is limited by the kinematic bounds of the

momentum relation $p_a - p_d = p_b + p_c$:

$$(E_c^* + E_d^*)^2 - (\sqrt{E_c^{*2} - m_c^2} + \sqrt{E_d^{*2} - m_d^2})^2 \leq m_{cd}^2$$

$$\leq (E_c^* + E_d^*)^2 - (\sqrt{E_c^{*2} - m_c^2} - \sqrt{E_d^{*2} - m_d^2})^2, \qquad (6.16)$$

$$(m_b + m_c)^2 \leq m_{bc}^2 \leq (m_a - m_d)^2. \qquad (6.17)$$

The upper bound in (6.17) is reached if particle d is produced at rest, the lower bound if b and c are at rest. This can typically be visualised in a DALITZ plot.

The phase space integration is simplified if some masses in the considered process are approximately zero, e.g. $m_c = m_d \approx 0$ [111]. In the application in Chap. 8, however, we will keep the exact masses.

7. The Narrow-Width Approximation

7.1. Standard NWA

The narrow-width approximation (NWA) is a useful way to simplify the calculation of complicated processes involving the resonant production of an unstable particle and its decay. The basic idea is to factorise the whole process into the on-shell production and the subsequent decay. The following picture in Fig. 7.1 visualises this splitting using the example of an arbitrary process $ab \rightarrow cef$.
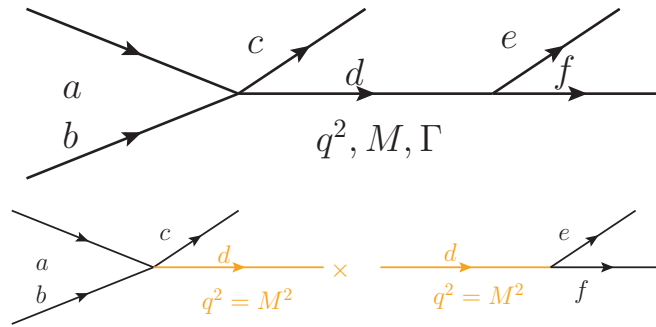
Figure 7.1.: The resonant process $ab \rightarrow cef$ (upper) is split into the production $ab \rightarrow cd$ and decay $d \rightarrow ef$ with particle d on-shell (lower).

In the following, we focus on scalar propagators. Nonetheless, although the production and decay are calculated independently, the spin of an intermediate particle can be taken into account by means of spin correlations [112].
The unstable scalar d with mass M and total width Γ is described by a Breit-Wigner propagator $\Delta^{BW}(q^2) = \frac{1}{q^2 - M^2 + iM\Gamma}$ so that the production becomes resonant near the pole at $q^2 = M^2 - iM\Gamma$. As the name of this approximation suggests, off-shell effects can only be neglected for small widths compared to the mass, $\Gamma \ll M$. Within its range of validity, the NWA leads to the result that the cross section of the full process is the product of the production cross section times the respective branching ratio:

$$\sigma_{ab \rightarrow cef} \simeq \sigma_{ab \rightarrow cd} \times BR_{d \rightarrow ef}. \tag{7.1}$$

The factorisation can be applied on cross sections as well as on decay rates. However, this useful approximation only holds under certain conditions, which are itemised in Sect. 7.1.1. The phase space properties and simplifications the obtained result is based on are explained in Sect. 7.1.2.

7.1.1. Conditions for the NWA

The NWA can only be expected to hold reliably if the following prerequisites are fulfilled [2, 113]:

1. A narrow mass peak is required in order to justify the on-shell approximation. Otherwise off-shell effects may become large.

2. Furthermore, the propagator needs to be separable from the matrix element. This never holds exactly, even if only scalar particles are involved since the phase space factor for the decay particles depends on q^2 for non-zero daughter masses. In cases when vector bosons or fermions are involved, the spin information can be accounted for by means of spin-density matrices.

3. Both sub-processes have to be kinematically allowed. For the production of the intermediate particle, this means that the centre of mass energy $\sqrt{s}$ must be well above the production threshold of the intermediate particle with mass M and the other particles in the final state of the production process, i.e. $\sqrt{s} \gg M + m_c$ for the process shown in Fig. 7.1. Otherwise, threshold effects must be considered [114].

4. On the other hand, the decay channel must be kinematically open and sufficiently far above the decay threshold, i.e. $M \gg \sum m_f$, where m_f are the masses of the particles in the final state of the decay process, here $m_e + m_f$.

5. As another crucial condition, interferences with other resonant or non-resonant diagrams have to be small because the mixed term would be neglected in the narrow-width approximation. The major part of the following chapters is dedicated to a generalisation of the NWA for the inclusion of interference effects based on [70].

7.1.2. Factorisation of the phase space and cross section

Eq. (7.1) is based on the property of the phase space and the matrix element to be factorisable into sub-processes. The phase space element $d\Phi_n$ with n particles in the final state as in Eq. (6.1) will now be expressed as a product of the k-particle phase

space Φ_k with $k < n$ and the remaining Φ_{n-k+1} [20, 111].

$$
\begin{aligned}
d\Phi_n \equiv \quad & dlips\,(P; p_1, ..., p_n) \overset{(6.1)}{=} (2\pi)^4 \delta^{(4)}(P - \sum_{f=1}^{n} p_f) \prod_{f=1}^{n} \frac{d^3 p_f}{(2\pi)^3 2E_i} \\
= \quad & (2\pi)^4 \delta^{(4)}(P - \sum_{f=1}^{k-1} p_f - q) \prod_{f=1}^{k-1} \frac{d^3 p_f}{(2\pi)^3 2E_i} \\
& d^4 q\, \delta^{(4)}(q - \sum_{f=k}^{n} p_f) \prod_{f=k}^{n} \frac{d^3 p_f}{(2\pi)^3 2E_i} \qquad (7.2) \\
= \quad & \underbrace{(2\pi)^4 \delta^{(4)}(P - (\sum_{f=1}^{k-1} p_f + q)) \frac{d^3 q}{(2\pi)^3 2E_q} \prod_{f=1}^{k-1} \frac{d^3 p_f}{(2\pi)^3 2E_i} \frac{dq^2}{2\pi}}_{dlips(P; p1, ..., p_{k-1}, q)} \\
& \underbrace{(2\pi)^4 \delta^{(4)}(q - \sum_{f=k}^{n} p_f) \prod_{f=k}^{n} \frac{d^3 p_f}{(2\pi)^3 2E_i}}_{dlips(q; p_k, ..., p_n)} \qquad (7.3) \\
= \quad & d\Phi_k \frac{dq^2}{2\pi} d\Phi_{n-k+1}. \qquad (7.4)
\end{aligned}
$$

Regarding the physical interpretation and relevance for following applications, by inserting unity

$$
1 = \int d^4 q\, \delta^{(4)}(q - \sum_{f=k}^{n} p_f)
$$

and by adding q to the $k-1$ final-state momenta in the first sub-phase space, q is treated as an external momentum in Φ_k and Φ_{n-k+1}. The nature of q being in fact an intermediate particle is accounted for by introducing an additional integration over dq^2.

Now Φ_k can be interpreted as the *production* phase space $P \to \{p_1, ..., p_{k-1}, q\}$ and Φ_{n-k+1} as the *decay* phase space $q \to \{p_k, ..., p_n\}$. Here it should be stated that no approximation has been made so far.

Next, we rewrite the amplitude with a scalar propagator as a product of the production (P) and decay (D) part:

$$
\mathcal{M} = \mathcal{M}_P \frac{1}{q^2 - M^2 + iM\Gamma} \mathcal{M}_D \qquad (7.5)
$$

$$
\Rightarrow |\mathcal{M}|^2 = |\mathcal{M}_P|^2 \frac{1}{(q^2 - M^2)^2 + (M\Gamma)^2} |\mathcal{M}_D|^2. \qquad (7.6)
$$

The flux factor for a scattering process $a, b \to X$ to any final state X (in particular $a, b \to c, e, f$ for the example in Fig. 7.1) is given by $F = 2\lambda^{1/2}(s, m_a^2, m_b^2)$ with the

kinematic function [111]

$$\lambda(x, y, z) := x^2 + y^2 + z^2 - 2(xy + yz + zx). \tag{7.7}$$

For a decay process $a \to X$ (for example $a \to c, e, f$), the flux factor is determined by the mass of the decaying particle, $F = 2m_a$. Then the full cross section is given as

$$\sigma = \frac{1}{F} \int d\Phi |\mathcal{M}|^2. \tag{7.8}$$

For the decomposition into production and decay, we do not only factorise the matrix elements as in Eq. (7.6). Based on Eq. (7.4), also the phase space of the full process is factorised into the production phase space Φ_P and the decay phase space Φ_D (here defined for the example process in Fig. 7.1, but they can be generalised to other external momenta), which depend on q, the momentum of the resonant particle:

$$\begin{aligned}
d\Phi &= dlips(\sqrt{s}; p_c, p_e, p_f) \\
d\Phi_P &= dlips(\sqrt{s}; p_c, q) \\
d\Phi_D &= dlips(q; p_e, p_f).
\end{aligned} \tag{7.9}$$

Then we can express the cross section in (7.8) as

$$\sigma = \frac{1}{F} \int \frac{dq^2}{2\pi} \left(\int d\Phi_P \overline{|\mathcal{M}_P|^2} \right) \frac{1}{(q^2 - M^2)^2 + (M\Gamma)^2} \left(\int d\Phi_D \overline{|\mathcal{M}_D|^2} \right). \tag{7.10}$$

In this analytical formula of the cross section, we separated the production and decay matrix elements and the sub-phase spaces from the Breit-Wigner propagator. However, the full q^2-dependence of the matrix elements and the phase space is retained. The off-shell production cross section of a scattering process with particles a, b in the initial state and the production flux factor $F_P = F = 2\lambda^{1/2}(s, m_a^2, m_b^2)$, or a decay process of particle a with flux factor $F_P = 2m_a$, reads

$$\sigma_P(q^2) = \frac{1}{F_P} \int d\Phi_P |\mathcal{M}_P(q^2)|^2. \tag{7.11}$$

The decay rate of the unstable particle, $d \to ef$, with energy $\sqrt{q^2}$ is obtained from the integrated squared decay matrix element divided by the decay flux factor $F_D = 2\sqrt{q^2}$,

$$\Gamma_D(q^2) = \frac{1}{F_D} \int d\Phi_D |\mathcal{M}_D(q^2)|^2. \tag{7.12}$$

Hence we can rewrite the full cross section from Eq. (7.10) as

$$\sigma = \int \frac{dq^2}{2\pi} \sigma_P(q^2) \frac{2\sqrt{q^2}}{(q^2 - M^2)^2 + (M\Gamma)^2} \Gamma_D(q^2). \tag{7.13}$$

Now we apply the first approximation by assuming that ΓM is small. Then the DIRAC δ-distribution can be used instead of the CAUCHY distribution

$$\frac{1}{\pi} \lim_{a \to 0} \frac{a}{a^2 + x^2} = \delta(x) \tag{7.14}$$

$$\Rightarrow \lim_{M\Gamma \to 0} \frac{1}{(q^2 - M^2)^2 + (M\Gamma)^2} = \delta(q^2 - M^2) \frac{\pi}{M\Gamma}. \tag{7.15}$$

For the integration of the δ-distribution, the integral boundaries are shifted from q_{max}^2, q_{min}^2, i.e. the upper and lower bound on q^2, respectively, to $\pm\infty$ because the contributions outside the narrow resonance region are expected to be small. So this extension of the integral should not significantly alter the result. The zero-width limit automatically implies to evaluate the production cross section, decay width and the factor $\sqrt{q^2}$ on-shell at $q^2 = M^2$. This applies both to the matrix elements and the phase space elements. The described approximation leads to the following simplification of the full cross section:

$$\sigma \overset{M\Gamma \to 0}{\to} \int\limits_{-\infty}^{+\infty} \frac{dq^2}{2\pi} \sigma_P(q^2) \, 2\sqrt{q^2} \, \delta(q^2 - M^2) \frac{\pi}{M\Gamma} \, \Gamma_D(q^2)$$

$$= \sigma_P(M^2) \cdot \frac{\Gamma_D(M^2)}{\Gamma} \equiv \sigma_P \cdot BR, \tag{7.16}$$

with the branching $BR := \frac{\Gamma_D}{\Gamma}$, where Γ_D denotes the partial decay width into the particles in the final state of the considered process, and Γ is the total decay width of the unstable particle.

Eq. (7.16) is exact in the limit $M\Gamma \to 0$. If the total width Γ is sufficiently small, it can still be used as an approximation with an error of $\mathcal{O}(\frac{\Gamma}{M})$ [115]. For the approximate treatment of finite width effects, the on-shell approximation can be applied on the matrix elements while keeping a finite width [2] in the integration over the Breit-Wigner propagator in the form of Eq. (7.13). This is motivated and justified by the consideration that the Breit-Wigner function is rapidly falling causing that only matrix elements close to the mass shell $q^2 = M^2$ contribute significantly. Bearing in mind the finite width when evaluating the matrix elements on-shell, the Breit-Wigner function is not substituted by a δ-distribution. This results in the

finite-narrow-width approximation improved for off-shell effects:

$$\sigma^{(ofs)} = \sigma_P(M^2) \left[\int \frac{dq^2}{2\pi} \frac{2\sqrt{q^2}}{(q^2 - M^2)^2 + (M\Gamma)^2} \right] \Gamma_D(M^2) \tag{7.17}$$

$$= \sigma_P(M^2) \left[\frac{i}{M\pi\Gamma} \left(\sqrt{M^2 + iM\Gamma}\, \text{arctanh} \left[\frac{\sqrt{q^2}}{\sqrt{M^2 + iM\Gamma}} \right] \right. \right.$$

$$\left. \left. - \sqrt{M^2 - iM\Gamma}\, \text{arctanh} \left[\frac{\sqrt{q^2}}{\sqrt{M^2 - iM\Gamma}} \right] \right) \right]_{q_{min}^2}^{q_{max}^2} \Gamma_D(M^2). \tag{7.18}$$

7.2. Generalised NWA for the inclusion of interference terms

If all conditions in Sect. 7.1.1 are met, the NWA works reliably within the error of $\mathcal{O}(\frac{\Gamma}{M})$. This section, however, addresses the issue how to include interference terms in the NWA [70]. Interference effects are expected to be large if there are several resonant diagrams whose intermediate particles are close in mass compared to their total decay width:

$$|M_1 - M_2| \lesssim \Gamma_1, \Gamma_2. \tag{7.19}$$

In these nearly mass-degenerate cases, the Breit-Wigner functions $\Delta_1^{BW}(q^2)$, $\Delta_2^{BW}(q^2)$ overlap strongly and an integral of the form

$$\int_{q_{min}^2}^{q_{max}^2} dq^2 \Delta_1^{BW}(q^2) \Delta_2^{*BW}(q^2) \cdot f(\mathcal{M}, p_i, ...), \tag{7.20}$$

may not just be neglected. The boundaries q_{min}^2, q_{max}^2 are the lower and upper limits of the allowed region of q^2 and f summarises a possible dependence on matrix elements $\mathcal{M}$ and momenta p_i in the phase space. Such interference effects might especially be enhanced in supersymmetric models with the enlarged particle spectrum and more possibilities for mass degeneracies in some parts of the parameter space. Let h_1, h_2 be two resonant intermediate particles, for example two Higgs bosons, with similar masses occurring in a process $ab \to cef$, i.e. $ab \to ch_i, h_i \to ef$ (cf.

Fig. 7.1 with $d = h_1, h_2$). Then the full matrix element is given by

$$
\begin{aligned}
\mathcal{M} = \quad & \mathcal{M}_{ab \to ch_1} \frac{1}{q^2 - M_1^2 + iM_1\Gamma_1} \mathcal{M}_{h_1 \to ef} + \mathcal{M}_{ab \to ch_2} \frac{1}{q^2 - M_2^2 + iM_2\Gamma_2} \mathcal{M}_{h_2 \to ef} \\
|\mathcal{M}|^2 = \quad & \frac{|\mathcal{M}_{ab \to ch_1}|^2 |\mathcal{M}_{h_1 \to ef}|^2}{(q^2 - M_1^2)^2 + M_1^2\Gamma_1^2} + \frac{|\mathcal{M}_{ab \to ch_2}|^2 |\mathcal{M}_{h_2 \to ef}|^2}{(q^2 - M_2^2)^2 + M_2^2\Gamma_2^2} \\
& + 2\mathrm{Re} \underbrace{ \left\{ \frac{\mathcal{M}_{ab \to ch_1} \mathcal{M}^*_{ab \to ch_2} \mathcal{M}_{h_1 \to ef} \mathcal{M}^*_{h_2 \to ef}}{(q^2 - M_1^2 + iM_1\Gamma_1)(q^2 - M_2^2 - iM_2\Gamma_2)} \right\} }_{\text{interference contribution}}.
\end{aligned}
\tag{7.21}
$$

So the full cross section from Eq. (7.13) with the matrix element from Eq. (7.21) can be written as

$$
\begin{aligned}
\sigma_{ab \to cef} = & \int \frac{dq^2}{2\pi} \left[\frac{\sigma_{ab \to ch_1}(q^2) \, 2\sqrt{q^2} \, \Gamma_{h_1 \to ef}(q^2)}{(q^2 - M_{h_1}^2)^2 + (M_{h_1}\Gamma_{h_1})^2} + \frac{\sigma_{ab \to ch_2}(q^2) \, 2\sqrt{q^2} \, \Gamma_{h_2 \to ef}(q^2)}{(q^2 - M_{h_2}^2)^2 + (M_{h_2}\Gamma_{h_2})^2} \right] \\
& + \int \frac{dlips(s; p_c, q) dq^2 dlips(q; p_e, p_f)}{2\pi \cdot 2\lambda^{1/2}(s, m_a^2, m_b^2)} 2\mathrm{Re} \left\{ \frac{\mathcal{M}_{ab \to ch_1} \mathcal{M}^*_{ab \to ch_2} \mathcal{M}_{h_1 \to ef} \mathcal{M}^*_{h_2 \to ef}}{(q^2 - M_1^2 + iM_1\Gamma_1)(q^2 - M_2^2 - iM_2\Gamma_2)} \right\}.
\end{aligned}
\tag{7.22}
$$

We will use Eq. (7.22) as the master formula and a starting point for approximations of this exact expression of the full cross section.

The first two terms can again be treated in the finite-narrow-width approximation according to Eq. (7.17) or summarised according to the usual narrow-width approximation in the limit of a vanishing width from Eq. (7.16) as $\sigma \times BR$. The interference term still consists of an integral over the q^2-dependent matrix elements, the product of Breit-Wigner propagators and the phase space.

7.2.1. Approximation with on-shell matrix elements

Our first approximation is to evaluate the production (P) and decay (D) matrix elements

$$
\mathcal{M}_{P_i} \equiv \mathcal{M}_{ab \to ch_i}, \quad \mathcal{M}_{D_i} \equiv \mathcal{M}_{h_i \to ef}
$$

on the mass shell of the external Higgs boson h_i. This is motivated by the assumption of a narrow resonance region $[M_{h_i} - \Gamma_{h_i}, M_{h_i} + \Gamma_{h_i}]$ so that off-shell contributions of the matrix elements in the integral are suppressed by non-resonant Breit-Wigner

factors. Then the interference term is approximated by

$$
\sigma_{int} = \int \frac{d\Phi_P dq^2 d\Phi_D}{2\pi F} 2\mathrm{Re} \left\{ \frac{\mathcal{M}_{P_1}(q^2)\mathcal{M}^*_{P_2}(q^2)\mathcal{M}_{D_1}(q^2)\mathcal{M}^*_{D_2}(q^2)}{(q^2 - M_1^2 + iM_1\Gamma_1)(q^2 - M_2^2 - iM_2\Gamma_2)} \right\} \tag{7.23}
$$

$$
= \frac{2}{F}\mathrm{Re}\left\{ \int \frac{dq^2}{2\pi} \left(\Delta_1^{BW}(q^2)\Delta_2^{*BW}(q^2) \left[\int d\Phi_P(q^2)\mathcal{M}_{P_1}(q^2)\mathcal{M}^*_{P_2}(q^2) \right] \right. \right.
$$
$$
\left. \left. \left[\int d\Phi_D(q^2)\mathcal{M}_{D_1}(q^2)\mathcal{M}^*_{D_2}(q^2) \right] \right) \right\} \tag{7.24}
$$

$$
\overset{\mathcal{M}\,os}{\approx} \frac{2}{F}\mathrm{Re}\left\{ \int \frac{dq^2}{2\pi} \left(\Delta_1^{BW}(q^2)\Delta_2^{*BW}(q^2) \left[\int d\Phi_P(q^2)\mathcal{M}_{P_1}(M_1^2)\mathcal{M}^*_{P_2}(M_2^2) \right] \right. \right.
$$
$$
\left. \left. \left[\int d\Phi_D(q^2)\mathcal{M}_{D_1}(M_1^2)\mathcal{M}^*_{D_2}(M_2^2) \right] \right) \right\}, \tag{7.25}
$$

At this stage, we have only evaluated the matrix elements on the mass shell of the particular Higgs boson (denoted by "$\mathcal{M}\,os$") by setting $q^2 = M_{h_i}^2$. But the dependence of the matrix elements on further invariants and momenta is retained. So the on-shell matrix elements can be taken out of the q^2-integral. For 2-body decays, it is possible to carry out the phase space integration without referring to the specific form of the matrix elements, as we will discuss in Sect. 8.2.3. In general, however, the matrix elements are functions of the phase space integration variables. The approximation in Eq. (7.25) is a slight simplification of the exact expression in Eq. (7.23) since the integrand of the q^2-integral is reduced. However, it is desirable to reduce the technical effort of the calculation if the agreement is still satisfactory. So we will further approximate the integral structure in the next section.

7.2.2. Approximation with on-shell phase space

On top of the on-shell approximation for matrix elements, one can also evaluate the production and decay phase spaces on-shell. This is based on the same argument as for the on-shell evaluation of the matrix elements because off-shell phase space elements are multiplied with non-resonant Breit-Wigner functions. Now the q^2-independent matrix elements and phase space integrals can be taken out of the q^2-integral, which is denoted by "$\mathcal{M}, \Phi\,os$":

$$
\sigma_{int} \overset{\mathcal{M},\Phi\,os}{\approx} \frac{2}{F}\mathrm{Re}\left\{ \left[\int d\Phi_P \mathcal{M}_{P_1}(M_1^2)\mathcal{M}^*_{P_2}(M_2^2) \right] \left[\int d\Phi_D \mathcal{M}_{D_1}(M_1^2)\mathcal{M}^*_{D_2}(M_2^2) \right] \right.
$$
$$
\left. \int \frac{dq^2}{2\pi} \Delta_1^{BW}(q^2)\Delta_2^{*BW}(q^2) \right\}. \tag{7.26}
$$

The choice at which mass, M_1 or M_2, to evaluate the production and decay phases is not unique. So we introduce a weighting factor between the two possible processes,

as an ansatz based on their production cross sections and branching ratios:

$$w_i := \frac{\sigma_{P_i} BR_i}{\sigma_{P_1} BR_1 + \sigma_{P_2} BR_2}. \tag{7.27}$$

Then we define the on-shell phase spaces as

$$d\Phi_{P/D} := w_1 d\,\Phi_{P/D}(q^2 = M_1^2) + w_2\,d\Phi_{P/D}(q^2 = M_2^2). \tag{7.28}$$

In the form of Eq. (7.26), a universal integral over the Breit-Wigner propagators emerges:

$$I := \int_{q_{min}^2}^{q_{max}^2} \frac{dq^2}{2\pi} \Delta_1^{BW}(q^2)\,\Delta_2^{*BW}(q^2)$$

$$\equiv \int_{q_{min}^2}^{q_{max}^2} \frac{dq^2}{2\pi} \left\{ \frac{1}{q^2 - M_1^2 + iM_1\Gamma_1} \cdot \frac{1}{q^2 - M_2^2 - iM_2\Gamma_1} \right\}. \tag{7.29}$$

The integral is analytically solvable,

$$I = \left[\frac{\arctan\left[\frac{\Gamma_1 M_1}{M_1^2 - q^2}\right] + \arctan\left[\frac{\Gamma_2 M_2}{M_2^2 - q^2}\right] + \frac{i}{2}\left(\ln\left[\Gamma_1^2 M_1^2 + \left(M_1^2 - q^2\right)^2\right] - \ln\left[\Gamma_2^2 M_2^2 + \left(M_2^2 - q^2\right)^2\right]\right)}{2\pi i \left(M_1^2 - M_2^2 - i(M_1\Gamma_1 + M_2\Gamma_2)\right)} \right]_{q_{min}^2}^{q_{max}^2}. \tag{7.30}$$

In the limit of equal masses and widths, $M = M_1 = M_2$ and $\Gamma = \Gamma_1 = \Gamma_2$, the product of Breit-Wigner propagators would become the absolute square, and the integral would be reduced to

$$I(M, \Gamma) = \int_{q_{min}^2}^{q_{max}^2} dq^2 \frac{1}{(q^2 - M^2)^2 + (M\Gamma)^2} = \left[-\frac{1}{M\Gamma} \arctan\left[\frac{M^2 - q^2}{M\Gamma}\right] \right]_{q_{min}^2}^{q_{max}^2}. \tag{7.31}$$

This absolute square of the Breit-Wigner function is also present in the usual NWA in Eq. (7.15), and for vanishing Γ it can be approximated by a δ-distribution. Here, however, we allow for different masses and widths from the two resonant propagators. We evaluate only the matrix elements and differential phase space on-shell, but we do not perform a zero-width approximation. This approach is analogous to the finite-narrow-width approximation without the interference term in Eq. (7.17).

7.2.3. Approximation with interference weight factors

As an additional simplification, we can try to express the interference part in terms of cross sections, branching ratios and other factors in order to avoid the explicit calculation of the product of unsquared amplitudes and their conjugates. This will also spare us the phase space integrals in the interference term as in Eq. (7.26).
For this purpose, each matrix element is written schematically as the coupling of the particular production or decay process, g_{P_i} or g_{D_i}, times the kinematic part $K_P(M_i)$ or $K_D(M_i)$, respectively,

$$\mathcal{M}_{P_i} \simeq g_{P_i} K_P(M_i), \qquad \mathcal{M}_{D_i} \simeq g_{D_i} K_{D_i}(M_i). \tag{7.32}$$

If we then assume $M_1 \simeq M_2$, the kinematical parts coincide, $K_{P/D}(M_1) \simeq K_{P/D}(M_2)$, thus the matrix elements differ just by fractions of their couplings,

$$\mathcal{M}_{P_2} = \frac{g_{P_2}}{g_{P_1}} \mathcal{M}_{P_1}, \qquad \mathcal{M}_{D_2} = \frac{g_{D_2}}{g_{D_1}} \mathcal{M}_{D_1}. \tag{7.33}$$

This enables us to replace the products of an amplitude involving the resonant particle 1 with a conjugate amplitude of resonant particle 2 by absolute squares of amplitudes as follows, where $i, j \in 1, 2$, $i \neq j$ and no summation over indices is implied:

$$\sigma_{int} \stackrel{(7.26)}{\approx} 2\mathrm{Re}\left\{ \left[\frac{1}{F} \int d\Phi_P \mathcal{M}_{P_1} \mathcal{M}_{P_2}^* \right] \left[\frac{1}{2M_i} \int d\Phi_D \mathcal{M}_{D_1} \mathcal{M}_{D_2}^* \right] 2M_i \right.$$
$$\left. \int \frac{dq^2}{2\pi} \Delta_1^{BW}(q^2) \Delta_2^{*BW}(q^2) \right\} \tag{7.34}$$

$$\stackrel{M_1 \simeq M_2}{\approx} 2\mathrm{Re}\left\{ \left[\frac{1}{F} \int d\Phi_P |\mathcal{M}_{P_i}|^2 \frac{g_{P_j}^*}{g_{P_i}^*} \right] \left[\frac{1}{2M_i} \int d\Phi_D |\mathcal{M}_{D_i}|^2 \frac{g_{D_j}^*}{g_{D_i}^*} \right] 2M_i \right.$$
$$\left. \int \frac{dq^2}{2\pi} \Delta_1^{BW}(q^2) \Delta_2^{*BW}(q^2) \right\} \tag{7.35}$$

$$\stackrel{(7.11, 7.12)}{=} \sigma_{P_i} \Gamma_{D_i} \cdot 2M_i \cdot 2\mathrm{Re}\left\{ \frac{g_{P_j}^* g_{D_j}^*}{g_{P_i}^* g_{D_i}^*} \int \frac{dq^2}{2\pi} \Delta_1^{BW}(q^2) \Delta_2^{*BW}(q^2) \right\} \tag{7.36}$$

$$= \sigma_{P_i} BR_i \cdot 2M_i \Gamma_i \cdot 2\mathrm{Re}\left\{ x_i \cdot I \right\}. \tag{7.37}$$

In the last step, we divided and multiplied by the total width Γ_i to obtain the branching ratio $BR_i = \frac{\Gamma_{D_i}}{\Gamma_i}$. The universal integral I over the overlapping Breit-Wigner propagators is given in Eq. (7.29). Furthermore, we defined a scaling factor as the ratio of couplings

$$x_i := \frac{g_{P_j}^* g_{D_j}^*}{g_{P_i}^* g_{D_i}^*} = \frac{g_{P_i} g_{P_j}^* g_{D_i} g_{D_j}^*}{|g_{P_i}|^2 |g_{D_i}|^2}. \tag{7.38}$$

Using Eq. (7.37) and the scaling factor x_i with $i = 1$, $j = 2$ or vice versa allows to express σ_{int} equivalently in terms of the cross section, branching ratio, mass and width of either the resonant particle 1 or 2. Since no summation over i or j is implied in Eq. (7.37), both contributions are accounted for by the weighting factor $w_i \in [0, 1]$ from Eq. (7.27).

Next, we summarise the components of σ_{int} apart from σ_{P_i} and BR_i, which also occur in the usual NWA, in an interference weight factor [70]

$$R_i := 2M_i \Gamma_i w_i \cdot 2\text{Re}\{x_i I\}. \tag{7.39}$$

Hence, in this approximation of on-shell matrix elements and production and decay phase spaces with the additional condition of equal masses, the interference can be written as the weighted sum

$$\sigma_{int} = \sigma_{P_1} BR_1 \cdot R_1 + \sigma_{P_2} BR_2 \cdot R_2. \tag{7.40}$$

Finally, we are able to express the cross section of the complete process, comprising the exchange of the resonant particles 1 and 2 as well as their interference, in the following compact form

$$\sigma \approx \sigma_{P_1} BR_1 \cdot (1 + R_1) + \sigma_{P_2} BR_2 \cdot (1 + R_2). \tag{7.41}$$

It is possible to replace the term $\sigma_i BR_i$ in the two separate processes without the interference term by the finite-width integral from Eq. (7.17).

7.2.4. Discussion of the steps of approximations

In the previous sections, we presented three levels of approximations for the interference term with two resonant particles. When comparing them, one should bear in mind the assumptions under which the approximations hold as well as the achievements for simplification of the computation and the costs for loss in generality.

The first approximation in Sect. 7.2.1 relies only on the on-shell evaluation of the matrix elements, justified by a narrow resonance region, but no further assumptions are implied. Different masses and finite widths are taken into account. This version requires the explicit calculation of unsquared on-shell amplitudes, preventing the use of e.g. convenient spinor trace rules. Furthermore, the phase space integration depends on q^2 so that the universal Breit-Wigner integral I from Eq. (7.29) does not appear here.

The second approximation in Sect. 7.2.2 goes beyond the first one in that it requires additionally, with the same argument as for the matrix elements, to set the differential Lorentz invariant phase spaces on-shell at either mass, scaled by a weighting factor. This makes the q^2-integration easier because only the universal integral I is left.

On the other hand, the third approximation in Sect. 7.2.3 avoids the cumbersome calculation of on-shell amplitudes in an explicit representation by expressing the interference part as an interference weight factor R in terms of cross sections, branching ratios, masses and widths, which are already needed in the simple NWA, plus the universal integral I and a scaling factor x which consists of the process-specific couplings.

Yet, this approximation holds only for equal masses. As discussed in the context of Eq. (7.20), the interference term is largest if the Breit-Wigner shapes overlap significantly due to the relation $\Delta M \lesssim \Gamma_i$. Nevertheless, the masses are not necessarily (nearly) equal in the interference region. Instead, the overlap criterion in Eq. (7.19) can as well be satisfied if one of the widths is relatively large. In this respect, the equal-mass condition goes beyond the overlap criterion.

However, the equal-mass constraint is just applied on the matrix elements, whereas different masses and widths are distinguished in the Breit-Wigner integral. The R-factor method is technically easiest to handle because the constituents of R can be obtained by standard routines in `FormCalc` and `FeynHiggs`.

All three versions can also be applied on decay rates instead of scattering cross sections. For one example process, this is done analytically in Chap. 8, and numerical results are presented in Chap. 9. An extension of the generalised narrow-width approximation to the 1-loop level for the R-factor method follows in Chap. 10.

8. Example process: neutralino decay

As a specific example, we want to discuss the decay of a heavy neutralino in this section. The concrete process under consideration is shown Fig. 8.1.

$$\tilde{\chi}_4^0 \to \tilde{\chi}_1^0 \tau^+ \tau^- : \tilde{\chi}_4^0 \to \tilde{\chi}_1^0 h/H, \ h/H \to \tau^+ \tau^-$$
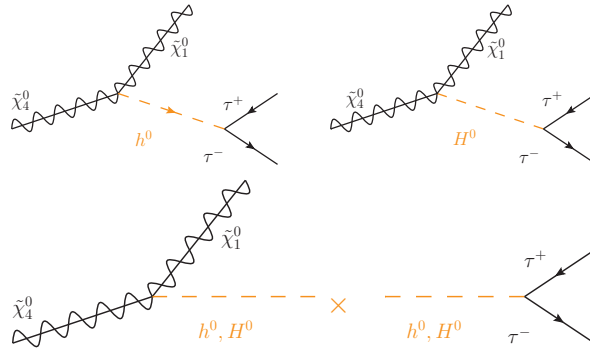
Figure 8.1.: $\tilde{\chi}_4^0 \to \tilde{\chi}_1^0 \tau^+ \tau^-$ with h or H as intermediate particle in the two interfering diagrams. The decay process is either considered as one 3-body decay or decomposed in two 2-body decays.

Assuming $\mathcal{CP}$-conservation in the MSSM with real parameters, only the two $\mathcal{CP}$-even states h, H mix instead of the 3×3-mixing of h, H, A in the complex case (see Sect. 3.5).
The decay width will be calculated both as a 3-body decay with the full matrix element and in the narrow-width approximation as a combination of two 2-body decays - with and without the interference term.

8.1. Calculation of the decay width

In this section we present the calculation of the full 3-body decay as well as the 2-body decays necessary in the simple NWA. The on-shell evaluation of matrix elements for the interference term is done in section 8.2.

Feynman rules for Majorana fermions One subtlety are the Feynman rules for Majorana fermions [116]. There is no conserved fermion number flow, so Majorana fermions do not carry arrows. Only the orientation of the momentum matters. For example, an incoming neutralino is treated as $u_s(p)$ and an outgoing one as $\bar{u}_s(p')$.

Couplings According to [117], the neutralino-Higgs couplings are (for $\tilde{\chi}_i^0 \tilde{\chi}_j^0 h_k$ with $i, j, k = 1, 2, 3, 4$ and the neutral Higgs bosons $h_{k=1,2,3,4} = \{h, H, A, G\}$)

$$C_{ijk}^R = -C_{ijk}^{L*} = \frac{ie}{2c_W \, s_W} c_{ijk}, \text{ with} \tag{8.1}$$

$$c_{ijk} = \begin{cases} (-s_\alpha N_{i3} - c_\alpha N_{i4})(s_W N_{j1} - c_W N_{j2}) + (i \leftrightarrow j), & k = 1 \\ (+c_\alpha N_{i3} - s_\alpha N_{i4})(s_W N_{j1} - c_W N_{j2}) + (i \leftrightarrow j), & k = 2 \\ (+is_\beta N_{i3} - ic_\beta N_{i4})(s_W N_{j1} - c_W N_{j2}) + (i \leftrightarrow j), & k = 3 \\ (-ic_\beta N_{i3} - is_\beta N_{i4})(s_W N_{j1} - c_W N_{j2}) + (i \leftrightarrow j), & k = 4. \end{cases}$$

Here, N is the unitary matrix which diagonalises the neutralino mass matrix Y as described in Eq. (3.24) The couplings of MSSM Higgs bosons to τ-leptons are equal to the SM coupling multiplied by the factors listed in Tab. (3.4.1):

$$C_{h\tau\tau} = +\frac{igm_\tau s_\alpha}{2M_W c_\beta} \tag{8.2}$$

$$C_{H\tau\tau} = -\frac{igm_\tau c_\alpha}{2M_W c_\beta}. \tag{8.3}$$

The couplings of the Higgs bosons h and H to neutralinos or to leptons are mixed by the Z-factors according to (4.48). From now on, the couplings $C_{h_k XY}$ always mean the mixed couplings

$$C_{h_k XY} \to \hat{\mathbf{Z}}_{h_k h_k} C_{h_k XY} + \hat{\mathbf{Z}}_{h_k h_l} C_{h_l XY}. \tag{8.4}$$

The 3-point function of the neutralino-Higgs sector at tree-level is

$$\Gamma_{\tilde{\chi}_1^0, \chi_j, h_k}^{tree} = \omega_R C_{ijk}^R \pm \omega_L C_{ijk}^L, \tag{8.5}$$

where the + applies to the $\mathcal{CP}$-even Higgs bosons h and H, whilst the - appears for the $\mathcal{CP}$-odd Higgs boson A and the Goldstone boson G.

In the case of $\mathcal{CP}$-conservation the calculation of the 3-body decay width is simplified. Real parameters in Y lead to a real matrix $\tilde{N}$ in Eq. (3.23). If all mass eigenvalues happen to be positive, then N is also a real matrix so that $C_{ijk}^R = C_{ijk}^L \equiv C_{ijk}$ for $k = 1, 2$. In this case, the γ_5-part in the coupling cancels although the γ_5-structure is present in the most general case. Yet, if the lth eigenvalue turns out to be negative, $i \neq l \neq j$, the coefficient c_{ijk} stays unaffected by the imaginary lth row of N. Thus, $C_{ijk}^R = C_{ijk}^L$ is still valid.

In our analysis, we only encountered a negative $m_{\tilde{\chi}_3}$, but the involved neutralinos are $\tilde{\chi}_1^0, \tilde{\chi}_4^0$. So the following analytical calculation makes use of the simplification discussed above whereas the general case is considered in the computation with `FormCalc`.

8.1.1. Full matrix element (3-body decay)

In this section, we calculate the amplitude and decay width of the 3-body decay, which is labelled as $p_1 \rightarrow p_2, p_3, p_4$ with $m_1 \equiv m_{\tilde{\chi}_4^0}, m_2 \equiv m_{\tilde{\chi}_1^0}, m_3 = m_4 \equiv m_\tau$.

$$
\mathcal{M}_{h_k} = iC_{h_k\tilde{\chi}_i^0\tilde{\chi}_j^0}C_{h_k\tau\tau}\bar{u}(p_4,s_4)v(p_3,s_3)\frac{1}{q^2 - M_{h_k}^2 + iM_{h_k}\Gamma_{h_k}}\bar{u}(p_2,s_2)u(p_1,s_1)
$$

$$
\overline{|\mathcal{M}_{h_k}|^2} = \frac{|C_{h_k\tilde{\chi}_1^0\tilde{\chi}_4^0}C_{h_k\tau\tau}|^2}{(q^2 - M_{h_k}^2 + iM_{h_k}\Gamma_{h_k})(q^2 - M_{h_k}^2 - iM_{h_k}\Gamma_{h_k})}\frac{1}{2}\sum_s \bar{u}_4 v_3 \bar{u}_2 u_1 \bar{u}_1 u_2 \bar{v}_3 u_4
$$

$$
= \frac{|C_{h_k\tilde{\chi}_1^0\tilde{\chi}_4^0}C_{h_k\tau\tau}|^2}{(q^2 - M_{h_k}^2)^2 + (M_{h_k}\Gamma_{h_k})^2}\frac{1}{2}\mathrm{Tr}[(\not{p}_4 + m_\tau)(\not{p}_3 - m_\tau)]\mathrm{Tr}[(\not{p}_1 + m_{\tilde{\chi}_4^0})(\not{p}_2 + m_{\tilde{\chi}_1^0})]
$$

$$
= \frac{|C_{h_k\tilde{\chi}_1^0\tilde{\chi}_4^0}C_{h_k\tau\tau}|^2}{(q^2 - M_{h_k}^2)^2 + (M_{h_k}\Gamma_{h_k})^2}8(p_3 p_4 - m_\tau^2)(p_1 p_2 + m_{\tilde{\chi}_1^0}m_{\tilde{\chi}_4^0})
$$

$$
\overline{|\mathcal{M}|^2} = \frac{1}{2}\sum_s \left(|\mathcal{M}_h|^2 + |\mathcal{M}_H|^2 + 2\mathrm{Re}[\mathcal{M}_h\mathcal{M}_H^*]\right)
$$

$$
= 8(p_1 p_2 + m_{\tilde{\chi}_1^0}m_{\tilde{\chi}_4^0})(p_3 p_4 - m_\tau^2) \tag{8.6}
$$

$$
\left(\frac{|C_{h\tilde{\chi}_1^0\tilde{\chi}_4^0}|^2|C_{h\tau\tau}|^2}{(q^2 - m_h^2)^2 + m_h^2\Gamma_h^2} + \frac{|C_{H\tilde{\chi}_1^0\tilde{\chi}_4^0}|^2|C_{H\tau\tau}|^2}{(q^2 - m_H^2)^2 + m_H^2\Gamma_H^2}\right.
$$

$$
\left. + 2\mathrm{Re}\left[C_{h\tilde{\chi}_1^0\tilde{\chi}_4^0}C_{H\tilde{\chi}_1^0\tilde{\chi}_4^0}^*C_{h\tau\tau}C_{H\tau\tau}^* \cdot \Delta_h^{BW}(q^2)\Delta_H^{*BW}(q^2)\right]\right) \tag{8.7}
$$

For Eq. (6.14) to be applicable, the products of momenta must be rewritten in terms of two combined invariant masses, here e.g. m_{23}, m_{24}.

$$
p_1 \cdot p_2 = p_2^2 + p_3 p_2 + p_4 p_2
$$

$$
= m_2^2 + \frac{1}{2}[m_{23}^2 - (m_3^2 + m_2^2)] + \frac{1}{2}[m_{24}^2 - (m_4^2 + m_2^2)] = \frac{1}{2}[m_{23}^2 + m_{24}^2] - m_\tau^2
$$

$$
p_3 \cdot p_4 = \frac{1}{2}\left[\underbrace{(p_3 + p_4)^2}_{=(p_1-p_2)^2} - p_3^2 - p_4^2\right] = \frac{1}{2}\left[m_1^2 + m_2^2 - m_{23}^2 - m_{24}^2\right]
$$

$$
q^2 = (p_1 - p_2)^2 = m_1^2 + m_2^2 - m_{23}^2 - m_{24}^2 \tag{8.8}
$$

In Eq. (6.14) $m_{bc} \equiv m_{23}, m_{cd} \equiv m_{24}$ are substituted which yield the partial width

$$\Gamma = \frac{1}{(2\pi)^3} \frac{1}{32 m_{\tilde{\chi}_4^0}^3} \int |\mathcal{M}|^2 dm_{23} dm_{24}. \tag{8.9}$$

The boundaries of the integration are defined in Eq. (6.17). The integral is solved numerically with `Mathematica`.

8.1.2. Decomposition into production and decay (2-body decays)

In this section, we calculate the 2-body decay widths of the subprocesses needed in the NWA. The matrix element for the production of $h_k = h^0, H^0$ is

$$
\begin{aligned}
\mathcal{M}_{\tilde{\chi}_4^0 \tilde{\chi}_1^0 h_k} &= i \bar{u}_2 C_{h_k \tilde{\chi}_4^0 \tilde{\chi}_1^0} u_1 \\
|\mathcal{M}_{\tilde{\chi}_4^0 \tilde{\chi}_1^0 h_k}|^2 &= |C_{h_k \tilde{\chi}_4^0 \tilde{\chi}_1^0}|^2 \frac{1}{2} \sum_{s1,s2} \bar{u}_2 u_1 \bar{u}_1 u_2 = |C_{h_k \tilde{\chi}_4^0 \tilde{\chi}_1^0}|^2 2(p_1 p_2 + m_{\tilde{\chi}_4^0} m_{\tilde{\chi}_1^0})
\end{aligned}
$$

In the rest frame of $\tilde{\chi}_4^0$ we have $p_1 p_2 = m_1 E_2$ with E_2 from Eq. (6.8). According to Eq. (6.12), the decay width of $\tilde{\chi}_4^0 \to \tilde{\chi}_1^0 h_k$ for the production of a $h_k = \{h^0, H^0\}$ is:

$$\Gamma(\tilde{\chi}_4^0 \to \tilde{\chi}_1^0 h_k) = \frac{|C_{h_k \tilde{\chi}_4^0 \tilde{\chi}_1^0}|^2}{16\pi m_{\tilde{\chi}_4^0}^3} ((m_{\tilde{\chi}_4^0} + m_{\tilde{\chi}_1^0})^2 - M_{h_k}^2) \sqrt{(m_{\tilde{\chi}_4^0}^2 - m_{\tilde{\chi}_1^0}^2 - M_{h_k}^2)^2 - 4 m_{\tilde{\chi}_1^0}^2 M_{h_k}^2} \tag{8.10}$$

A fermion couples to Higgs bosons proportionally to its mass. Thus assuming that h^0 and H^0 decay exclusively into pairs of the most massive available fermions τ and b, the total width of the Higgs is $\Gamma_{h_k} \simeq \Gamma(h_k \to \tau^+ \tau^-) + \Gamma(h_k \to b\bar{b})$. We sum over the final spins (and colours of the b).

$$\Gamma(h \to \tau\tau) = \frac{1}{\pi} |C_{h\tau\tau}|^2 \frac{\left[\frac{m_h^2}{4} - m_\tau^2\right]^{3/2}}{m_h^2}, \qquad \Gamma(H \to \tau\tau) = \frac{1}{\pi} |C_{H\tau\tau}|^2 \frac{\left[\frac{m_H^2}{4} - m_\tau^2\right]^{3/2}}{m_H^2} \tag{8.11}$$

$$\Gamma(h \to b\bar{b}) = \frac{3}{\pi} |C_{hbb}|^2 \frac{\left[\frac{m_h^2}{4} - m_b^2\right]^{3/2}}{m_h^2}, \qquad \Gamma(H \to b\bar{b}) = \frac{3}{\pi} |C_{Hbb}|^2 \frac{\left[\frac{m_H^2}{4} - m_b^2\right]^{3/2}}{m_H^2} \tag{8.12}$$

$$BR_k = \frac{\Gamma(h_k \to \tau^+ \tau^-)}{\Gamma(h_k \to \tau^+ \tau^-) + \Gamma(h_k \to b\bar{b})} \tag{8.13}$$

8.2. On-shell evaluation of unsquared matrix elements

For the calculation of the interference term according to Eq. (7.25), we need the on-shell matrix elements of the production and decay part. Instead of evaluating absolute values of squared, spin-averaged matrix elements by applying spinor traces, we now aim at expressing the unsquared matrix elements explicitly in order to evaluate them on the appropriate mass shell. Therefore, we need to represent spinors in terms of energy and mass. Following Ref. [118], a spinor with an arbitrary helicity can be written as

$$u(p) = \begin{pmatrix} \sqrt{E+m}\,\chi \\ \sqrt{E-m}\,\vec{\sigma}\cdot\vec{p}\,\chi \end{pmatrix} \tag{8.14}$$

where χ is a spinor with two components. The eigenstates of the helicity operator $\vec{\sigma}\cdot\vec{p}$ with eigenvalues $\lambda = \pm\frac{1}{2}$ can be expressed in the following way:

$$\left[\frac{1}{2}\vec{\sigma}\cdot\vec{p}\right]\chi_\lambda \overset{!}{=} \lambda\chi_\lambda \quad\Rightarrow\quad \chi_{1/2} = \begin{pmatrix} \cos\frac{\theta}{2} \\ e^{i\phi}\sin\frac{\theta}{2} \end{pmatrix}, \quad \chi_{-1/2} = \begin{pmatrix} -e^{-i\phi}\sin\frac{\theta}{2} \\ \cos\frac{\theta}{2} \end{pmatrix}. \tag{8.15}$$

For the specific choice of $\vec{p} \propto \hat{e}_z$ we have $\theta = 0$ and ϕ is arbitrary so that it can be set to 0. Thus, the 2-spinors take the simpler form

$$\chi_{1/2}(\hat{p} = \hat{e}_z) = \begin{pmatrix} 1 \\ 0 \end{pmatrix}, \qquad\qquad \chi_{-1/2}(\hat{p} = \hat{e}_z) = \begin{pmatrix} 0 \\ 1 \end{pmatrix}. \tag{8.16}$$

These are indeed eigenstates of the simplified helicity operator,

$$\left[\frac{1}{2}\vec{\sigma}\cdot\vec{p}\right]\chi_{+1/2} = \left[\frac{1}{2}\sigma_3\hat{e}_z\right]\chi_{+1/2}. = +\frac{1}{2}\chi_{+1/2} \tag{8.17}$$

$$\left[\frac{1}{2}\vec{\sigma}\cdot\vec{p}\right]\chi_{-1/2} = \left[\frac{1}{2}\sigma_3\hat{e}_z\right]\chi_{-1/2} = -\frac{1}{2}\chi_{-1/2} \tag{8.18}$$

Hence, the 4-spinor u can be written as

$$u_{+1/2}(E,0,0,p) = \begin{pmatrix} \sqrt{E+m}\begin{pmatrix}1\\0\end{pmatrix} \\ \sqrt{E-m}\begin{pmatrix}1\\0\end{pmatrix} \end{pmatrix}, \quad u_{-1/2}(E,0,0,p) = \begin{pmatrix} \sqrt{E+m}\begin{pmatrix}0\\1\end{pmatrix} \\ -\sqrt{E-m}\begin{pmatrix}0\\1\end{pmatrix} \end{pmatrix}. \tag{8.19}$$

8.2.1. Higgs production

In order to obtain the spin-averaged matrix element of the 2-body neutralino decay $\mathcal{M}_{\tilde{\chi}_4^0 \tilde{\chi}_1^0 h} \equiv \mathcal{M}(\tilde{\chi}_4^0 \to \tilde{\chi}_1^0 h)$, we need to compute the spinor products $\bar{u}_{\lambda_2}^h(p_2) \cdot u_{\lambda_1}(p_1)$ for all combinations of $\lambda_1, \lambda_2 = \pm 1/2$.

$$
\bar{u}_{2,+} u_{1,+} = \left(\begin{pmatrix} \sqrt{E_2 + m_2} \begin{pmatrix} 1 \\ 0 \end{pmatrix} \\ \sqrt{E_2 - m_2} \begin{pmatrix} 1 \\ 0 \end{pmatrix} \end{pmatrix} \right)^{*T} \begin{pmatrix} 1 & & \\ & 1 & \\ & & -1 \\ & & & -1 \end{pmatrix} \begin{pmatrix} \sqrt{E_1 + m_1} \begin{pmatrix} 1 \\ 0 \end{pmatrix} \\ \sqrt{E_1 - m_1} \begin{pmatrix} 1 \\ 0 \end{pmatrix} \end{pmatrix}
$$

$$
= \sqrt{(E_2 + m_2)(E_1 + m_1)} - \sqrt{(E_2 - m_2)(E_1 - m_1)}
$$

$$
\bar{u}_{2,-} u_{1,-} = \left(\begin{pmatrix} \sqrt{E_2 + m_2} \begin{pmatrix} 0 \\ 1 \end{pmatrix} \\ -\sqrt{E_2 - m_2} \begin{pmatrix} 0 \\ 1 \end{pmatrix} \end{pmatrix} \right)^{*T} \begin{pmatrix} 1 & & \\ & 1 & \\ & & -1 \\ & & & -1 \end{pmatrix} \begin{pmatrix} \sqrt{E_1 + m_1} \begin{pmatrix} 0 \\ 1 \end{pmatrix} \\ -\sqrt{E_1 - m_1} \begin{pmatrix} 0 \\ 1 \end{pmatrix} \end{pmatrix}
$$

$$
= \sqrt{(E_2 + m_2)(E_1 + m_1)} - \sqrt{(E_2 - m_2)(E_1 - m_1)} \equiv \bar{u}_{2,+} u_{1,+} \tag{8.20}
$$

The mixed products, however, vanish: $\bar{u}_{2,-} u_{1,+} = \bar{u}_{2,+} u_{1,-} = 0$. With $\tilde{\chi}_4^0$ at rest, hence $E_1 = m_{\tilde{\chi}_4^0}$, we can insert the kinematic relations of the 2-body decay $\tilde{\chi}_4^0 \to \tilde{\chi}_1^0 h$:

$$
E_2 \equiv E_2^h = \frac{m_{\tilde{\chi}_4^0}^2 + m_{\tilde{\chi}_1^0}^2 - M_h^2}{2 m_{\tilde{\chi}_4^0}} \tag{8.21}
$$

This yields the averaged on-shell matrix element

$$
\overline{\mathcal{M}_{\tilde{\chi}_4^0 \tilde{\chi}_1^0 h}} = i C_{h \tilde{\chi}_1^0 \tilde{\chi}_4^0} \frac{1}{2} \sum_{\lambda_1, \lambda_2} \bar{u}_{\lambda_2}^h(p_2) \cdot u_{\lambda_1}(p_1)
$$

$$
= i C_{h \tilde{\chi}_1^0 \tilde{\chi}_4^0} \sqrt{\left(\frac{m_{\tilde{\chi}_4^0}^2 + m_{\tilde{\chi}_1^0}^2 - M_h^2}{2 m_{\tilde{\chi}_4^0}} + m_{\tilde{\chi}_1^0} \right) \cdot 2 m_{\tilde{\chi}_4^0}}
$$

$$
= i C_{h \tilde{\chi}_1^0 \tilde{\chi}_4^0} \sqrt{(m_{\tilde{\chi}_1^0} + m_{\tilde{\chi}_4^0})^2 - M_h^2}. \tag{8.22}
$$

Analogously, the result for the 2-body decay on-shell matrix element for H-production reads

$$
\mathcal{M}_{\tilde{\chi}_4^0 \tilde{\chi}_1^0 H} = i C_{H \tilde{\chi}_1^0 \tilde{\chi}_4^0} \sqrt{(m_{\tilde{\chi}_1^0} + m_{\tilde{\chi}_4^0})^2 - M_H^2}. \tag{8.23}
$$

8.2.2. Higgs decay

In the 2-body decay $h_k \to \tau^+ \tau^-$ we also need an explicit representation of antiparticles. With the charge conjugation operator $C = i\gamma_0\gamma_2$, the spinor of the antiparticle, v, can be expressed as

$$v(p) = C\bar{u}^T(p) = i\gamma_0\gamma_2 \left(u(p)^\dagger \gamma_0\right)^T = -i\gamma_0^2\gamma_2 u^*(p)$$

$$= \begin{pmatrix} & & & -1 \\ & & 1 & \\ & 1 & & \\ -1 & & & \end{pmatrix} \begin{pmatrix} +\sqrt{E-m}\,\chi_\lambda \\ -2\lambda\sqrt{E+m}\,\chi_\lambda \end{pmatrix}$$

$$\Rightarrow v_{+1/2}(E,0,0,p) = \begin{pmatrix} \sqrt{E-m}\begin{pmatrix}0\\1\end{pmatrix} \\ -\sqrt{E+m}\begin{pmatrix}0\\1\end{pmatrix} \end{pmatrix}, \quad v_{-1/2}(E,0,0,p) = \begin{pmatrix} \sqrt{E-m}\begin{pmatrix}1\\0\end{pmatrix} \\ \sqrt{E+m}\begin{pmatrix}1\\0\end{pmatrix} \end{pmatrix}.$$

$$(8.24)$$

For the summation over all spin combinations in the final state, we calculate the products $\bar{u}_{\lambda_4}(p_4) \cdot v_{\lambda_3}(p_3)$:

$$\bar{u}_{4,+}v_{3,+} = \begin{pmatrix} \sqrt{E_4+m_4}\begin{pmatrix}1\\0\end{pmatrix} \\ \sqrt{E_4-m_4}\begin{pmatrix}1\\0\end{pmatrix} \end{pmatrix}^{*T} \begin{pmatrix} & & & -1 \\ & & 1 & \\ & 1 & & \\ -1 & & & \end{pmatrix} \begin{pmatrix} \sqrt{E_1+m_1}\begin{pmatrix}0\\1\end{pmatrix} \\ \sqrt{E_1-m_1}\begin{pmatrix}0\\1\end{pmatrix} \end{pmatrix} = 0 = \bar{u}_{4,-}v_{3,-}$$

$$\bar{u}_{4,+}v_{3,-} = \sqrt{(E_4+m_4)(E_3-m_3)} + \sqrt{(E_4-m_4)(E_3+m_3)} = \bar{u}_{4,-}v_{3,+}. \qquad (8.25)$$

Thus, only the mixed spin combinations contribute here. Inserting $m_3 = m_4 = m_\tau$ and the energy of one of the Higgs bosons $E_3 = E_4 = \frac{M_h}{2} =: E$ from h decaying at rest, we obtain the averaged matrix element,

$$\overline{\mathcal{M}_{h\tau\tau}} = iC_{h\tau\tau} \sum_{\lambda_1,\lambda_2} \bar{u}_{\lambda_2}^h(p_2) \cdot u_{\lambda_1}(p_1)$$

$$= 2iC_{h\tau\tau} \cdot 2\sqrt{(E+m_\tau)(E-m_\tau)} = 4iC_{h\tau\tau}\sqrt{\frac{M_h^2}{4} - m_\tau^2}. \qquad (8.26)$$

Accordingly, the averaged matrix element for the decay of the H-boson is obtained:

$$\overline{\mathcal{M}_{H\tau\tau}} = 4iC_{H\tau\tau}\sqrt{\frac{M_H^2}{4} - m_\tau^2}.$$

Finally, the product of the on-shell matrix elements reads

$$
\mathcal{M}_{\tilde{\chi}_4^0 \tilde{\chi}_1^0 h}\, \mathcal{M}_{\tilde{\chi}_4^0 \tilde{\chi}_1^0 H}^*\, \mathcal{M}_{h\tau\tau}\, \mathcal{M}_{H\tau\tau}^* = C_{41h}^*\, C_{41h}^*\, C_{h\tau\tau}\, C_{H\tau\tau}^* \cdot
$$
$$
4\sqrt{((m_{\tilde{\chi}_1^0} + m_{\tilde{\chi}_4^0})^2 - M_h^2)((m_{\tilde{\chi}_1^0} + m_{\tilde{\chi}_4^0})^2 - M_H^2)(M_h^2 - 4m_\tau^2)(M_H^2 - 4m_\tau^2)}.
$$
(8.27)

8.2.3. Interference term

In this section we want to apply the methods from Sect. 7.2 to approximate the interference term on-shell in three steps.

Method of on-shell matrix elements The first step is the on-shell evaluation of the production and decay matrix elements according to Eq. (7.25). In the rest frame of m_{34}^2, i.e. $q = p_3 + p_4 = p_1 - p_2$ as in Sect. 8.1.1, we choose m_{24}^2 as the other independent invariant mass square for the parametrisation of the phase space integration. Its bounds of integration $m_{24,min/max}^2(q^2)$ are then functions of $q^2 = m_{34}^2$ and given by Eq. (6.16). As justified in Sect. 7.2.1, we take the on-shell matrix elements out of the q^2-integral and obtain the following approximation of Eq. (8.9) for the interference term:

$$
\sigma_{int} \simeq \frac{1}{(2\pi)^3\, 32 M^3} 2\mathrm{Re}\left\{ [\mathcal{M}_{\tilde{\chi}_4^0 \tilde{\chi}_1^0 h}\mathcal{M}_{h\tau\tau}]_{M_h^2} [\mathcal{M}_{\tilde{\chi}_4^0 \tilde{\chi}_1^0 H}\mathcal{M}_{H\tau\tau}]_{M_H^2} \right.
$$
$$
\left. \int\limits_{(m_3+m_4)^2}^{(m_1-m_2)^2} dq^2 \int\limits_{m_{24,min}^2(q^2)}^{m_{24,max}^2(q^2)} dm_{24}^2\, \Delta^{BW}(q^2)\Delta^{*BW}(q^2) \right\}.
$$
(8.28)

Method of on-shell phase space The factorised 3-body phase space for the process $p_1 \rightarrow p_2, p_3, p_4$ is given by

$$
d\Phi_3(p_1 \rightarrow p_2, p_3, p_4) = d\Phi_P(p_1 \rightarrow p_2, q) \frac{dq^2}{2\pi} d\Phi_D(q \rightarrow p_3, p_4)
$$
$$
= \frac{1}{4\pi} \frac{|\vec{p}_2|}{m_1} \frac{d\Omega_P}{4\pi} \frac{dq^2}{2\pi} \frac{1}{4\pi} \frac{|\vec{p}_3|}{\sqrt{q^2}} \frac{d\Omega_D}{4\pi}.
$$
(8.29)

In 2-body decays, the momenta are determined by the relations in Sect. 6.2, and in our process $m_3 = m_4$ leads to a simplification of the decay phase space:

$$
|\vec{p}_2|^2 = \frac{\sqrt{(m_1^2 - (\sqrt{q^2} + m_2)^2)(m_1^2 - (\sqrt{q^2} - m_2)^2)}}{2m_1}
$$
(8.30)

$$
|\vec{p}_3|^2 = \frac{\sqrt{(q^2 - (m_3 + m_4)^2)(q^2 - (m_3 - m_4)^2)}}{2\sqrt{q^2}} \stackrel{m_3 = m_4}{=} \frac{\sqrt{(q^2 - 4m_3^2)}}{2}
$$
(8.31)

The phase space can also be evaluated on the mass shell of one of the Higgs bosons, see Sect. 7.2.2. Since the choice is not unique, both possibilities are taken into account in the weighted phase space according to Eq. (7.27),

$$d\Phi = w_h \, d\Phi(M_h^2) + w_H \, d\Phi(M_H^2). \tag{8.32}$$

Method of interference weight factors   Using the definition of the interference weight factor in Eq. (7.39) and considering that we are not calculating a cross section, but a partial width, Eq. (7.41) becomes

$$\Gamma_{\tilde{\chi}_4^0 \to \tilde{\chi}_1^0 \tau^+ \tau^-} \simeq \Gamma_{\tilde{\chi}_4^0 \to \tilde{\chi}_1^0 h} BR_{h \to \tau^+ \tau^-} (1 + R_h) + \Gamma_{\tilde{\chi}_4^0 \to \tilde{\chi}_1^0 H} BR_{H \to \tau^+ \tau^-} (1 + R_H). \tag{8.33}$$

We found agreement between our analytical calculation and the 2- and 3-body decays computed by `FormCalc`. In the next chapter we will present numerical results for the full calculation and the generalised narrow-width approximation applied to the discussed neutralino decay at tree-level. Vertex corrections will be discussed in Chap. 10.

9. Numerical results for the generalised NWA at tree-level

In this chapter we will analyse in which parameter regions interference effects between the neutral $\mathcal{CP}$-even Higgs bosons h^0, H^0 are relevant. The calculation of the separate contribution of both Higgs bosons to the full processes, as well as the interference term considered as a full 3-body decay, are compared to the generalised NWA in order to investigate its validity, accuracy and limitations.

In Sect. 9.1 we define the scenario of parameters chosen for the numerical analysis. Next, the method of our computation is described in Sect. 9.2. The following Sect. 9.3 contains a discussion of the dependence of the decay width on the Higgs sector parameters $M_{H^\pm}$ and $\tan\beta$, and on M_1 from the neutralino sector. In the subsequent Sect. 9.4, the accuracy of the simple and generalised narrow-width approximation is analysed with respect to the full 3-body decay width. In this context, the ratio between the difference of the two Higgs masses and the maximum of both total widths serves as a control parameter for the size of the interference term.

9.1. Scenario

The aim here is not to determine the parameters which are most likely realised in nature[1], but to provide a setting in which interference effects between h and H become large in order to investigate the performance of the generalised narrow-width approximation.

The m_h^{max} scenario is defined such that the loop corrections to the mass M_h in Eq. (3.15) reach their maximum for fixed $\tan\beta$ and M_A. This requires a large SUSY breaking scale $M_{SUSY} = \sqrt{m_{\tilde{t}_1} m_{\tilde{t}_2}}$ and a large stop mixing of $X_t = \sqrt{6}M_S$ at 1-loop level or $X_t = 2M_S$ at 2-loop level. How close the masses M_h and M_H get, is already influenced by parameters that enter at tree-level, such as a rather light pseudoscalar Higgs boson or equivalently a light charged Higgs boson, so a low M_{A^0} or $M_{H^\pm}$, and a high value of $\tan\beta$. On the other hand, $\tan\beta$ must not be chosen too large because otherwise the bottom Yukawa couplings would be enhanced so strongly that they would render perturbation theory unreliable.

However, the m_h^{max} scenario does not necessarily lead to a minimal difference of M_H

---

[1]Although in our scenario the Higgs masses are $M_h \simeq 126\,\mathrm{GeV}$ and $M_H \simeq 127\,\mathrm{GeV}$ in the interference region, i.e. close to the excess observed by ATLAS[14] and CMS[15].

and M_h if the loop corrections to M_H turn out to be large as well. So we work in a m_h^{max}-like scenario where M_h is as close to M_H as possible at the cross-over point, potentially within the total width.

For a later extension to $\mathcal{CP}$-violating mixings we choose $M_H^{\pm}$ instead of M_A, which is more commonly used in the MSSM without complex phases, as one of the Higgs sector input parameters, fixed at 153 GeV or scanned over in Sect. 9.3.1. If not varied as in Sect. 9.3.2, we set $\tan \beta = 50$. The gaugino parameters M_1 and M_2 are treated independently, no GUT relation is assumed. M_1 is varied in Sect. 9.3.3 or fixed at 100 GeV otherwise.

We set $M_S = 1$ TeV and assume universal trilinear couplings

$$A_f = A_t = |X_t + \mu \cot \beta|.$$

We work in the MSSM with real parameters, hence all complex phases vanish. For an overview, the parameter values are listed in Tab. 9.1.

Table 9.1.: Parameter settings in the numerical analysis. Values in brackets indicate that these parameters are varied otherwise.

M_1	M_2	M_3	M_{SUSY}	X_t	μ	$M_{H^{\pm}}$	t_{β}
(100 GeV)	200 GeV	800 GeV	1 TeV	2.5 TeV	200 GeV	(153 GeV)	(50)

9.2. Method

The following results are produced using `FeynArts, FormCalc` and `FeynHiggs` (see Chap. 5). We incorporated the Z-factors into the MSSM model file by modifying the couplings of the Higgs bosons to particles $X, Y = \tilde{\chi}_4^0, \tilde{\chi}_1^0$ or τ^+, τ^- according to Eq. (8.4). The Higgs masses, widths and Z-factors are calculated by `FeynHiggs` and the width is added by hand to the tree-level propagator in the 3-body calculation following the fixed-width scheme. A running width is not considered here.

For the NWA, `FeynArts` and `FormCalc` generate the production 2-body process $\Gamma(\tilde{\chi}_4^0 \to \tilde{\chi}_1^0 h_k)$ and the 2-body decay $\Gamma(h_k \to \tau^+\tau^-)$ at tree-level with all external particles on-shell. Finally, the product of both 2-body widths is divided by $\Gamma_{h_k}^{tot}$ obtained from `FeynHiggs`.

The interference term is calculated separately in three different versions according to Eqs. (8.28), (8.32) and (8.33) with the matrix elements derived in Sect. 8.2. The inserted couplings are obtained from `FeynHiggs` at tree-level, but mixed by the 2-loop Z-factors. Also the masses and widths in the interference term are evaluated at 2-loop level using `FeynHiggs`. So in order to ensure a consistent treatment of the branching ratios and decay widths in the calculation of a 3-body decay and the NWA,

one cannot just use the 2-loop corrected branching ratios available in `FeynHiggs` because the corresponding $h_k\tau^+\tau^-$ vertex in the 3-body decay does not include corrections. Moreover, for a consistent comparison between the full process with an intermediate Higgs boson and the on-shell approximation split into production and decay, Z-matrices are also invoked in the former case although they formally only apply to external Higgs bosons whereas internal Higgs bosons are mixed by an analogous U-matrix. But in the analysis of the final result, the effects from the different application of U- or Z-factors could not be disentangled from effects of the NWA. Hence, Z-factors are applied in either case, keeping in mind that actually the Higgs bosons are no external particles in the 3-body decay.

9.3. Parameter dependence of the interference term

The approach of this section is to first examine the dependence of the Higgs masses and total widths on the respective parameter and to identify the interval in which $\Delta M \equiv M_H - M_h \leq max\{\Gamma_h, \Gamma_H\}$. Here the overlap of the two Breit-Wigner propagators is large so that a significant interference term is expected. Second, the narrow-width approximation for $\tilde{\chi}_4^0 \to \tilde{\chi}_1^0\tau^+\tau^-$ is confronted with the full calculation of this process. To be precise, this is done in three parts, namely the contribution of either Higgs exchange to the process as well as the interference term. While the interference term is present in the full calculation and in the generalised narrow-width approximation, it is neglected in the simple narrow-width approximation. The dependence of the numerical size of the interference term on several parameters from different sectors is investigated. A large interference term can be attributed to a small mass difference compared to the total width.

9.3.1. Dependence on $M_{H^\pm}$

The left plot in Fig. 9.1 shows the predictions for the masses of h^0 (in light blue) and of H^0 (in dark blue) as functions of the charged Higgs mass, computed with `FeynHiggs` including corrections at the 2-loop level. While $M_H \simeq 127\,\text{GeV}$ is nearly constant up to $M_{H^\pm} = 153\,\text{GeV}$, it increases for larger values of $M_{H^\pm}$. M_h approaches $126.5\,\text{GeV}$ from below. The difference between the two Higgs masses, which is shown as the red line in the plot on the right-hand side of Fig. 9.1, reaches a minimum of $\Delta M_{hH} \equiv M_H - M_h \simeq 2\,\text{GeV}$ at around $M_{H^\pm} = 153\,\text{GeV}$. This mass splitting is even less than one of the total widths Γ_h, Γ_H (in light/ dark blue) in the interval of $150\,\text{GeV} \lesssim M_{H^\pm} \lesssim 156\,\text{GeV}$. So we will focus on this parameter interval in the investigation of the interference term. Around $M_{H^\pm} \simeq 153\,\text{GeV}$, there is a cross-over of h, H, i.e. they change their character, leading to a swap of the state that couples SM-like.

Fig. 9.2 shows the full result of the decay width $\Gamma(\tilde{\chi}_4^0 \overset{h,H}{\to} \tilde{\chi}_1^0\tau^+\tau^-)\hat{=}|h + H|^2$. This
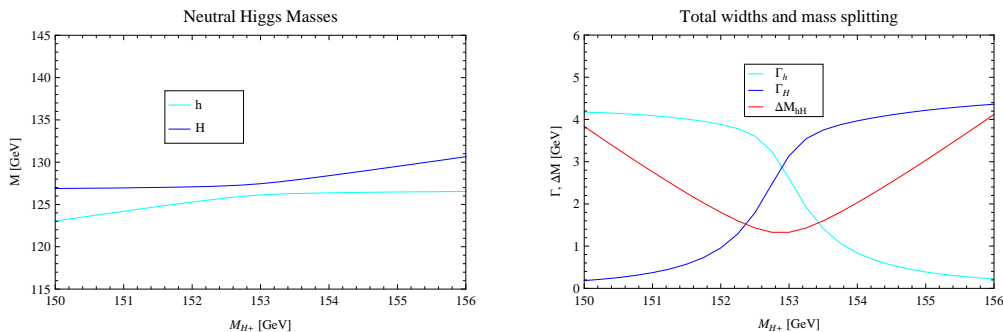
Figure 9.1.: **Left:** The masses of the neutral, $\mathcal{CP}$-even Higgs bosons M_h, M_H in light/ dark blue as a function of $M_{H^\pm}$, calculated by `FeynHiggs` at the 2-loop level for $\tan\beta = 50$ and $M_1 = 100\,\text{GeV}$ fixed. **Right:** The total widths Γ_h, Γ_H (blue) depending on $M_{H^\pm}$ are compared to the mass difference $\Delta M_{hH} = M_H - M_h$ in red. The region where the red line lies below one of the widths is most relevant for interference effects.

shall be approximated by the NWA. First, the simple NWA (sNWA) in orange is composed of the *incoherent* sum

$$\Gamma(\tilde\chi_4^0 \xrightarrow{h} \tilde\chi_1^0 \tau^+\tau^-) + \Gamma(\tilde\chi_4^0 \xrightarrow{H} \tilde\chi_1^0 \tau^+\tau^-) \hat{=} |h|^2 + |H|^2, \qquad (9.1)$$

where the contribution from h is represented by the light blue line and H by the dark blue one. Solid lines and "3" denote the calculation as a 3-body decay width whereas dashed lines and "2" stand for the factorisation of the process into the on-shell production of one of the Higgs bosons from a 2-body decay and its subsequent 2-body decay.

Confronting Fig. 9.1 (right) with 9.2 reveals that the contribution from h dominates if $\Gamma_h < \Gamma_H$ (for $M_{H^\pm} \gtrsim 153\,\text{GeV}$) and vice versa. The reason is that a large total width suppresses either the Breit-Wigner propagator $\Delta_{h_k}^{BW} = \frac{1}{q^2 - M_{h_k}^2 + iM_{h_k}\Gamma_{h_k}}$ in the 3-body calculation or in the branching ratio $BR = \frac{\Gamma(h_k \to \tau^+\tau^-)}{\Gamma_{h_k}}$. The comparison between the dashed and solid lines for h and H each serves as a consistency check of the usual NWA before dealing at all with the interference effects because here both processes are treated separately. If also the other four conditions from Chap. 7.1.1 hold, the NWA should agree with the $1 \to 3$ decay to $\mathcal{O}\left(\frac{\Gamma_{h_k}}{M_{h_k}}\right) \le 4\%$. The widths are small enough compared to the masses, and the scalar propagator is separable from the matrix elements. Besides, our scenario is far away from the production and decay threshold since $M_{h_k} \gg 2m_\tau$ holds independently of the parameters, and with neutralino masses of $m_{\tilde\chi_4^0} \simeq 264.9\,\text{GeV}$ and $m_{\tilde\chi_1^0} \simeq 92.6\,\text{GeV}$, also $m_{\tilde\chi_4^0} - (m_{\tilde\chi_4^0} + M_{h_k}) > 32\,\text{GeV}$ does not violate the condition. The neutralino masses are independent of $M_{H^\pm}$.
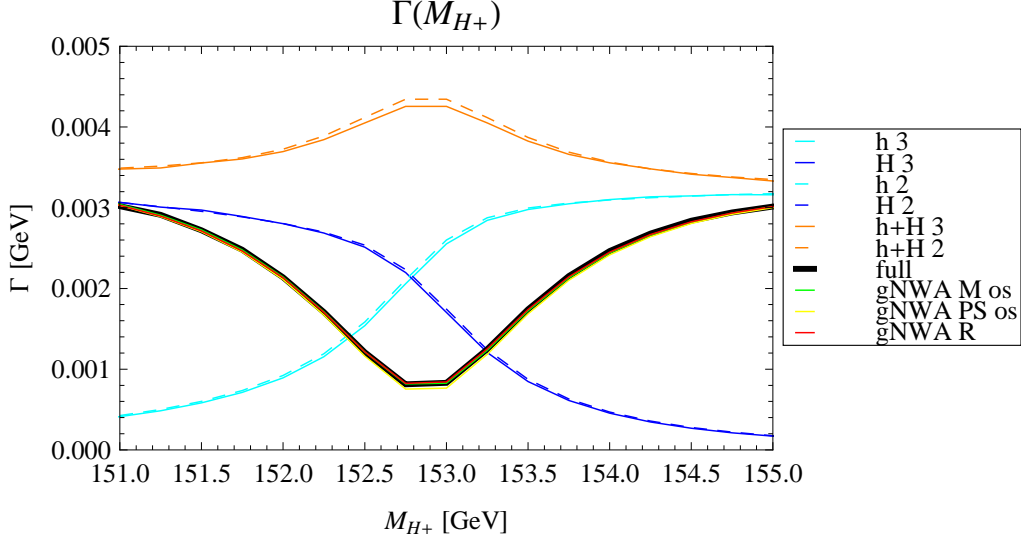
Figure 9.2.: The decay width $\Gamma(\tilde{\chi}_4^0 \to \tilde{\chi}_1^0 \tau^+ \tau^-)$ as a function of $M_{H^\pm}$ with $\tan\beta = 50$, $M_1 = 100\,\text{GeV}$. The full 3-body decay width (represented by the thick black line) consists of three summands: the contribution from h (light blue) and H (dark blue) and the interference term. The *incoherent* sum of $|h|^2 + |H|^2$ (orange), i.e. the sNWA, does not contain the interference term and deviates strongly from the full result. The gNWA (green, yellow, red) takes the interference into account and approximates the full result significantly better. The green line represents the on-shell evaluation of the matrix elements in the interference term. On top of this on-shell approximation, the yellow line stands for a constant phase space factor in the interference term. The red curve is based on the R-factor method. 3 denotes a 3-body calculation (solid lines), whereas 2 stands for the decomposition into two 2-body decays (dashed).

Thus, the NWA is applicable for the individual contributions of h and H. Nevertheless, the slight deviation of the dashed from the solid lines indicates that the 2- and 3-body calculations do not exactly agree. This can be seen in the difference between the dashed and solid blue lines for the contribution of h and H and their sum in orange. However, as we will further investigate in Sect. 9.4, this inaccuracy does not exceed Γ_{h_k}/M_{h_k}, thus it lies within the expected error of the NWA. In the later discussion of the relative accuracy of the NWA, we distinguish between several sources for the slight deviation of the final result from the full 3-body decay width. Already here we want to state that one part of it is due to the inaccuracy of the NWA itself even before the inclusion of the interference term.

approximation (dashed orange line) does not approximate the incoherent sum of the two 3-body decays perfectly. In the later discussion of the relative accuracy

of the NWA in Sect. 9.4 we distinguish between several sources for the slight deviation of the final result. Already here we want to state that one part of it is due to the inaccuracy of the NWA itself even before the inclusion of the interference term.

Improvement by the generalised NWA   Apart from this inspection of the partial decay rates involving h or H only, Fig. 9.2 also demonstrates how the simple NWA is limited by interference effects. The discrepancy between the sNWA and the full result (orange and thick black line) is enormous especially around $M_{H^\pm} \simeq 153\,\mathrm{GeV}$ and also throughout the plotted interval where ΔM_{hH} is below one of the total widths. In the centre of the analysed interval, the simple NWA overestimates the full result by over 100% because h and H interfere destructively resulting in a negative interference term. This points out the importance of including the interference in a generalised NWA.

Towards the boundaries of the considered interval, the interference effects decrease with the growing mass difference compared to the total width as shown in Fig. 9.1. The mass difference ΔM_{hH} is large compared to the widths Γ_h, Γ_H outside the interval shown in the plot so that the interference term is small so that the sNWA approximates the full result sufficiently well.

The green line shows the gNWA as the sum of the sNWA and that version of the approximated interference term in which the matrix elements are evaluated on-shell, but the phase space dependence on the momentum transfer q^2 is kept as in Eq. (7.25). In contrast, a weighted on-shell phase space factor is used for the approximation of the interference term in the gNWA according to Eq. (7.26), denoted by the yellow line. The red line represents the gNWA based on the R-factor method in Eq. (7.40). The numerical difference between the three versions of the gNWA are found to be small. All of them are in excellent agreement with the full result, in contrast to the sNWA, even in the region of the largest interference term. The relative deviations, investigating the individual contributions from h, H and the interference term, are quantified in Sect. 9.4.

Summarising the $M_{H^\pm}$-dependence, we observe that the simple NWA is insufficient in the parameter interval of $M_{H^\pm}$ where ΔM_{hH} is exceeded by the total widths of one of the Higgs bosons because the occurring interference effect violates one of the conditions for the NWA. This is cured by the generalised NWA.

9.3.2. Dependence on $\tan\beta$

After the analysis of the $M_{H^\pm}$-dependence, we will now discuss in a similar way which impact $\tan\beta$ has on the Higgs masses and widths and on the interference term. Therefore Fig. 9.3 shows M_h and M_H as a function of $\tan\beta$ as well as their difference and the total widths Γ_h, Γ_H. Given that the mass difference ΔM_{hH} decreases towards larger values of $\tan\beta$ and lies below one of the widths only for

Figure 9.3.: **Left:** Predictions for the masses M_h, M_H of the neutral, $\mathcal{CP}$-even Higgs bosons in light/ dark blue as a function of $\tan\beta$ from `FeynHiggs`, incorporating 2-loop corrections, for $M_{H^\pm} = 153\,\text{GeV}$ and $M_1 = 100\,\text{GeV}$ fixed. **Right:** The total widths Γ_h, Γ_H (blue) depending on $\tan\beta$ in comparison to the mass difference $\Delta M_{hH} = M_H - M_h$ in red. The region where the red line is close to or below one of the widths is most relevant for interference effects.

Figure 9.4.: The decay width $\Gamma(\tilde{\chi}_4^0 \to \tilde{\chi}_1^0 \tau^+ \tau^-)$ as a function of $\tan\beta$ with $M_{H^\pm} = 153\,\text{GeV}$, $M_1 = 100\,\text{GeV}$. The single contributions from h and H are shown as 3-body decays and in the NWA. The full 3-body decay taking h- and H-exchange into account is compared to the simple and generalised NWA in its different versions. Including the negative interference term, the gNWA is close to the full result. Colour code as in Fig. 9.2.

$\tan\beta \gtrsim 43$, there are no significant interference effects between h and H at low $\tan\beta$ in the $\mathcal{CP}$-conserving case. However, $\tan\beta$ is limited from above by perturbativity of the bottom Yukawa coupling, so we do not take any $\tan\beta > 50$ into account. In the MSSM with complex parameters, a significant interference between

H and *A* could be possible at lower $\tan\beta$, though. But here we consider the MSSM with real parameters.

In Fig. 9.4 the dependence of the decay width $\Gamma(\tilde{\chi}_4^0 \to \tilde{\chi}_1^0 \tau^+ \tau^-)$ on $\tan\beta$ is shown. The colour code is the same as in Fig. 9.1, so the light and dark blue lines represent the individual contributions of *h* and *H*, respectively. The difference between the simple NWA (dashed orange) and the full result (black) shows the negative interference term. Its approximations are included in the generalised NWA (green, yellow and red corresponding to on-shell matrix elements, an on-shell phase space factor and the R-factor method, respectively, as defined in Sect. 7.2) yielding a result comparable to the full 3-body decay. A discussion of the relative accuracy follows in Sect. 9.4.

Inspecting Fig. 9.2 and 9.4, we can state that the size of the interference term depends strongly on the input parameters of the Higgs sector because the difference of M_h and M_H is small compared to the widths only in a certain parameter region. The interference term is of the order of 100% if both propagators become resonant and approaches zero for an increasing mass splitting. Yet, independently of the analysed parameters, the interference is destructive.

9.3.3. Dependence on M_1

Due to the external neutralinos, we also analyse the dependence on M_1, a parameter from the neutralino sector. Varying M_1 from 50 to 140 GeV alters the neutralino masses from $m_{\tilde{\chi}_1^0} = 47.1$ GeV to 122.7 GeV and $m_{\tilde{\chi}_4^0} = 264.1$ GeV to 266.1 GeV, and changes therefore the kinematics, but it leaves the masses and widths of *h* and *H* essentially constant, see Fig. 9.5. By fixing $M_{H^\pm} = 153$ GeV and $\tan\beta = 50$, the parameter configuration remains in a scenario where the total widths of both Higgs bosons are rather large and $\Delta M_{hH} < \Gamma_h, \Gamma_H$. So the interference effect is important throughout the scan of M_1.

Fig. 9.6 shows the decay width $\Gamma(\tilde{\chi}_4^0 \to \tilde{\chi}_1^0 \tau^+ \tau^-)$ depending on M_1. The contributions from *h* and *H* shown in light and dark blue are quite precisely approximated by the NWA (dashed). The remaining deviations correspond to that one in the interference region of Fig. 9.2. Their sum contributes to the difference between the simple NWA (dashed orange) and the incoherent sum of the 3-body decays $\Gamma(\tilde{\chi}_4^0 \xrightarrow{h} \tilde{\chi}_1^0 \tau^+ \tau^-) + \Gamma(\tilde{\chi}_4^0 \xrightarrow{H} \tilde{\chi}_1^0 \tau^+ \tau^-)$ which is still of $\mathcal{O}\left(\frac{\Gamma_{h_k}}{M_{h_k}}\right)$.

However, comparing the orange with the black line reveals that the simple NWA overestimates the full width by a factor of about 2 to 5 in the complete parameter interval because of the sizable negative interference term which is neglected in the sNWA. However, the generalised NWA (red) approximates the full result reliably. The slight deviations are quantified in Sect. 9.4. As a conclusion we observe that the decay width $\Gamma(\tilde{\chi}_4^0 \to \tilde{\chi}_1^0 \tau^+ \tau^-)$ depends on M_1 due to the neutralino masses in the
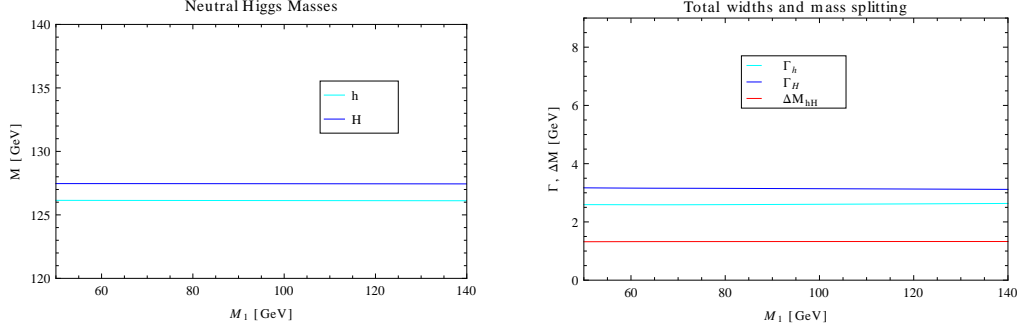
Figure 9.5.: **Left:** Predictions for the masses M_h, M_H of the neutral, $\mathcal{CP}$-even Higgs bosons in light/ dark blue as a function of $\tan\beta$ from `FeynHiggs`, incorporating 2-loop corrections, for $M_{H^\pm} = 153\,\text{GeV}$ and $\tan\beta = 50$ fixed. **Right:** The total widths Γ_h, Γ_H (blue) depending on $\tan\beta$ in comparison to the mass difference $\Delta M_{hH} = M_H - M_h$ in red which remains smaller than Γ_h, Γ_H.
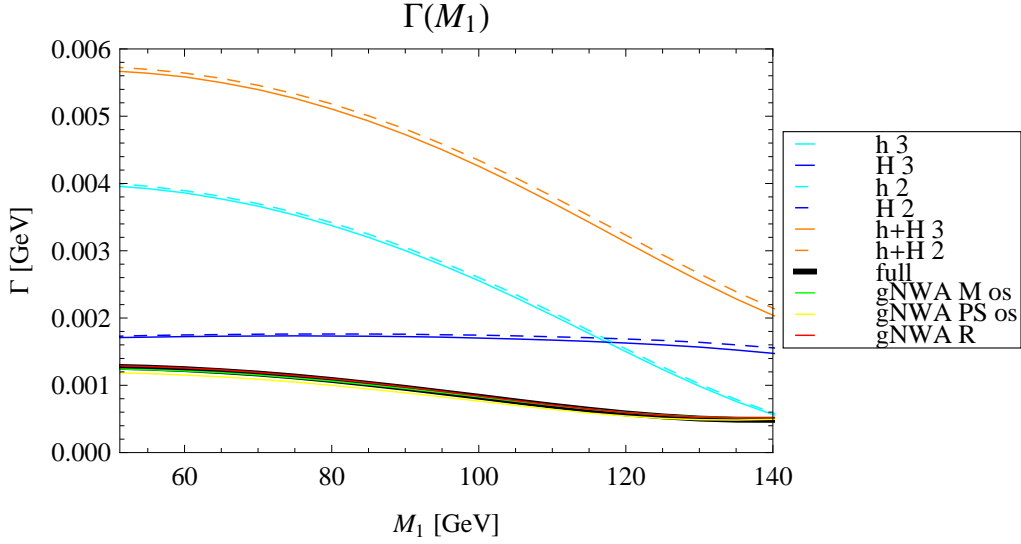
Figure 9.6.: The decay width $\Gamma(\tilde{\chi}_4^0 \rightarrow \tilde{\chi}_1^0 \tau^+\tau^-)$ as a function of M_1 with $\tan\beta = 50$, $M_{H^\pm} = 153\,\text{GeV}$. The single contributions from h and H are shown as 3-body decays and in the NWA. The full 3-body decay taking h- and H-exchange into account is compared to the simple and generalised NWA. Colour code as in Fig. 9.2.

available phase space. But by fixing $M_{H^\pm}$ and $\tan\beta$ in such a way that the Higgs mass difference stays smaller than one of the total widths, the size of the interference term is large at the order of at least 100%, irrespective of the variation of M_1.

9.4. Accuracy of the generalised NWA

In this section we want to examine the relative accuracy of the narrow-width approximation. For this purpose we study first the relative deviation of the three contributions from h, H and the interference term each in order to be able to tell apart the different sources of a possible difference in the final result. Second, we confront the simple and the generalised narrow-width approximation with the full 3-body result and comment on the improvement of the accuracy by including the interference term in the gNWA.

Impact of $M_{H^\pm}$ The left plot in Fig. 9.7 shows the absolute deviation of $\Gamma(\tilde{\chi}_4^0 \to \tilde{\chi}_1^0 h) \cdot BR(h \to \tau^+\tau^-)$ and $\Gamma(\tilde{\chi}_4^0 \to \tilde{\chi}_1^0 H) \cdot BR(H \to \tau^+\tau^-)$, computed in the NWA, from the 3-body decays $\Gamma^{(3)}(\tilde{\chi}_4^0 \overset{h}{\to} \tilde{\chi}_1^0 \tau^+\tau^-)$, $\Gamma^{(3)}(\tilde{\chi}_4^0 \overset{H}{\to} \tilde{\chi}_1^0 \tau^+\tau^-)$, respectively (in light/ dark blue), as well as the interference term in the different versions of the on-shell approximation compared to the full q^2-dependence (in yellow, green and red). In the right plot, the differences are normalised to the respective term computed as a 3-body process. For clarity, we list the plotted ratios here, where *os* denotes one of the three versions of the on-shell approximation:

$$h : \left(\Gamma(\tilde{\chi}_4^0 \to \tilde{\chi}_1^0 h) \;\cdot\; BR(h \to \tau^+\tau^-) - \Gamma^{(3)}(\tilde{\chi}_4^0 \overset{h}{\to} \tilde{\chi}_1^0 \tau^+\tau^-)\right) / \Gamma^{(3)}(\tilde{\chi}_4^0 \overset{h}{\to} \tilde{\chi}_1^0 \tau^+\tau^-)$$

$$H : \left(\Gamma(\tilde{\chi}_4^0 \to \tilde{\chi}_1^0 H) \cdot BR(H \to \tau^+\tau^-) - \Gamma^{(3)}(\tilde{\chi}_4^0 \overset{H}{\to} \tilde{\chi}_1^0 \tau^+\tau^-)\right) / \Gamma^{(3)}(\tilde{\chi}_4^0 \overset{H}{\to} \tilde{\chi}_1^0 \tau^+\tau^-)$$

$$int : \left(\Gamma_{int}^{(os)} - \Gamma_{int}^{(q^2)}\right) / \Gamma_{int}^{(q^2)}. \tag{9.2}$$
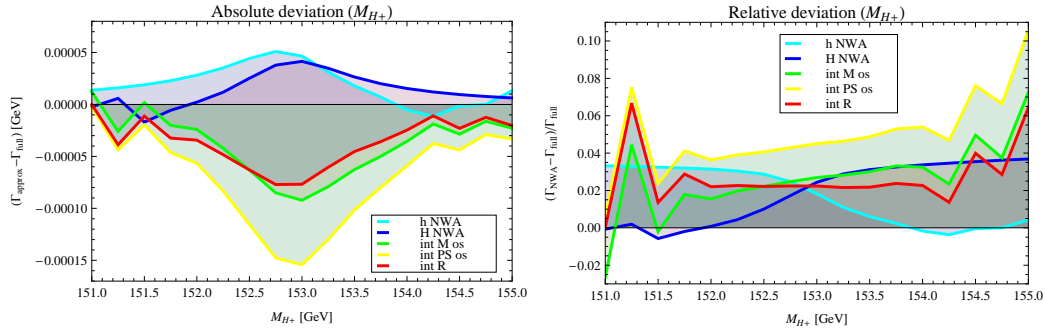
Figure 9.7.: **Left:** Absolute deviation of NWA contributions of h, H (light/ dark blue) and the interference term (green: only matrix elements on-shell, yellow: also on-shell phase space factor, red: R-factor method) from the respective term of the full calculation, depending on $M_{H^\pm}$. **Right:** Relative deviation normalised by the respective term of comparison.

We observe that all terms have their maximum absolute deviation from the full

result around $M_{H^+} \simeq 153\,\text{GeV}$, i.e. where the difference of M_H and M_h is minimal and both total widths relatively large, see Fig. 9.1. The factorised calculations of the separate decay widths with either h or H yield a slightly too large result. Also the absolute value of the interference term is overestimated by all three approximations. However, owing to the negative sign of the interference term, this results in a negative deviation in the left plot of Fig. 9.7. So the errors of different sign partly compensate each other in the total result in Fig. 9.2.

Concerning the relative deviation, the Γ/M behaviour becomes evident in that the relative deviation from h is largest for $M_{H^+} \lesssim 153\,\text{GeV}$, i.e., where Γ_h^{tot} is large, and accordingly with H for $M_{H^+} \gtrsim 153\,\text{GeV}$. Large relative differences between the approximated and the exact interference term can arise from a small absolute value of the interference term in the normalisation for M_{H^+} away from $153\,\text{GeV}$. The method of evaluating only the matrix elements on-shell, but integrating over the phase space (green) and the R-factor method (red) turn out to approximate the interference term nearly equally well, in the interference region with an accuracy of $\sim 3\%$. The method using a weighted phase space factor (yellow) introduces an uncertainty of $\sim 4-5\%$.

In Fig. 9.8, the performance of the simple and generalised NWA with respect to the full result is analysed. We plot the ratios

$$sNWA : \left(\Gamma^{(NWA,h)} + \Gamma^{(NWA,H)} - \Gamma^{(3,full)} \right) / \Gamma^{(3,full)}$$

$$gNWA : \left(\Gamma^{(NWA,h)} + \Gamma^{(NWA,H)} + \Gamma_{int}^{(os)} - \Gamma^{(3,full)} \right) / \Gamma^{(3,full)}, \qquad (9.3)$$

versus the interference control parameter

$$\frac{\Delta M_{hH}}{\Gamma_{max}} \equiv \frac{M_H - M_h}{\max \{\Gamma_h, \Gamma_H\}}. \qquad (9.4)$$

The region most relevant for interference effects is where $\frac{\Delta M_{hH}}{\Gamma_{max}} < 1$. Due to the masses and widths in Fig. 9.1, this ratio goes down to 0.4. The points of the sNWA accuracy that are close to each other, but not equal, arise as there are several combinations of ΔM_{hH} and Γ_{max} yielding a similar ratio, but different magnitudes of the interference term which is largest around $M_{H^\pm} \simeq 153\,\text{GeV}$. In the interference region the sNWA overestimates the full result by up to 450% because the sizable negative interference term is neglected. However, all three versions of the gNWA approximate the full result to an accuracy of better than 3%. Towards ratios of $\frac{\Delta M_{hH}}{\Gamma_{max}} \gtrsim 1$, the interference term vanishes so that the sNWA approaches the gNWA.
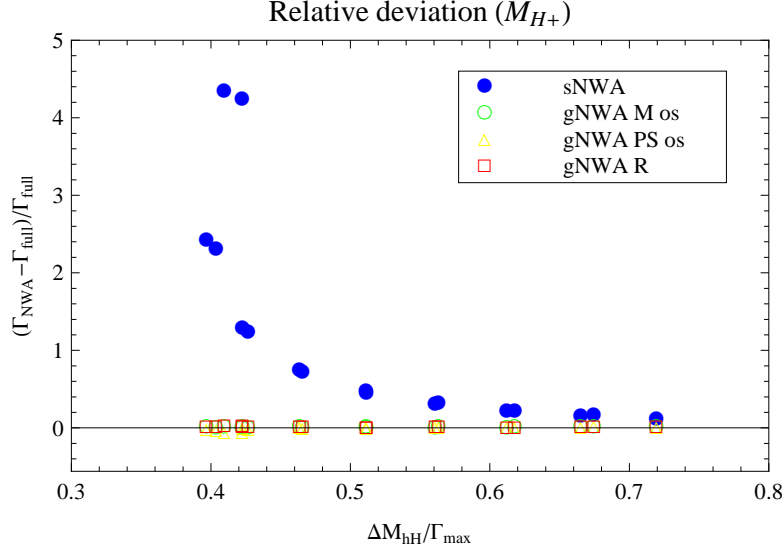
Figure 9.8.: Relative deviation of the final result in the simple NWA (sNWA, blue) and generalised NWA (gNWA, green, yellow, red) from the full decay width, versus the ratio $\Delta M_{hH}/\max\{\Gamma_h, \Gamma_H\}$.

Impact of $\tan\beta$ Next, we apply the same procedure as above to evaluate the absolute and relative deviations from Fig. 9.4 also as functions of $\tan\beta$. The results are shown in Fig. 9.9. The left plot in Fig. 9.9 shows that all terms except h differ
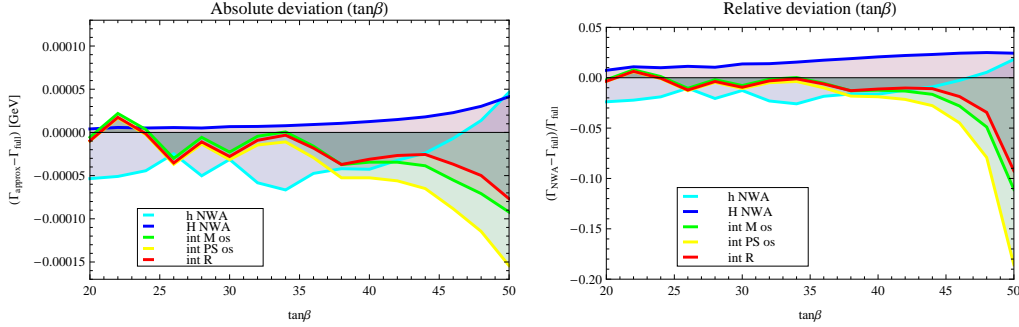
Figure 9.9.: **Left:** Absolute deviation of the separate contributions involving h and H (light/ dark blue) and the interference term (green: only matrix elements on-shell, yellow: also on-shell phase space factor, red: R-factor method) from the corresponding terms of the full calculation, depending on $\tan\beta$. **Right:** Relative accuracy normalised by the respective term of comparison.

by the biggest amount from the exact result for $\tan\beta \gtrsim 40$, i.e. where the mass

difference is smallest and the total widths are largest. The separate contributions of h and H stay within $1-3\%$ accuracy whereas at $\tan\beta = 50$ the relative deviation of the interference term amounts to 10% for the R-factor method, 12% for the on-shell matrix elements and 20% for the weighted phase space factor.
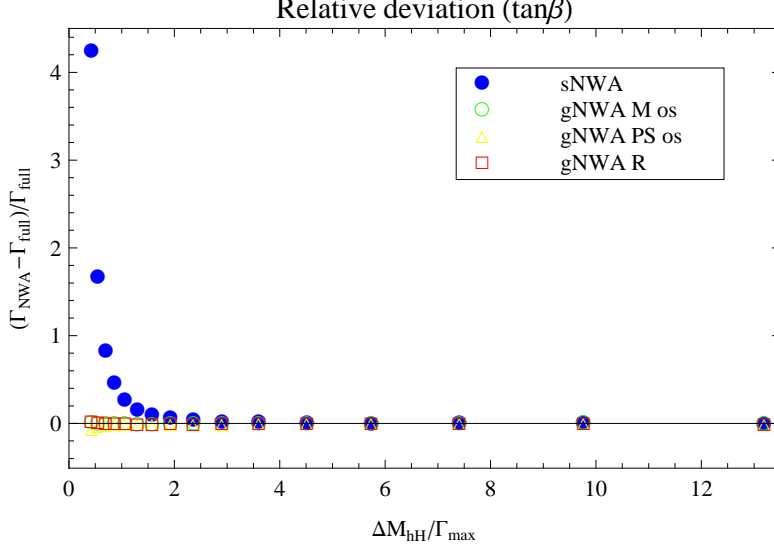
Figure 9.10.: Relative accuracy of the final result in the simple NWA (sNWA, blue) and generalised NWA (gNWA, green, yellow, red) versus the ratio $\Delta M_{hH}/\max\{\Gamma_h, \Gamma_H\}$.

Fig. 9.10 shows that the sNWA overestimates the full width by up to 423% for a ratio of $\frac{\Delta M_{hH}}{\Gamma_{max}} = 0.42$. Moreover, the sNWA approaches the full width in the limit of large $\frac{\Delta M_{hH}}{\Gamma_{max}}$ when the interference term vanishes. In contrast to the $M_{H^\pm}$-dependence, for $\tan\beta$ it is a monotonic behaviour because the mass difference decreases and the maximum width increases with growing $\tan\beta$ in the parameter interval under consideration. The gNWA, however, differs from the full result by at most 3% also in the region of strong interference.

Impact of M_1 As already noted in Fig. 9.6, with constant Higgs masses and rather large and constant widths Γ_h, Γ_H, the expected error of the order $\Gamma_{h_h}/M_{h_k} \simeq 3\%$ lies in the range from 1% to 5% of the relative deviation of the h- and H-contributions in the NWA from the full result. The relative deviation in the interference term with on-shell matrix elements (green) and the R-factor method (red) of 1% to 3.5% is exceeded by the phase space factor method (yellow) which ranges from 3% to 6.5%, as shown in Fig. 9.11.

Varying M_1 hardly changes the masses and total widths of the Higgs bosons so that

the control parameter stays rather constant and is fixed by the parameter choice $M_{H^\pm} = 153$ GeV and $\tan\beta = 50$ at a ratio around 0.42, thus always below 1 (see Fig. 9.12). While the sNWA deviates from the full result by 130% to 453% due to the quite constantly large interference term, the difference between the gNWA and the full width does not exceed 7%.
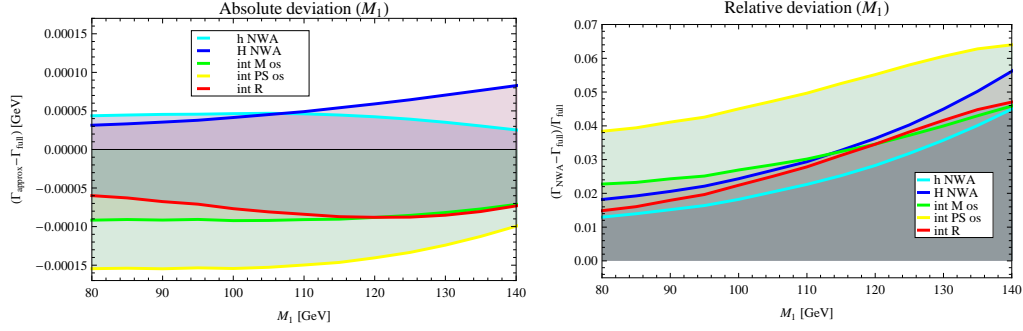
Figure 9.11.: **Left:** Absolute deviation of h, H (light/ dark blue) and the interference term (green: only matrix elements on-shell, yellow: also on-shell phase space factor, red: R-factor method) from the corresponding terms of the full calculation, depending on M_1. **Right:** Relative accuracy normalised by the respective term of comparison.
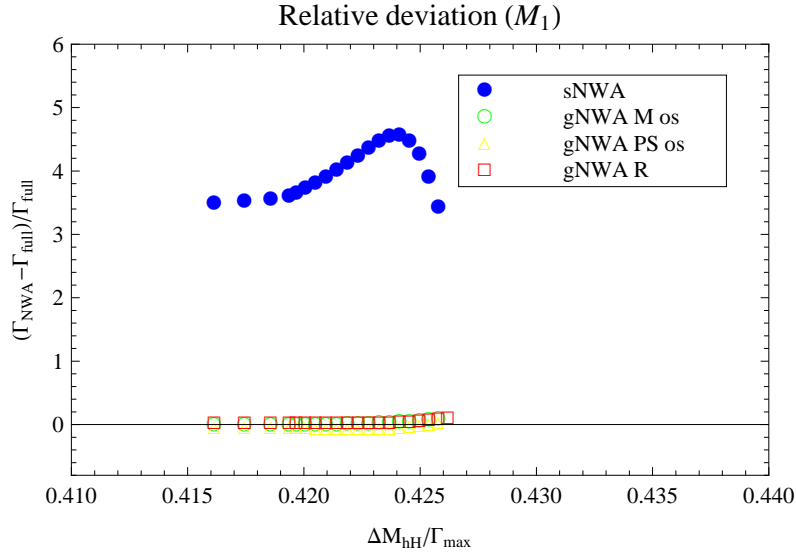
Figure 9.12.: Relative accuracy of the final result in the simple NWA (sNWA, blue) and generalised NWA (gNWA, green, yellow, red) versus the ratio $\Delta M_{hH}/\max\{\Gamma_h, \Gamma_H\}$.

10. Vertex corrections in the generalised NWA

In this chapter, we want to discuss 1-loop corrections to the vertex with one Higgs boson h_k^0 and two neutralinos $\tilde{\chi}_i^0, \tilde{\chi}_j^0$. Sect. 10.1 contains the structure of the 1-loop amplitudes and of the counterterm, the procedure of a check for UV-finiteness as well as numerical results for the decay width of $\tilde{\chi}_4^0 \to \tilde{\chi}_1^0 h/H$ at the 1-loop level. Subsequently in Sect. 10.2, the loop-corrected 2-body decays for the Higgs production are implemented into the narrow-width approximation including the interference term. Without performing a full 1-loop calculation of the 3-body process, we obtain an approximate prediction for the decay width $\Gamma(\tilde{\chi}_4^0 \to \tilde{\chi}_1^0 \tau^+ \tau^-)$ with vertex corrections. This is meant as an illustration of the practicability of the generalised NWA at higher orders.

10.1. Corrections to the neutralino-Higgs vertex

10.1.1. Vertex counterterm

The vertex counterterm with a $\mathcal{CP}$-even/ odd neutral Higgs boson h_k reads

$$\delta\Gamma_{\tilde{\chi}_i^0 \tilde{\chi}_j^0 h_k} = \omega_R \delta C_{ijk}^R \pm \omega_L \delta C_{ijk}^L, \tag{10.1}$$

which involves the following parameter and field renormalisation using the coupling defined in Eq. (8.1) and the renormalisation constants from Chap. 4.3, listed in Tab. 10.1. The explicit expression for δc_{ijk} reads

$$\delta c_{ijk} = (a_k N_{i3} + b_k N_{i4})(\delta s_W N_{j1} - \delta c_W N_{j2}) + (a_k N_{j3} + b_k N_{j4})(\delta s_W N_{i1} - \delta c_W N_{i2}). \tag{10.2}$$

Adding all terms, we obtain the full coupling counterterm [70]

$$\delta C_{ijk}^{R/L} = \frac{e}{2 c_W s_W} \delta c_{ijk}^{(*)} + \left(\delta Z_e - \frac{\delta s_W}{s_W} - \frac{\delta c_W}{c_W} \right) C_{ijk}^{R/L}$$
$$+ \frac{1}{2} \sum_{l=1}^4 (\delta Z_{li}^{R/L} C_{ljk}^{R/L} + \delta \bar{Z}_{jl}^{L/R} C_{ilk}^{R/L} + Z_{h_k h_l} C_{ijk}^{R/L}). \tag{10.3}$$

Table 10.1.: Constituents of the coupling counterterm from the renormalisation constants of the parameters and fields.

renormalisation constant	counterterm
$c_{ijk}^{(*)} \to \delta c_{ijk}^{(*)}$	$\frac{e}{2c_W s_W} \delta c_{ijk}^{(*)}$
$e \to e(1 + \delta Z_e)$	$\frac{e\,\delta Z_e}{2c_W s_W} c_{ijk}^{(*)} = C_{ijk}^{R/L} \delta Z_e$
$s_W \to s_W + \delta s_W$	$-\frac{e}{2c_W s_W^2} c_{ijk}^{(*)} = -C_{ijk}^{R/L} \frac{\delta s_W}{s_W}$
$c_W \to c_W + \delta c_W$	$-\frac{e}{2c_W^2 s_W} c_{ijk}^{(*)} = -C_{ijk}^{R/L} \frac{\delta c_W}{c_W}$
$\tilde{\chi}_l^0 \to (1 + \frac{1}{2}\delta Z_{li}^{0R/L})\tilde{\chi}_i^0$	$\frac{1}{2}\sum_{l=1}^4 \delta Z_{li}^{0R/L} C_{ljk}^{R/L}$
$\bar{\tilde{\chi}}_l^0 \to \bar{\tilde{\chi}}_j^0(1 + \frac{1}{2}\delta\bar{Z}_{jl}^{0L/R})$	$\frac{1}{2}\sum_{l=1}^4 \delta\bar{Z}_{jl}^{0L/R} C_{ilk}^{L/R}$
$h_k \to h_k + \frac{1}{2}\sum_{l=1}^4 \delta Z_{h_k h_l} h_l$	$\frac{1}{2}\sum_{l=1}^4 \delta Z_{h_k h_l} h_l C_{ijk}^{R/L}$

This is illustrated in Fig. 10.1.
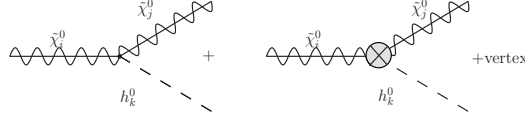
Figure 10.1.: Born graph and counterterm of the $\tilde{\chi}_i^0 \tilde{\chi}_j^0 h_k$-vertex. The vertex triangle diagrams are shown in Fig. 10.2.

The renormalisation has been worked out in Sects. 4.2 and 4.3. We implemented the calculated renormalisation constants and the structure of the counterterm into the `FeynArts` MSSM model file (`MSSM.mod`) because they are not contained in the distributed version. After the generation of counterterm topologies (out of which we exclude tadpoles and wave function corrections) with `FeynArts`, this allows for the calculation of the counterterm amplitude (CT) in `FormCalc`. Upon invocation of `CalcRenConst[CT]` the renormalisation constants in the counterterm are returned. These counterterms are required to absorb the divergences from the 1-loop triangle vertex corrections displayed schematically in Fig. 10.2.

10.1.2. 1-loop triangle diagrams

The complete set of 1-loop triangle diagrams can be divided into several UV-finite and gauge invariant subsets of diagrams if the same particle restrictions are imposed on the self-energies in the renormalisation constants in the counterterm, such as each generation of quarks and squarks or leptons and sleptons, respectively. On the other hand, the class of gauge and Higgs bosons, gauginos and higgsinos cannot further be

partitioned. The first row of Fig. 10.2 represents the fermion-sfermion triangles in
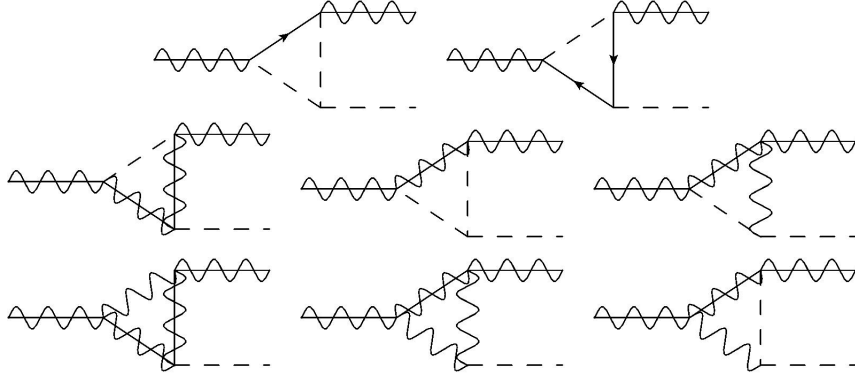
Figure 10.2.: Classes of triangle diagrams as 1-loop corrections of the $\tilde{\chi}_i^0 \tilde{\chi}_j^0 h_k$-vertex. The **first row** contains the (s)fermion triangles. The fermion arrows can be reversed and there are two states for each scalar superpartner except for sneutrinos (which couple only to h, H). Massless neutrinos do not couple to any Higgs boson. So there are 24 diagrams per (s)quark generation. For the leptons, there 10 (8) insertions into the left diagram if h_k is $\mathcal{CP}$-even (odd) and 4 into the right one, so in total 14 (12). The remaining diagrams in the **second and third row** containing neutral or charged gauge bosons, neutralinos or charginos and neutral or charged Higgs bosons form together one gauge invariant and UV-finite subset.

which the fermion arrows can also occur in reversed direction so that these diagrams have to be considered twice. Counting the total number of particle insertions, one has to keep in mind that each SM fermion $f_{L/R}$ with left- and right-handed states has two scalar superpartners $\tilde{f}_{1,2}$. But due to the absence of right-handed neutrinos in the SM, there is only one sneutrino per generation. Sneutrinos only couple to the $\mathcal{CP}$-even Higgs bosons h, H ($k = 1, 2$). Furthermore, massless neutrinos do not couple to Higgs bosons.

So the upper left diagram yields $2 \cdot (4 + \delta_{k1} + \delta_{k2})$ possibilities and the upper right one $2 \cdot 2$ per lepton generation, in total 14 (12) for a $\mathcal{CP}$-even (odd) external Higgs boson.

Concerning the (s)quarks, the left diagram allows for two squarks with two possibilities each, times two flavours per generation, multiplied by two for the fermion arrow, whereas the right diagram with only one squark gives rise to half as many insertions, i.e. $2 \cdot (8 + 4) = 24$ possibilities per (s)quark generation as illustrated for one example in Fig. 10.3.
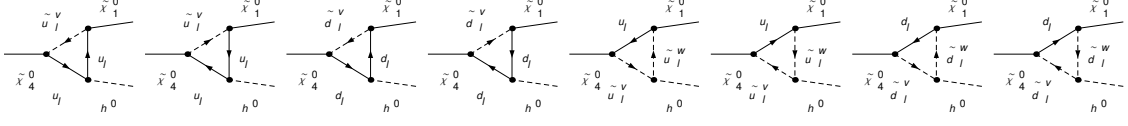
Figure 10.3.: Example from Fig.10.2, generated with `FeynArts`: Triangle diagram corrections of the $\tilde{\chi}_4^0 \tilde{\chi}_1^0 h$-vertex with up- and down-type (s)quarks from one generation (squark indices $v, w \in \{1, 2\}$).

For the example of a triangle consisting of one sfermion and two fermion lines with momentum labels as indicated in Fig. 10.4, we calculate the amplitude

$$\mathcal{M} = -\int \frac{d^4 q_1}{(2\pi)^4} \frac{\bar{u}_1 \left(\omega_L C^L_{\tilde{f}_v f \tilde{\chi}_j^0} + \omega_R C^R_{\tilde{f}_v f \tilde{\chi}_j^0}\right) (\slashed{q}_1 + m_{\tilde{f}_v}) \left(\omega_L C^L_{\tilde{f}_v f \tilde{\chi}_i^0} + \omega_R C^R_{\tilde{f}_v f \tilde{\chi}_i^0}\right)}{[q_1^2 - m_{\tilde{f}_v}^2][(q_1 - k_1)^2 - m_f^2][(q_1 - k_1 - k_2)^2 - m_f^2]}.$$
(10.4)
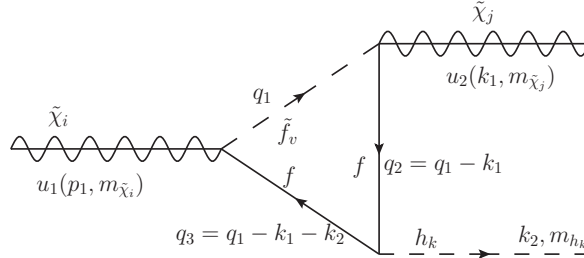
Figure 10.4.: Triangle vertex correction with one sfermion and two fermions, external momenta p_1 in the initial and k_1, k_2 in the final state, loop momenta q_1, q_2, q_3.

`FormCalc` algebraically simplifies this amplitude by contracting indices, calculating traces and abbreviating spinor chains.

In the framework of Passarino-Veltman reduction [119], the loop integrals are then expanded by `FormCalc` into all possible Lorentz covariant tensor structures. Subsequently, the coefficients are determined by contraction with Lorentz covariants with the matching rank of indices. In this process, in addition to 2-point functions from the self-energies, 3-point integrals C from the vertex diagrams are encountered,

namely[1]

$$\{C_0; C_\mu; C_{\mu\nu}\} = \frac{(2\pi\mu)^{4-D}}{i\pi^2} \int d^D q \frac{\{1; q_\mu; q_{\mu\nu}\}}{[q^2 - m_1^2][(q+p_1)^2 - m_2^2][(q+p_1+p_2)^2 - m_3]}. \tag{10.5}$$

The tensor integrals C_μ and $C_{\mu\nu}$ can be decomposed in the following way,

$$C_\mu = \sum_{i=1}^{2} k_{i\mu} C_i \tag{10.6}$$

$$C_{\mu\nu} = g_{\mu\nu} C_{00} + \sum_{i,j=1}^{2} k_{i\mu} k_{j\nu} C_{ij}. \tag{10.7}$$

Apart from a finite part, expressions proportional to $C_0, C_1, C_2, C_{00}, C_{11}, C_{12}$ and C_{22} occur out of which only C_{00} is divergent. The divergence is manifest in the form of

$$\Delta \equiv \frac{1}{\epsilon} = \frac{2}{4 - D}. \tag{10.8}$$

Numerical values are obtained with `LoopTools`.

10.1.3. Check for UV-finiteness

For a first check of the UV-finiteness of the considered process using the extension of the MSSM model file with the counterterms specified in Chap. 4, we restrict the particle content in the triangles and simultaneously in the loops of the self-energies to quarks and squarks of the third generation, i.e. $t, b, \tilde{t}_{1,2}, \tilde{b}_{1,2}$, because their contribution is dominating and they are technically easiest to handle.

This restriction simplifies the explicit expression of the Higgs doublet renormalisation constants, $\delta Z_{\mathcal{H}_{1,2}}^{\overline{DR}}$, defined in Eqs. (4.26) and (4.27).

$$-\text{Re}\left[\Sigma_{HH(f_3,\tilde{f}_3)}^{'(div)}(m_H^2)\right] = -\text{Re}\left[\Delta\left(\frac{3\alpha_{em}s_\alpha^2 m_t^2}{8\pi M_W^2 s_\beta^2 s_W^2} + \frac{3\alpha_{em}c_\alpha^2 m_b^2}{8\pi M_W^2 c_\beta^2 s_W^2}\right)\right]$$

$$\stackrel{\alpha=0}{\rightarrow} -\text{Re}\left[\Delta\frac{3\alpha_{em}m_b^2}{8\pi M_W^2 c_\beta^2 s_W^2}\right] = \delta Z_{\mathcal{H}_1}^{\overline{DR}} \tag{10.9}$$

$$-\text{Re}\left[\Sigma_{hh(f_3,\tilde{f}_3)}^{'(div)}(m_h^2)\right] = -\text{Re}\left[\Delta\left(\frac{3\alpha_{em}c_\alpha^2 m_t^2}{8\pi M_W^2 s_\beta^2 s_W^2} + \frac{3\alpha_{em}s_\alpha^2 m_b^2}{8\pi M_W^2 c_\beta^2 s_W^2}\right)\right]$$

$$\stackrel{\alpha=0}{\rightarrow} -\text{Re}\left[\Delta\frac{3\alpha_{em}m_t^2}{8\pi M_W^2 s_\beta^2 s_W^2}\right] = \delta Z_{\mathcal{H}_2}^{\overline{DR}} \tag{10.10}$$

---

[1]In the convention of Ref. [120] instead of Ref. [119]

According to the restriction to loop contributions of the third generation fermions and sfermions, we generate the triangle amplitudes and, with the help of the extended model file, the vertex counterterm. One possibility is to check analytically by means of the function `UVDivergentPart` whether the coefficients in front of the divergence cancel exactly. This, however, is not feasible for long expressions involving many parameters as those from the neutralino mixing matrix. So instead, we test the UV-finiteness numerically by varying the parameter Δ. If all coefficients in front of the divergence cancel within the numerical precision, the final result of the loop contribution must not change notably. In our check, the result remained constant within the numerical precision, also when we extended the allowed particle spectrum in loops to include the fermions and sfermions of all three generations.

10.1.4. Numerical results for (s)fermion vertex corrections

We computed the 2-body decay widths $\Gamma(\tilde{\chi}_4^0 \to \tilde{\chi}_1^0 h)$ and $\Gamma(\tilde{\chi}_4^0 \to \tilde{\chi}_1^0 H)$ including vertex corrections at the 1-loop level with fermions and sfermions. In addition to the vertex triangle diagrams and the counterterm defined in Eq. (10.3), we take 2×2 mixing of the external Higgs bosons h, H into account by means of Z-factors, see Sect. 4.2.3. They are applied both on the tree-level amplitudes $\mathcal{M}^{tree}$ and on the sum of the 1-loop amplitudes $\mathcal{M}^{1-loop}$ and the counterterms $\delta\mathcal{M}$,

$$\mathcal{M}_h^Z = \hat{\mathbf{Z}}_{hh}\mathcal{M}_h + \hat{\mathbf{Z}}_{hH}\mathcal{M}_H \tag{10.11}$$

$$\mathcal{M}_H^Z = \hat{\mathbf{Z}}_{Hh}\mathcal{M}_h + \hat{\mathbf{Z}}_{HH}\mathcal{M}_H. \tag{10.12}$$

This does not introduce any new divergences because the Z-factors are finite and the divergences cancel in the combination $\mathcal{M}^{1-loop} + \delta\mathcal{M}$. Technically, the amplitudes are collated in `FormCalc` as follows:

$$\mathcal{M}_{h_k}^{Z,tree} = \hat{\mathbf{Z}}_{h_kh}\mathcal{M}_h + \hat{\mathbf{Z}}_{h_kH}\mathcal{M}_H \tag{10.13}$$

$$\mathcal{M}_{h_k}^{Z,1-loop} = \hat{\mathbf{Z}}_{h_kh}(\mathcal{M}_h^{1-loop} + \delta\mathcal{M}_h) + \hat{\mathbf{Z}}_{h_kH}(\mathcal{M}_H^{1-loop} + \delta\mathcal{M}_H). \tag{10.14}$$

From now on, we drop the Z-superscripts and implicitly understand all amplitudes as mixed by the Z-factors in the manner defined above. The perturbative expansion of the squared matrix element in the coupling α is

$$|\mathcal{M}|^2 = |\mathcal{M}^{tree}|^2 + 2\text{Re}[\mathcal{M}^{tree}(\mathcal{M}^{1-loop})^*]$$
$$+ |\mathcal{M}^{1-loop}|^2 + 2\text{Re}[\mathcal{M}^{tree}(\mathcal{M}^{2-loop})^*] + \mathcal{O}(\alpha^3). \tag{10.15}$$

Formally, the term $|\mathcal{M}^{1-loop}|^2$ is not contained in the one-loop result because it is of order α^2. If it is included, for consistency one should in general also include the term $2\text{Re}[\mathcal{M}^{tree}(\mathcal{M}^{2-loop})^*]$ of the same order in α. However, if the tree level amplitude happens to be extremely small compared to the 1-loop amplitude, then the terms

in $|\mathcal{M}|^2$ which are multiplied by the tree-level amplitude are also suppressed. In this case it is not only consistent, but also necessary to include the $|\mathcal{M}^{1-loop}|^2$ term because it can be much larger than $2\text{Re}[\mathcal{M}^{tree}(\mathcal{M}^{2-loop})^*]$, which is suppressed by the small tree-level amplitude. In case of a strongly negative contribution of $\mathcal{O}(\alpha)$, it might also be necessary to complete the square of $|\mathcal{M}^{tree}+\mathcal{M}^{1-loop}|$ by adding the squared 1-loop term in order to obtain a non-negative cross section or decay width. In our numerical analysis, we encounter small tree-level contributions of $\Gamma(\tilde{\chi}_4^0 \to \tilde{\chi}_1^0 h_k)$ for either h or H, depending on the parameter point. For a positive decay width, we use the option `LoopSquare` in `FormCalc` to add also the squared 1-loop amplitude. The results are shown in Fig. 10.5 where we varied the parameters $M_{H^\pm}, \tan\beta$ and M_1 as in Chap. 9.
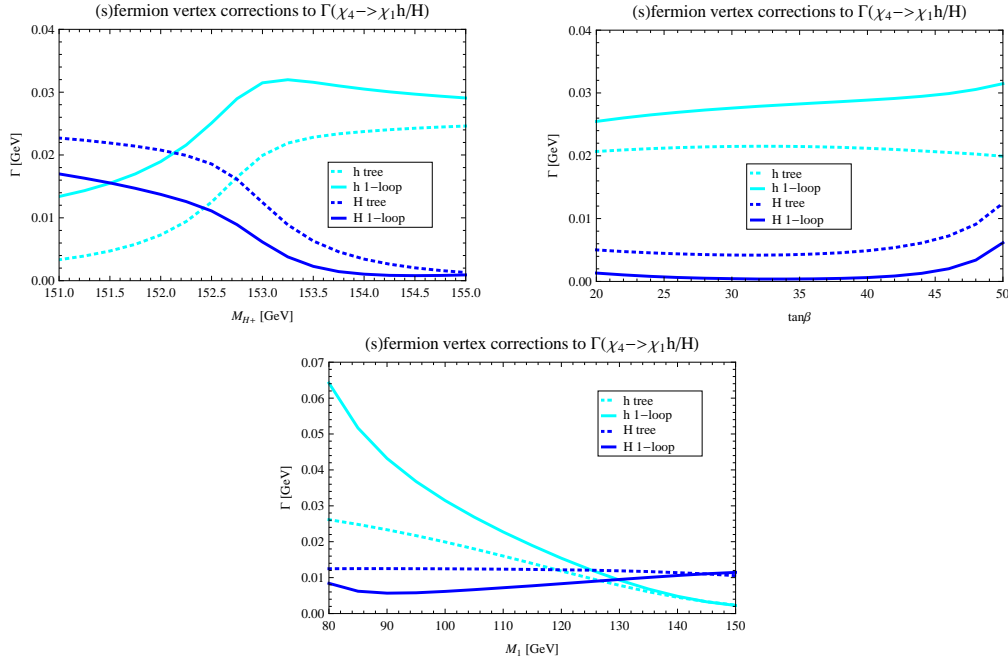
Figure 10.5.: 2-body decay widths $\Gamma(\tilde{\chi}_4^0 \to \tilde{\chi}_1^0 h/H)$ with (s)fermion vertex corrections as a function of $M_{H^\pm}$ (upper left), $\tan\beta$ (upper right) and M_1 (lower row). The dotted lines represent tree-level results, the solid lines the sum of tree-level and 1-loop results, including the squared 1-loop matrix element.

Positive loop corrections are found for h and negative ones for H. As a consequence, the decay width $\Gamma(\tilde{\chi}_4^0 \to \tilde{\chi}_1^0 H)$ is smaller than $\Gamma(\tilde{\chi}_4^0 \to \tilde{\chi}_1^0 h)$ in the complete interval of $\tan\beta$ and in most of the M_1-interval. The variation of $M_{H^\pm}$ causes a cross-over effect in the mixing between h and H so that the Z-factors mix both contributions of $\Gamma(\tilde{\chi}_4^0 \to \tilde{\chi}_1^0 h_k)$. But the loop-corrected width of the H-production from a $\tilde{\chi}_4^0$-decay

exceeds the h production only at low values of $M_{H^\pm}$.

In total, the loop corrections turn out to be rather large in the analysed parameter settings, which motivates to take them into account in the production part of the NWA. This is done in the next Sect. 10.2.

10.2. Extension of the generalised NWA to the one-loop level

10.2.1. One-loop approximation of the interference term

Finally, we incorporate the vertex corrections to the Higgs production processes $\Gamma(\tilde{\chi}_4^0 \to \tilde{\chi}_1^0 h)$ and $\Gamma(\tilde{\chi}_4^0 \to \tilde{\chi}_1^0 H)$ into the generalised narrow-width approximation. Among the three versions for the interference term, we choose the R-factor method. At tree-level, it exhibited a remarkably precise performance with respect to the full 3-body decay despite its strongest assumptions in the approximation. It is technically better feasible than the other two versions because it is not based on the on-shell evaluation of unsquared tree-level and 1-loop matrix elements, but the computed decay widths and branching ratios can be directly used. So the formula for the approximation is

$$\Gamma^{gNWA,1-loop}_{\tilde{\chi}_4^0 \to \tilde{\chi}_1^0 \tau^+ \tau^-} = \Gamma^{1-loop}(\tilde{\chi}_4^0 \to \tilde{\chi}_1^0 h) \cdot BR^{tree}(h \to \tau^+ \tau^-)(1 + R_h^{1-loop})$$
$$+ \Gamma^{1-loop}(\tilde{\chi}_4^0 \to \tilde{\chi}_1^0 H) \cdot BR^{tree}(H \to \tau^+ \tau^-)(1 + R_H^{1-loop}), \quad (10.16)$$

$$R_{h_k} = \frac{M_{h_k}^{2-loop}\Gamma_{h_k}^{2-loop}}{\pi} w_{h_k} 2\text{Re}[x_k \int dq^2 \Delta_h^{BW}(q^2) \Delta_H^{BW*}(q^2)], \quad (10.17)$$

with the weight factors

$$w_{h_k} = \frac{\Gamma^{1-loop}(\tilde{\chi}_4^0 \to \tilde{\chi}_1^0 h_k) \cdot BR^{tree}(h_k \to \tau^+ \tau^-)}{\sum\limits_{h_k=h,H} \Gamma^{1-loop}(\tilde{\chi}_4^0 \to \tilde{\chi}_1^0 h_k) \cdot BR^{tree}(h_k \to \tau^+ \tau^-)}, \quad i = 1, 2, \quad (10.18)$$

and with the fraction x_k of loop-corrected couplings from `FeynHiggs`. The results can be seen in Fig. 10.6. The negative or positive 1-loop corrections to the production of H and h, respectively, affect the partial width of $\tilde{\chi}_4^0 \to \tilde{\chi}_1^0 \tau^+ \tau^-$ in such a way that it gets even closer to zero than in Figs. 9.2, 9.4 and 9.6 in the parameter regions of strongest negative interference effects.
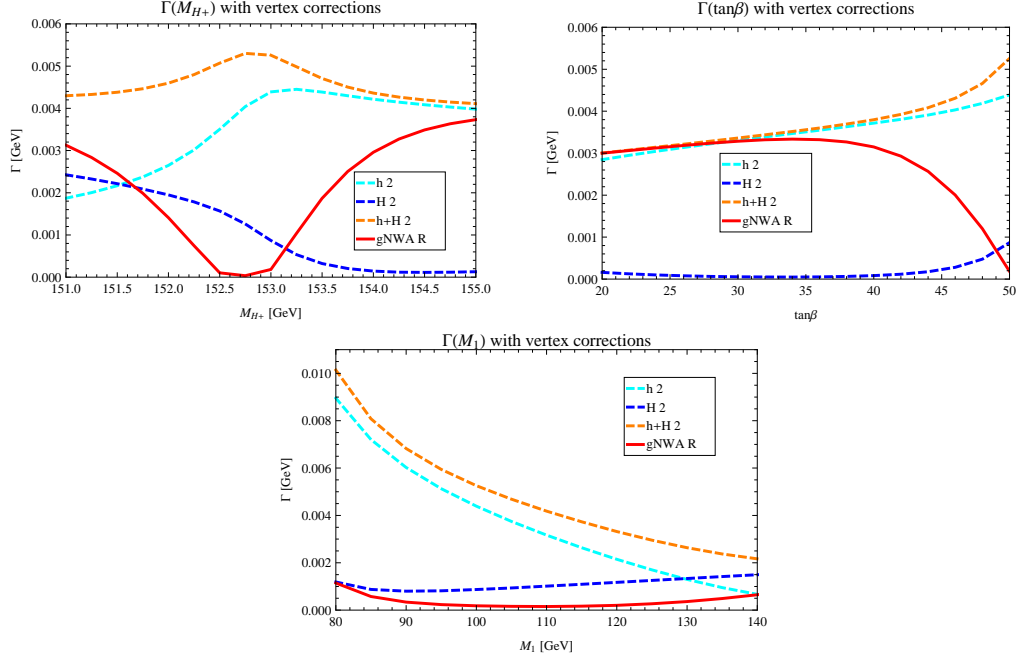
Figure 10.6.: Generalised NWA of the decay width $\Gamma(\tilde{\chi}_4^0 \to \tilde{\chi}_1^0 \tau^+ \tau^-)$ with vertex corrections in the Higgs production as a function of $M_{H^\pm}$ (upper left), $\tan\beta$ (upper right) and M_1 (lower). Dashed lines allude to the fact that no 3-body decay is calculated. The incoherent sum (orange) of the separate Higgs contributions in the NWA (light/ dark blue) deviates strongly from the prediction of Γ including the interference term according to the R-factor method of the gNWA (red).

10.2.2. Impact of vertex corrections

The absolute and relative contribution of the (s)fermion loop-corrections can be seen in Fig. 10.2.2, depending on $M_{H^\pm}$, $\tan\beta$ and M_1. The left column shows the decay width $\Gamma(\tilde{\chi}_4^0 \to \tilde{\chi}_1^0 \tau^+ \tau^-)$ at 1-loop level (solid lines) in comparison to the tree-level results (dotted), both in the simple NWA (orange) and in the gNWA (red) based on the R-factor method applied in Eqs. (10.17) and (10.18). For both approximations, the ratios of vertex-corrected and leading order result, the so-called K-factors, are shown in the right column,

$$K = \Gamma^{1-loop}(\tilde{\chi}_4^0 \to \tilde{\chi}_1^0 \tau^+ \tau^-)/\Gamma^{tree}(\tilde{\chi}_4^0 \to \tilde{\chi}_1^0 \tau^+ \tau^-). \tag{10.19}$$

We note that the K-factor of the sNWA is essentially constant as a function of $M_{H^\pm}$ and $\tan\beta$. It strongly increases for low values of M_1. On the other hand, the K-factor of the gNWA is characterised by the different behaviour of the interference

term at leading order or with the vertex corrections. As a function of $M_{H\pm}$ and $\tan\beta$, it varies most strongly and reaches its minimum in the interference region with the negative interference that has the largest absolute value. Depending on M_1, the K-factor of the gNWA is less than one in most of the analysed parameter interval.
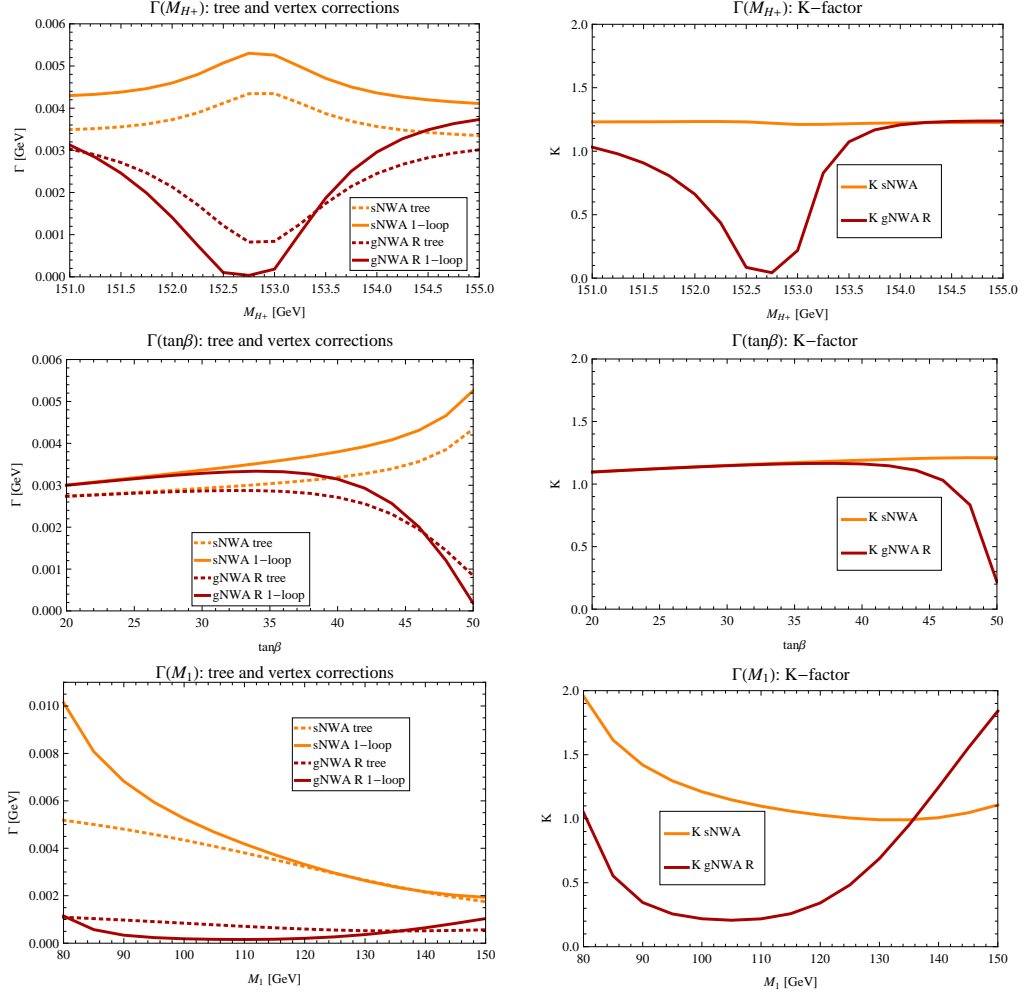
Figure 10.7.: **Left column:** Comparison of tree-level (dotted) and 1-loop (solid) results for the decay width $\Gamma(\tilde{\chi}_4^0 \to \tilde{\chi}_1^0 \tau^+ \tau^-)$ in the simple (orange) and generalised NWA with interference weight factor R (red). **Right column:** K-factor $\Gamma^{1-loop}/\Gamma^{tree}$ in the sNWA and gNWA.
Upper row: Dependence of Γ and K on $M_{H\pm}$. **Central row:** Dependence of Γ and K on $\tan\beta$. **Lower row:** Dependence of Γ and K on M_1.

Of course, this is only a first step towards a full one-loop treatment. First, the particle spectrum in the loops will be extended to all MSSM particles. Second, triangle diagrams and counterterms also have to be calculated for the decay process $h_k \to \tau^+\tau^-$. A comparison to the other two methods of approximating the interference term will be interesting.

Anyway, the purpose of this section was to obtain a prediction for the process $\Gamma(\tilde{\chi}_4^0 \to \tilde{\chi}_1^0 h/H)$ at the 1-loop level without calculating the full process. The generalised NWA provides the possibility to calculate higher-order corrections to several parts of the diagram, such as the production and the decay vertex and propagators or external legs, and, if all conditions for the underlying assumptions and applied approximations are met, to put them together in an appropriate way.

11. Conclusion

11.1. Summary

Interference effects of nearly mass-degenerate resonances can contribute substantially to cross sections and decay widths. Therefore the usual narrow-width approximation (NWA) cannot always be applied to split a longer process into subsequent production and decay processes, neglecting interference terms. The MSSM contains an extended particle spectrum which allows for such mass degeneracies.

In this thesis, a generalisation of the usual NWA was studied that includes an approximation of the interference term. Analogously to the usual NWA, it is based on the factorisation of the matrix elements and the phase space into their production and decay part. The on-shell evaluation of the matrix elements and optional further approximations simplify the calculation of the interference term compared to the calculation of the full process.

The computation was performed using `FeynArts`, `FormCalc` and `LoopTools`. Tree-level results were supplemented by 2-loop corrections from `FeynHiggs` to Higgs masses, total widths and wave-function normalisation Z-factors for correct on-shell properties of external Higgs bosons. In addition, 1-loop corrections of the neutralino-Higgs vertex were calculated with an on-shell renormalisation of the neutralino sector and a mixed on-shell and $\overline{\text{DR}}$-scheme for the Higgs sector.

We studied the example of interferences between the MSSM Higgs bosons h and H, which are produced in a decay of a heavy neutralino and then decay into a pair of τ-leptons. In a scenario with a small difference of the masses M_h and M_H, the interference term was found to be large and negative. In our scenario, the usual NWA leads to an overestimation of the full result of up to a factor of 5. The generalised NWA, however, approximates the full result within an accuracy of a few percent. The impact of the interference term strongly depends on the input parameters from the Higgs sector and is less sensitive to parameters from the neutralino sector.

One-loop vertex corrections to the production part were included into the usual and the generalised NWA. A large interference term was also encountered at loop-level. As an illustration of feasibility, we demonstrated how higher-order corrections of sub-processes could be incorporated into the interference-improved generalised NWA without calculating the full process. This can be useful for the application to more complicated processes for which the factorisation into different sub-processes will be essential to enable the computation of higher-order contributions.

11.2. **Outlook**

The results obtained in this thesis will be extended and the generalised narrow-width approximation will be applied in a more general context.

We will include the full one-loop corrections to the neutralino decay. Furthermore, we will consider complex phases in the most general case of the MSSM in order to allow for $\mathcal{CP}$-violating mixing. In preparation, we have already implemented the counterterms for the neutralino sector of the MSSM with complex parameters. Taking the interference between all three neutral Higgs bosons with mass eigenstates h_1, h_2, h_3 into account, we will calculate production cross sections of these Higgs bosons in association with bottom quarks and their subsequent decay. The goal is to use the state-of-the-art results for cross sections and branching ratios in the usual narrow width approximation and to combine those results with an appropriate prediction for the interference term.

Further studies of decay widths and cross sections with interferences from various sectors of the MSSM will be performed.

A. Derivation of on-shell neutralino field renormalisation constants

In addition to the summary of the on-shell field renormalisation constants $\delta Z_{ij}^{R/L}$ and $\delta \bar{Z}_{ij}^{R/L}$ in the neutralino sector in Sect. 4.3.2, we derive them in detail in this appendix.

First, we require that external on-shell (anti-) particles do not mix.

$$\hat{\Gamma}_{ij}\tilde{\chi}_j^0(p)|_{p^2=m_{\tilde{\chi}_j^0}^2} = 0 \tag{A.1}$$

$$\overline{\tilde{\chi}_i^0}(p)\hat{\Gamma}_{ij}|_{p^2=m_{\tilde{\chi}_i^0}^2} = 0 \tag{A.2}$$

Second, the residues of the diagonal propagators are normalised to unity.

$$\lim_{p^2\to m_{\tilde{\chi}_i^0}^2} \frac{1}{\not{p}-m_{\tilde{\chi}_i^0}}\hat{\Gamma}_{ii}\tilde{\chi}_i^0(p) = i\tilde{\chi}_i^0 \tag{A.3}$$

$$\lim_{p^2\to m_{\tilde{\chi}_i^0}^2} \overline{\tilde{\chi}_i^0}(p)\hat{\Gamma}_{ii}\frac{1}{\not{p}-m_{\tilde{\chi}_i^0}} = i\overline{\tilde{\chi}_i^0} \tag{A.4}$$

In order to ensure the same Lorentz structure of the renormalised diagonal propagator as at tree level when taking the on-shell limit, the γ_5-dependence needs to be eliminated. This requirement leads to equal coefficients of the right- and left-handed projection operators, $\omega_{R/L}$ and therewith to equal right- and left-handed renormalised diagonal self-energies evaluated on-shell at the tree-level mass, both for the scalar and vector components,

$$\hat{\Sigma}_{ii}^L(m_{\tilde{\chi}_i^0}^2) = \hat{\Sigma}_{ii}^R(m_{\tilde{\chi}_i^0}^2), \tag{A.5}$$

$$\hat{\Sigma}_{ii}^{SL}(m_{\tilde{\chi}_i^0}^2) = \hat{\Sigma}_{ii}^{SR}(m_{\tilde{\chi}_i^0}^2), \tag{A.6}$$

so that the vector and scalar structure of the diagonal propagator can be summarised as

$$
\hat{S}_{ii}^{-1}(p)|_{p^2=m_{\tilde{\chi}_i^0}^2} \equiv -i\hat{\Gamma}_{ii}(p)|_{p^2=m_{\tilde{\chi}_i^0}^2}
$$

$$
\overset{(4.59,4.65,A.5,A.6)}{=} \left[\frac{\not{p}(1+\hat{\Sigma}_{ii}(m_{\tilde{\chi}_i^0}^2)) + m_{\tilde{\chi}_i^0} - \hat{\Sigma}_{ii}^S(m_{\tilde{\chi}_i^0}^2)}{m_{\tilde{\chi}_i^0}^2(1+\hat{\Sigma}_{ii}(m_{\tilde{\chi}_i^0}^2))^2 - (m_{\tilde{\chi}_i^0} - \hat{\Sigma}_{ii}^S(m_{\tilde{\chi}_i^0}^2))^2} \right]_{p^2=m_{\tilde{\chi}_i^0}^2} . \tag{A.7}
$$

Off-diagonal renormalisation constants $(i \neq j)$ For $i \neq j$, we would like to derive the off-diagonal renormalisation constants $\delta Z_{0,ij}^{R/L}$, $\delta \bar{Z}_{0,ij}^{R/L}$. Requiring that the ith and jth neutralinos do not mix in the on-shell limit, we obtain

$$
\hat{\Gamma}_{ij}\tilde{\chi}_j^0(p)|_{p^2=m_{\tilde{\chi}_j^0}^2} \overset{(4.65)}{=} [i(\not{p}-m_{\tilde{\chi}_i^0})\delta_{ij} + i\hat{\Sigma}_{ij}(p^2)]\tilde{\chi}_j^0(p)|_{p^2=m_{\tilde{\chi}_j^0}^2, i\neq j}
$$

$$
= i\hat{\Sigma}_{ij}(p^2)\tilde{\chi}_j^0(p)|_{p^2=m_{\tilde{\chi}_j^0}^2} \overset{(A.1)}{=} 0. \tag{A.8}
$$

Furthermore, since the axial part of the projection operators $\omega_{L/R}$ anticommutes with the γ_μ matrices in $\not{p}$, the L/R coefficients are switched in front of the vector parts $\hat{\Sigma}_{ij}^{L/R}$,

$$
\not{p}\omega_{L/R}\tilde{\chi}_j^0(p)|_{p^2=m_{\tilde{\chi}_j^0}^2} = \omega_{R/L}\not{p}\tilde{\chi}_j^0(p)|_{p^2=m_{\tilde{\chi}_j^0}^2} = \omega_{R/L}m_{\tilde{\chi}_j^0}\tilde{\chi}_j^0(p^2=m_{\tilde{\chi}_j^0}^2). \tag{A.9}
$$

Now we write Eq. (A.8) explicitly as

$$
i\hat{\Sigma}_{ij}(p^2)\tilde{\chi}_j^0(p)|_{p^2=m_{\tilde{\chi}_j^0}^2} = i[(\hat{\Sigma}_{ij}^L\omega_R + \hat{\Sigma}_{ij}^R\omega_L)m_{\tilde{\chi}_j^0} + \omega_L\hat{\Sigma}_{ij}^{SL} + \omega_R\hat{\Sigma}_{ij}^{SR}]\tilde{\chi}_j^0(p)|_{p^2=m_{\tilde{\chi}_j^0}^2} = 0
$$

$$
= i\omega_R\underbrace{[m_{\tilde{\chi}_j^0}\hat{\Sigma}_{ij}^L + \hat{\Sigma}_{ij}^{SR}]}_{=C_R} + i\omega_L\underbrace{[m_{\tilde{\chi}_j^0}\hat{\Sigma}_{ij}^R + \hat{\Sigma}_{ij}^{SL}]}_{=C_L}. \tag{A.10}
$$

Due to the cancellation of $\frac{m_{\tilde{\chi}_j^0}}{2}\delta \bar{Z}_{ij}^L$ in the right-handed coefficient C_R and $\frac{m_{\tilde{\chi}_j^0}}{2}\delta \bar{Z}_{ij}^R$ in the left-handed coefficient C_L, they read

$$
C_R = m_{\tilde{\chi}_j^0}\Sigma_{ij}^L(m_{\tilde{\chi}_j^0}^2) + \frac{m_{\tilde{\chi}_j^0}}{2}\delta Z_{ij}^L + \Sigma_{ij}^{SR}(m_{\tilde{\chi}_j^0}^2) - (N\delta Y^\dagger N^T)_{ij} - \frac{m_{\tilde{\chi}_i^0}}{2}\delta Z_{ij}^R \tag{A.11}
$$

$$
C_L = m_{\tilde{\chi}_j^0}\Sigma_{ij}^R(m_{\tilde{\chi}_j^0}^2) + \frac{m_{\tilde{\chi}_j^0}}{2}\delta Z_{ij}^R + \Sigma_{ij}^{SL}(m_{\tilde{\chi}_j^0}^2) - (N^*\delta Y N^\dagger)_{ij} - \frac{m_{\tilde{\chi}_i^0}}{2}\delta Z_{ij}^L. \tag{A.12}
$$

Thus, we rewrite Eq. (A.10) as

$$0 = \frac{1}{2}(1 + \gamma_5)C_R + \frac{1}{2}(1 - \gamma_5)C_L = \frac{1}{2}(C_R + C_L) + \frac{1}{2}\gamma_5(C_R - C_L) \qquad \text{(A.13)}$$

After separating the axial part, both terms have to vanish simultaneously, so we can conclude that both coefficients, C_L and C_R must be identical to zero;

$$C_R + C_L = 0 \wedge C_R - C_L = 0 \Leftrightarrow C_L = C_R = 0. \qquad \text{(A.14)}$$

Moreover, in order to solve for δZ_{ij}^L, we take a linear combination of Eqs. (A.11, A.12):

$$0 = m_{\tilde{\chi}_j^0} \cdot C_R + m_{\tilde{\chi}_i^0} \cdot C_L$$

$$= m_{\tilde{\chi}_j^0}^2 \Sigma_{ij}^L(m_{\tilde{\chi}_j^0}^2) + \frac{m_{\tilde{\chi}_j^0}^2}{2}\delta Z_{ij}^L + \Sigma_{ij}^{SR}(m_{\tilde{\chi}_j^0}^2)m_{\tilde{\chi}_j^0} - m_{\tilde{\chi}_j^0}(N\delta Y^\dagger N^T)_{ij}$$

$$+ m_{\tilde{\chi}_i^0} m_{\tilde{\chi}_j^0} \Sigma_{ij}^R(m_{\tilde{\chi}_j^0}^2) - \frac{m_{\tilde{\chi}_i^0}^2}{2}\delta Z_{ij}^L + \Sigma_{ij}^{SL}(m_{\tilde{\chi}_j^0}^2)m_{\tilde{\chi}_i^0} - m_{\tilde{\chi}_i^0}(N^*\delta Y N^\dagger)_{ij}. \qquad \text{(A.15)}$$

Likewise, we add $m_{\tilde{\chi}_i^0} \cdot C_R + m_{\tilde{\chi}_j^0} \cdot C_L = 0$ to solve for δZ_{ij}^R with the solution in Eq. (4.66). Next, we proceed with the same method, but using Eq. (A.2) instead of (A.1) in order to solve for $\delta\bar{Z}_{ij}^{L/R}$. Inserting the mass $m_{\tilde{\chi}_i^0}$,

$$\overline{\tilde{\chi}_i^0}(p)\,\slashed{p}\,\omega_{L/R}\,\hat{\Sigma}_{ij}^{(S)L/R}\big|_{p^2=m_{\tilde{\chi}_i^0}^2} = m_{\tilde{\chi}_i^0}\overline{\tilde{\chi}_i^0}(p)\,\omega_{L/R}\,\hat{\Sigma}_{ij}^{(S)L/R}\big|_{p^2=m_{\tilde{\chi}_i^0}^2}, \qquad \text{(A.16)}$$

we obtain the following equations with coefficients $C_{\bar{L}}$, $C_{\bar{R}}$

$$i\overline{\tilde{\chi}_i^0}(p)\hat{\Sigma}_{ij}(m_{\tilde{\chi}_i^0}^2)\big|_{p^2=m_{\tilde{\chi}_i^0}^2} = i\overline{\tilde{\chi}_i^0}(p)[\omega_R C_{\bar{R}} + \omega_L C_{\bar{L}}]\big|_{p^2=m_{\tilde{\chi}_i^0}^2} = 0 \quad \forall\tilde{\chi}_i^0. \qquad \text{(A.17)}$$

As this relation has to hold for all $\overline{\tilde{\chi}_i^0}$, we conclude

$$\omega_R C_{\bar{R}} + \omega_L C_{\bar{L}} = 0, \qquad \text{(A.18)}$$

where coefficients labelled with bars are expressed in terms of barred field renormalisation constants;

$$C_{\bar{R}} = m_{\tilde{\chi}_i^0}\Sigma_{ij}^R(m_{\tilde{\chi}_i^0}^2) + \Sigma_{ij}^{SR}(m_{\tilde{\chi}_i^0}^2) - (N\delta Y^\dagger N^T)_{ij} + \frac{m_{\tilde{\chi}_i^0}}{2}\delta\bar{Z}_{ij}^R - \frac{m_{\tilde{\chi}_j^0}}{2}\delta\bar{Z}_{ij}^L \qquad \text{(A.19)}$$

$$C_{\bar{L}} = m_{\tilde{\chi}_i^0}\Sigma_{ij}^L(m_{\tilde{\chi}_i^0}^2) + \Sigma_{ij}^{SL}(m_{\tilde{\chi}_i^0}^2) - (N^*\delta Y N^\dagger)_{ij} + \frac{m_{\tilde{\chi}_i^0}}{2}\delta\bar{Z}_{ij}^L - \frac{m_{\tilde{\chi}_j^0}}{2}\delta\bar{Z}_{ij}^R. \qquad \text{(A.20)}$$

From the γ_5-independence of Eq. (A.18), we can conclude that $C_{\bar{R}} = 0 = C_{\bar{L}}$. Hence, taking the linear combinations

$$0 = m_{\tilde{\chi}_i^0} C_{\bar{R}} + m_{\tilde{\chi}_j^0} C_{\bar{L}} = m_{\tilde{\chi}_j^0} C_{\bar{R}} + m_{\tilde{\chi}_i^0} C_{\bar{L}} \tag{A.21}$$

enables us to solve for $\delta \bar{Z}_{ij}^R$ and $\delta \bar{Z}_{ij}^L$, respectively, to obtain Eq. (4.67).

Diagonal renormalisation constants ($i = j$)   For the diagonal renormalisation constants $\delta Z_{ii}, \delta \bar{Z}_{ii}$, we set use Eq. (A.3) and insert the 2-point vertex function $\hat{\Gamma}_{ii}$ from Eq. (4.65).

$$i\tilde{\chi}_i^0 = \lim_{p^2 \to m_{\tilde{\chi}_i^0}^2} \frac{1}{\not{p} - m_{\tilde{\chi}_i^0}} \hat{\Gamma}_{ii} \tilde{\chi}_i^0(p) = \lim_{p^2 \to m_{\tilde{\chi}_i^0}^2} i \left[1 + \frac{\hat{\Sigma}_{ii}(p^2)}{\not{p} - m_{\tilde{\chi}_i^0}} \right] \tilde{\chi}_i^0(p) \tag{A.22}$$

Subtracting $i\tilde{\chi}_i^0$ on both sides leads to

$$0 = \lim_{p^2 \to m_{\tilde{\chi}_i^0}^2} \frac{\not{p}\omega_L \hat{\Sigma}_{ii}^L(p^2) + \not{p}\omega_R \hat{\Sigma}_{ii}^R(p^2) + \omega_L \hat{\Sigma}_{ii}^{SL}(p) + \omega_R \hat{\Sigma}_{ii}^{SR}(p^2)}{\not{p} - m_{\tilde{\chi}_i^0}} \tag{A.23}$$

For a simplification of this limit, we rewrite

$$\not{p}\omega_{L/R} \hat{\Sigma}_{ii}^{L/R} = m_{\tilde{\chi}_i^0} \omega_{L/R} \hat{\Sigma}_{ii}^{L/R} + (\not{p} - m_{\tilde{\chi}_i^0})\omega_{L/R} \hat{\Sigma}_{ii}^{L/R} \text{ and} \tag{A.24}$$

$$\frac{1}{\not{p} - m_{\tilde{\chi}_i^0}} = \frac{\not{p} + m_{\tilde{\chi}_i^0}}{p^2 - m_{\tilde{\chi}_i^0}^2} \tag{A.25}$$

in Eq. (A.23) to obtain

$$0 = \lim_{p^2 \to m_{\tilde{\chi}_i^0}^2} \frac{\not{p} + m_{\tilde{\chi}_i^0}}{p^2 - m_{\tilde{\chi}_i^0}^2} \left[m_{\tilde{\chi}_i^0} \omega_L \hat{\Sigma}_{ii}^L(p^2) + m_{\tilde{\chi}_i^0} \omega_R \hat{\Sigma}_{ii}^R(p^2) + \omega_L \hat{\Sigma}_{ii}^{SL}(p^2) \right.$$

$$\left. + \omega_R \hat{\Sigma}_{ii}^{SR}(p^2) \right] \tilde{\chi}_i^0(p) + \lim_{p^2 \to m_{\tilde{\chi}_i^0}^2} \underbrace{\frac{(\not{p} + m_{\tilde{\chi}_i^0})(\not{p} - m_{\tilde{\chi}_i^0})}{p^2 - m_{\tilde{\chi}_i^0}^2}}_{=1} \left[\omega_L \hat{\Sigma}_{ii}^L(p^2) + \omega_R \hat{\Sigma}_{ii}^R(p^2) \right] \tilde{\chi}_i^0(p).$$

$$\tag{A.26}$$

Taking the on-shell limit $p^2 \to m_{\tilde{\chi}_i^0}^2$ of the second square bracket simply affects the evaluation of the renormalised, diagonal self-energies, whereas the first square bracket requires an expansion about the mass $m_{\tilde{\chi}_i^0}^2$,

$$\hat{\Sigma}_{ii}^{(S)L/R}(p^2) = \hat{\Sigma}_{ii}^{(S)L/R}(m_{\tilde{\chi}_i^0}^2) + \hat{\Sigma}_{ii}'^{(S)L/R}(m_{\tilde{\chi}_i^0}^2) \cdot (p^2 - m_{\tilde{\chi}_i^0}^2) + \mathcal{O}\left((p^2 - m_{\tilde{\chi}_i^0}^2)^2 \right), \tag{A.27}$$

where $\hat{\Sigma}'_{ii}(p2) = \frac{\partial \hat{\Sigma}_{ii}(p^2)}{\partial(p^2)}$ is the derivative of the self-energy. Now we impose an on-shell condition for the mass:

$$\hat{\Sigma}_{ii}^{(S)L/R}(m_{\tilde{\chi}_i^0}^2) = 0. \tag{A.28}$$

The difference between the evaluation of the self-energy at the pole mass $M_{\tilde{\chi}_i^0}^2$ or tree-level mass $m_{\tilde{\chi}_i^0}^2$ is of two-loop order. So the first term in the expansion in Eq. (A.27) vanishes and at one-loop order only the term with the derivative of the self-energy times $(p^2 - m_{\tilde{\chi}_i^0}^2)$ remains. This is applied on the first limit in Eq. (A.26). Furthermore, with Eq. (A.9) we can derive

$$\lim_{p^2 \to m_{\tilde{\chi}_i^0}^2} \frac{\not{p} + m_{\tilde{\chi}_i^0}}{p^2 - m_{\tilde{\chi}_i^0}^2} \left[m_{\tilde{\chi}_i^0}(\omega_L \hat{\Sigma}_{ii}^{\prime L} + \omega_R \hat{\Sigma}_{ii}^{\prime R}) + \omega_L \hat{\Sigma}_{ii}^{\prime SL} + \omega_R \hat{\Sigma}_{ii}^{\prime SR} \right] (p^2 - m_{\tilde{\chi}_i^0}^2) \tilde{\chi}_i^0(p)$$

$$= [m_{\tilde{\chi}_i^0}^2((\omega_L + \omega_R)\hat{\Sigma}_{ii}^{\prime L}(m_{\tilde{\chi}_i^0}^2) + (\omega_R + \omega_L)\hat{\Sigma}_{ii}^{\prime R}(m_{\tilde{\chi}_i^0}^2))$$
$$+ m_{\tilde{\chi}_i^0}((\omega_L + \omega_R)\hat{\Sigma}_{ii}^{\prime SL}(m_{\tilde{\chi}_i^0}^2) + (\omega_R + \omega_L)\hat{\Sigma}_{ii}^{\prime SR}(m_{\tilde{\chi}_i^0}^2))]\tilde{\chi}_i^0(p)|_{p^2 = m_{\tilde{\chi}_i^0}^2}. \tag{A.29}$$

Thus, we deduce the left- and right-handed coefficients $C_{L/R}^D$ (where D denotes diagonal) for the determination of the diagonal field renormalisation constants from Eqs. (A.27, A.29).

$$0 = \omega_L C_L^D + \omega_R C_R^D \quad \text{with } C_L^D = 0 = C_R^D \text{ and}$$
$$C_L^D = \hat{\Sigma}_{ii}^L(m_{\tilde{\chi}_i^0}^2) + \underbrace{m_{\tilde{\chi}_i^0}^2 \left[\hat{\Sigma}_{ii}^{\prime L}(m_{\tilde{\chi}_i^0}^2) + \hat{\Sigma}_{ii}^{\prime R}(m_{\tilde{\chi}_i^0}^2) \right] + m_{\tilde{\chi}_i^0} \left[\hat{\Sigma}_{ii}^{\prime SL}(m_{\tilde{\chi}_i^0}^2) + \hat{\Sigma}_{ii}^{\prime SR}(m_{\tilde{\chi}_i^0}^2) \right]}_{=:R_L(m_{\tilde{\chi}_i^0}^2)}$$
$$\tag{A.30}$$
$$C_R^D = \hat{\Sigma}_{ii}^R(m_{\tilde{\chi}_i^0}^2) + \underbrace{m_{\tilde{\chi}_i^0}^2 \left[\hat{\Sigma}_{ii}^{\prime R}(m_{\tilde{\chi}_i^0}^2) + \hat{\Sigma}_{ii}^{\prime L}(m_{\tilde{\chi}_i^0}^2) \right] + m_{\tilde{\chi}_i^0} \left[\hat{\Sigma}_{ii}^{\prime SR}(m_{\tilde{\chi}_i^0}^2) + \hat{\Sigma}_{ii}^{\prime SL}(m_{\tilde{\chi}_i^0}^2) \right]}_{=:R_R(m_{\tilde{\chi}_i^0}^2)}.$$
$$\tag{A.31}$$

We summarised the remaining expression of the coefficients apart from the renormalised self-energies in the functions $R_{L/R}(p^2)$. Using the renormalised self-energies from Eq. (4.60) leads to the following relations for the sum of barred or unbarred diagonal neutralino field renormalisation constants in the left- or right-handed case:

$$\frac{1}{2}\left(\delta Z_{ii}^{L/R} + \delta \bar{Z}_{ii}^{L/R}\right) = -\Sigma_{ii}^{L/R}(m_{\tilde{\chi}_i^0}^2) - R_{ii}^{L/R}(m_{\tilde{\chi}_i^0}^2). \tag{A.32}$$

In the following, we shall collect linear combinations of the diagonal neutralino field renormalisation constants in a system of equations. Its solution will determine these

field renormalisation constants $\delta Z_{ii}^{L/R}$, $\delta \bar{Z}_{ii}^{L/R}$. For brevity, we define the coefficients b_i, $i = 1, 2, 3, 4$ as the explicit expressions of sums and differences of the renormalisation constants in order to use them more conveniently in a the linear system of equations;

$$b_1 := \delta Z_{ii}^L + \delta \bar{Z}_{ii}^L = -2 \left(\Sigma_{ii}^L(m_{\tilde{\chi}_i^0}^2) + m_{\tilde{\chi}_i^0}^2 \left[\hat{\Sigma}_{ii}^{\prime L}(m_{\tilde{\chi}_i^0}^2) + \hat{\Sigma}_{ii}^{\prime R}(m_{\tilde{\chi}_i^0}^2) \right] \right.$$
$$\left. + m_{\tilde{\chi}_i^0} \left[\hat{\Sigma}_{ii}^{\prime SL}(m_{\tilde{\chi}_i^0}^2) + \hat{\Sigma}_{ii}^{\prime SR}(m_{\tilde{\chi}_i^0}^2) \right] \right) \tag{A.33}$$

$$b_2 := \delta Z_{ii}^R + \delta \bar{Z}_{ii}^R = -2 \left(\Sigma_{ii}^R(m_{\tilde{\chi}_i^0}^2) + m_{\tilde{\chi}_i^0}^2 \left[\hat{\Sigma}_{ii}^{\prime L}(m_{\tilde{\chi}_i^0}^2) + \hat{\Sigma}_{ii}^{\prime R}(m_{\tilde{\chi}_i^0}^2) \right] \right.$$
$$\left. + m_{\tilde{\chi}_i^0} \left[\hat{\Sigma}_{ii}^{\prime SL}(m_{\tilde{\chi}_i^0}^2) + \hat{\Sigma}_{ii}^{\prime SR}(m_{\tilde{\chi}_i^0}^2) \right] \right). \tag{A.34}$$

Since the remaining terms, summarised as $R_{L/R} \equiv R_{ii}(m_{\tilde{\chi}_i^0}^2)$ in Eqs. (A.30, A.31), are equal, the on-shell renormalisation conditions trivially lead to Eq. (A.5),

$$0 = \hat{\Sigma}_{ii}^L(m_{\tilde{\chi}_i^0}^2) + R_{ii}(m_{\tilde{\chi}_i^0}^2) = \hat{\Sigma}_{ii}^R(m_{\tilde{\chi}_i^0}^2) + R_{ii}(m_{\tilde{\chi}_i^0}^2), \tag{A.35}$$

and $\hat{\Sigma}_{ii}^L(m_{\tilde{\chi}_i^0}^2) = \hat{\Sigma}_{ii}^R(m_{\tilde{\chi}_i^0}^2)$ follows automatically. In order to fix the renormalisation constants, we also need the condition in Eq. (A.6) into which the definitions (4.63, 4.64) of the renormalised scalar self-energies are inserted. This leads to the following linear combination of renormalisation constants, which is summarised by the coefficient b_3 for the system of equations:

$$b_3 := \delta Z_{ii}^R - \delta \bar{Z}_{ii}^R + \delta \bar{Z}_{ii}^L - \delta Z_{ii}^L$$
$$= \frac{2 \left(\Sigma_{ii}^{SR}(m_{\tilde{\chi}_i^0}^2) - \Sigma_{ii}^{SL}(m_{\tilde{\chi}_i^0}^2) + (N^* \delta Y N^\dagger)_{ii} - (N \delta Y^\dagger N^T)_{ii} \right)}{m_{\tilde{\chi}_i^0}}. \tag{A.36}$$

This means that so far there are three conditions, but the aim is to fix the four constants $\delta Z_{ii}^{L/R}, \delta \bar{Z}_{ii}^{L/R}$. Having already exploited all renormalisation conditions, the fourth determining equation is of free choice. For symmetry reasons and according to [70], we choose

$$b_4 := \delta Z_{ii}^L - \delta \bar{Z}_{ii}^L + \delta Z_{ii}^R - \delta \bar{Z}_{ii}^R \overset{!}{=} 0. \tag{A.37}$$

Since the four equations (A.33, A.34, A.36, A.37) are linearly independent, the solution is unique and given by this linear system of equations

$$\begin{pmatrix} +1 & +1 & 0 & 0 \\ 0 & 0 & +1 & +1 \\ -1 & +1 & +1 & -1 \\ +1 & -1 & +1 & -1 \end{pmatrix} \cdot \begin{pmatrix} \delta Z_{ii}^L \\ \delta \bar{Z}_{ii}^L \\ \delta Z_{ii}^R \\ \delta \bar{Z}_{ii}^R \end{pmatrix} = \begin{pmatrix} b_1 \\ b_2 \\ b_3 \\ b_4 \end{pmatrix}. \tag{A.38}$$

Applying Gauß's algorithm or using `Mathematica`, this system is solved by

$$\delta Z_{ii}^{L/R} = \frac{2b_1 \mp b_3 + b_4}{4}$$

$$\delta \bar{Z}_{ii}^{L/R} = \frac{2b_1 \pm b_3 - b_4}{4}$$

The explicit results for $\delta Z_{ii}^{L/R}$ and $\delta \bar{Z}_{ii}^{L/R}$ are given in Eqs. (4.68, 4.69).
While in the off-diagonal case the requirement of vanishing coefficients $C_{L/R}, C_{\bar{L}/\bar{R}}$ provided four independent equations, the solution of the equations in the diagonal case required two additional conditions (A.36, A.37).

Acknowledgements

Bibliography

[1] J. Reuter, "Off-Shell and Interference Effects for SUSY Particle Production," `arXiv:0709.0068 [hep-ph]`.

[2] D. Berdine, N. Kauer, and D. Rainwater, "Breakdown of the Narrow Width Approximation for New Physics," *Phys. Rev. Lett.* **99** (2007) 111601, `arXiv:hep-ph/0703058`.

[3] J. Kalinowski, W. Kilian, J. Reuter, T. Robens, and K. Rolbiecki, "Pinning down the Invisible Sneutrino," *JHEP* **10** (2008) 090, `arXiv:0809.3997 [hep-ph]`.

[4] C. F. Uhlemann, "Narrow-Width Approximation in the Minimal Supersymmetric Standard Model." Diploma Thesis, Würzburg, 2007.

[5] M. Bohm, A. Denner, and H. Joos, "Gauge theories of the strong and electroweak interaction,".

[6] A. Denner, "Techniques for calculation of electroweak radiative corrections at the one loop level and results for W physics at LEP-200," *Fortsch.Phys.* **41** (1993) 307–420, `arXiv:0709.1075 [hep-ph]`.

[7] S. Glashow, "Partial Symmetries of Weak Interactions," *Nucl.Phys.* **22** (1961) 579–588.

[8] A. Salam, "Weak and Electromagnetic Interactions," *Conf.Proc.* **C680519** (1968) 367–377.

[9] S. Weinberg, "A Model of Leptons," *Phys. Rev. Lett.* **19** (Nov, 1967) 1264–1266. `http://link.aps.org/doi/10.1103/PhysRevLett.19.1264`.

[10] S. Glashow, J. Iliopoulos, and L. Maiani, "Weak Interactions with Lepton-Hadron Symmetry," *Phys.Rev.* **D2** (1970) 1285–1292.

[11] Barate, R. and others, LEP Working Group for Higgs boson searches, ALEPH Collaboration, DELPHI Collaboration, L3 Collaboration, OPAL Collaboration, "Search for the standard model Higgs boson at LEP," *Phys.Lett.* **B565** (2003) 61–75, `arXiv:hep-ex/0306033 [hep-ex]`.

[12] "Combination of Higgs Boson Searches with up to 4.9 fb-1 of pp Collisions Data Taken at a center-of-mass energy of 7 TeV with the ATLAS Experiment at the LHC," Tech. Rep. ATLAS-CONF-2011-163, Dec 2011.

[13] The CMS Collaboration, "Search for Neutral Higgs Bosons Decaying to Tau Pairs in pp Collisions at sqrts=7 TeV." CMS-PAS-HIG-11-029, 2011.

[14] ATLAS Collaboration, "Combined search for the Standard Model Higgs boson using up to 4.9 fb-1 of pp collision data at sqrt(s) = 7 TeV with the ATLAS detector at the LHC," `arXiv:1202.1408 [hep-ex]`.

[15] CMS Collaboration, "Combined results of searches for the standard model Higgs boson in pp collisions at sqrt(s) = 7 TeV," `arXiv:1202.1488 [hep-ex]`.

[16] The TEVNPH Working Group for the CDF and D0 Collaborations, "Combined CDF and D0 Search for Standard Model Higgs Boson Production with up to 10/fb of Data," `arXiv:1203.3774 [hep-ex]`.

[17] Tevatron Electroweak Working Group, for the CDF and D0 Collaborations, "Combination of CDF and D0 results on the mass of the top quark using up to 5.8 fb-1 of data," `arXiv:1107.5255 [hep-ex]`.

[18] "Measurement of the top quark mass from 2011 ATLAS data using the template method," Tech. Rep. ATLAS-CONF-2011-120, Aug 2011.

[19] The CMS Collaboration, "Measurement of the top quark mass in the l+jets channel," Tech. Rep. CMS-PAS-TOP-10-009, 2011.

[20] K. Nakamura et al. (Particle Data Group), "Review of Particle Physics," *JP G* **37** (2010) 075021.

[21] N. Cabibbo, "Unitary Symmetry and Leptonic Decays," *Phys.Rev.Lett.* **10** (1963) 531–533.

[22] M. Kobayashi and T. Maskawa, "CP Violation in the Renormalizable Theory of Weak Interaction," *Prog. Theor. Phys.* **49** (1973) 652–657.

[23] P. W. Higgs, "Broken symmetries, massless particles and gauge fields," *Phys.Lett.* **12** (1964) 132–133.

[24] P. W. Higgs, "Broken Symmetries and the Masses of Gauge Bosons," *Phys.Rev.Lett.* **13** (1964) 508–509.

[25] F. Englert and R. Brout, "Broken Symmetry and the Mass of Gauge Vector Mesons," *Phys.Rev.Lett.* **13** (1964) 321–322.

[26] G. Guralnik, C. Hagen, and T. Kibble, "Global Conservation Laws and Massless Particles," *Phys.Rev.Lett.* **13** (1964) 585–587.

[27] T. Kibble, "Symmetry breaking in nonAbelian gauge theories," *Phys.Rev.* **155** (1967) 1554–1561.

[28] J. Goldstone, A. Salam, and S. Weinberg, "Broken Symmetries," *Phys. Rev.* **127** (1962) 965–970.

[29] Y. Nambu and G. Jona-Lasinio, "Dynamical Model of Elementary Particles Based on an Analogy with Superconductivity. 1.," *Phys.Rev.* **122** (1961) 345–358.

[30] D. Collaboration, "Measurement of the W Boson Mass with the D0 Detector," `arXiv:1203.0293 [hep-ex]`.

[31] C. Collaboration, "Precise measurement of the *W*-boson mass with the CDF II detector," `arXiv:1203.0275 [hep-ex]`.

[32] S. P. Martin, "A Supersymmetry Primer," `arXiv:hep-ph/9709356`.

[33] I. J. R. Aitchison, "Supersymmetry and the MSSM: An Elementary introduction," `arXiv:hep-ph/0505105`.

[34] D. Chung, L. Everett, G. Kane, S. King, J. D. Lykken, *et al.*, "The Soft supersymmetry breaking Lagrangian: Theory and applications," *Phys.Rept.* **407** (2005) 1–203, `arXiv:hep-ph/0312378 [hep-ph]`.

[35] H. P. Nilles, "Supersymmetry, Supergravity and Particle Physics," *Phys.Rept.* **110** (1984) 1–162.

[36] M. S. Carena, S. Pokorski, and C. Wagner, "On the unification of couplings in the minimal supersymmetric Standard Model," *Nucl.Phys.* **B406** (1993) 59–89, `arXiv:hep-ph/9303202 [hep-ph]`.

[37] S. Abel, S. Khalil, and O. Lebedev, "EDM constraints in supersymmetric theories," *Nucl.Phys.* **B606** (2001) 151–182, `arXiv:hep-ph/0103320 [hep-ph]`.

[38] J. R. Ellis, J. S. Lee, and A. Pilaftsis, "Electric Dipole Moments in the MSSM Reloaded," *JHEP* **0810** (2008) 049, `arXiv:0808.1819 [hep-ph]`.

[39] Y. Li, S. Profumo, and M. Ramsey-Musolf, "A Comprehensive Analysis of Electric Dipole Moment Constraints on CP-violating Phases in the MSSM," *JHEP* **1008** (2010) 062, `arXiv:1006.1440 [hep-ph]`.

[40] S. R. Coleman and J. Mandula, "All Possible Symmetries of the S Matrix," *Phys. Rev.* **159** (1967) 1251–1256.

[41] R. Haag, J. T. Lopuszanski, and M. Sohnius, "All Possible Generators of Supersymmetries of the s Matrix," *Nucl. Phys.* **B88** (1975) 257.

[42] S. Weinberg, *The Quantum Theory of Fields, Volume III: Supersymmetry.* Cambridge University Press, New York, 2000.

[43] G. 't Hooft, "Symmetry Breaking Through Bell-Jackiw Anomalies," *Phys.Rev.Lett.* **37** (1976) 8–11.

[44] G. R. Farrar and P. Fayet, "Phenomenology of the Production, Decay, and Detection of New Hadronic States Associated with Supersymmetry," *Phys.Lett.* **B76** (1978) 575–579.

[45] H. Goldberg, "Constraint on the Photino Mass from Cosmology," *Phys.Rev.Lett.* **50** (1983) 1419.

[46] J. R. Ellis, J. Hagelin, D. V. Nanopoulos, K. A. Olive, and M. Srednicki, "Supersymmetric Relics from the Big Bang," *Nucl.Phys.* **B238** (1984) 453–476.

[47] L. O'Raifeartaigh, "Spontaneous Symmetry Breaking for Chiral Scalar Superfields," *Nucl.Phys.* **B96** (1975) 331.

[48] P. Fayet and J. Iliopoulos, "Spontaneously Broken Supergauge Symmetries and Goldstone Spinors," *Phys.Lett.* **B51** (1974) 461–464.

[49] M. Dine and A. E. Nelson, "Dynamical supersymmetry breaking at low-energies," *Phys.Rev.* **D48** (1993) 1277–1287, `arXiv:hep-ph/9303230 [hep-ph]`.

[50] L. Randall and R. Sundrum, "Out of this world supersymmetry breaking," *Nucl.Phys.* **B557** (1999) 79–118, `arXiv:hep-th/9810155 [hep-th]`.

[51] H. E. Haber and R. Hempfling, "Can the mass of the lightest Higgs boson of the minimal supersymmetric model be larger than m(Z)?," *Phys.Rev.Lett.* **66** (1991) 1815–1818.

[52] J. R. Ellis, G. Ridolfi, and F. Zwirner, "Radiative corrections to the masses of supersymmetric Higgs bosons," *Phys.Lett.* **B257** (1991) 83–91.

[53] R. Barbieri and M. Frigeni, "The Supersymmetric Higgs searches at LEP after radiative corrections," *Phys.Lett.* **B258** (1991) 395–398.

[54] J. R. Ellis, G. Ridolfi, and F. Zwirner, "On radiative corrections to supersymmetric Higgs boson masses and their implications for LEP searches," *Phys.Lett.* **B262** (1991) 477–484.

[55] J. Espinosa and M. Quiros, "Two loop radiative corrections to the mass of the lightest Higgs boson in supersymmetric standard models," *Phys.Lett.* **B266** (1991) 389–396.

[56] S. Heinemeyer, W. Hollik, and G. Weiglein, "The Masses of the neutral CP - even Higgs bosons in the MSSM: Accurate analysis at the two loop level," *Eur. Phys. J.* **C9** (1999) 343–366, `arXiv:hep-ph/9812472`.

[57] J. F. Gunion and H. E. Haber, "The CP conserving two Higgs doublet model: The Approach to the decoupling limit," *Phys.Rev.* **D67** (2003) 075019, `arXiv:hep-ph/0207010 [hep-ph]`.

[58] T. Hahn, "Routines for the diagonalization of complex matrices," `arXiv:0607103v2 [pysics.comp-ph]`.

[59] T. Takagi, "On an algebraic problem related to an analytic theorem of Carathéodory and Fejér and on an allied theorem of Landau.," *Japanese J. Math.* **1** (1927) 83.

[60] A. J. Buras, "Minimal flavor violation," *Acta Phys.Polon.* **B34** (2003) 5615–5668, `arXiv:hep-ph/0310208 [hep-ph]`.

[61] S. AbdusSalam, B. Allanach, H. Dreiner, J. Ellis, U. Ellwanger, *et al.*, "Benchmark Models, Planes, Lines and Points for Future SUSY Searches at the LHC," *Eur.Phys.J.* **C71** (2011) 1835, `arXiv:1109.3859 [hep-ph]`.

[62] G. L. Kane, C. F. Kolda, L. Roszkowski, and J. D. Wells, "Study of constrained minimal supersymmetry," *Phys.Rev.* **D49** (1994) 6173–6210, `arXiv:hep-ph/9312272 [hep-ph]`.

[63] The ATLAS Collaboration, "ATLAS SUSY searches." `https://twiki.cern.ch/twiki/bin/view/AtlasPublic/CombinedSummaryPlots`.

[64] The CMS Collaboration, "CMS SUSY searches." `https://twiki.cern.ch/twiki/bin/view/CMSPublic/PhysicsResultsSUS`.

[65] H. Anlauf, "Radiative Corrections in Gauge Theories." Lecture notes, Split 2001.

[66] G. Weiglein, "Renormalisation and precision physics." Lecture notes, Feldberg 2005.

[67] G. 't Hooft and M. Veltman, "Regularization and Renormalization of Gauge Fields," *Nucl.Phys.* **B44** (1972) 189–213.

[68] W. Hollik and H. J. Timme, "Renormalization scheme dependence of electroweak radiative corrections," *Z. Phys.* **C33** (1986) 125.

[69] G. 't Hooft, "Renormalization of Massless Yang-Mills Fields," *Nucl.Phys.* **B33** (1971) 173–199.

[70] A. Fowler, "Higher order and CP-violating effects in the neutralino and Higgs boson sectors of the MSSM." PhD Thesis, Durham, 2010.

[71] M. Steinhauser, "Leptonic contribution to the effective electromagnetic coupling constant up to three loops," *Phys.Lett.* **B429** (1998) 158–161, `arXiv:hep-ph/9803313 [hep-ph]`.

[72] H. Burkhardt and B. Pietrzyk, "Low energy hadronic contribution to the QED vacuum polarization," *Phys.Rev.* **D72** (2005) 057501, `arXiv:hep-ph/0506323 [hep-ph]`.

[73] M. Bohm, H. Spiesberger, and W. Hollik, "On the One Loop Renormalization of the Electroweak Standard Model and Its Application to Leptonic Processes," *Fortsch.Phys.* **34** (1986) 687–751.

[74] D. Capper, D. Jones, and P. van Nieuwenhuizen, "Regularization by Dimensional Reduction of Supersymmetric and Nonsupersymmetric Gauge Theories," *Nucl.Phys.* **B167** (1980) 479.

[75] W. Siegel, "Supersymmetric Dimensional Regularization via Dimensional Reduction," *Phys.Lett.* **B84** (1979) 193.

[76] W. Hollik, E. Kraus, M. Roth, C. Rupp, K. Sibold, and D. Stöckinger, "Renormalization of the minimal supersymmetric standard model," *Nucl.Phys.* **B639** (2002) 3–65, `arXiv:hep-ph/0204350 [hep-ph]`.

[77] A. Signer and D. Stockinger, "Factorization and regularization by dimensional reduction," *Phys.Lett.* **B626** (2005) 127–138, `arXiv:hep-ph/0508203 [hep-ph]`.

[78] D. Stockinger, "Regularization by dimensional reduction: consistency, quantum action principle, and supersymmetry," *JHEP* **0503** (2005) 076, `arXiv:hep-ph/0503129 [hep-ph]`.

[79] F. del Aguila, A. Culatti, R. Munoz Tapia, and M. Perez-Victoria, "Techniques for one loop calculations in constrained differential renormalization," *Nucl.Phys.* **B537** (1999) 561–585, `arXiv:hep-ph/9806451 [hep-ph]`.

[80] T. Hahn and M. Perez-Victoria, "Automatized one-loop calculations in four and D dimensions," *Comput. Phys. Commun.* **118** (1999) 153–165, `arXiv:hep-ph/9807565`.

[81] M. Frank, T. Hahn, S. Heinemeyer, W. Hollik, H. Rzehak, and G. Weiglein, "The Higgs boson masses and mixings of the complex MSSM in the Feynman-diagrammatic approach," *JHEP* **02** (2007) 047, `arXiv:hep-ph/0611326`.

[82] A. Freitas and D. Stockinger, "Gauge dependence and renormalization of tan beta in the MSSM," *Phys.Rev.* **D66** (2002) 095014, `arXiv:hep-ph/0205281 [hep-ph]`.

[83] M. Frank, S. Heinemeyer, W. Hollik, and G. Weiglein, "FeynHiggs1.2: Hybrid MS-bar / on-shell renormalization for the CP even Higgs boson sector in the MSSM," `arXiv:hep-ph/0202166 [hep-ph]`.

[84] S. Heinemeyer, W. Hollik, and G. Weiglein, "FeynHiggs: a program for the calculation of the masses of the neutral CP-even Higgs bosons in the MSSM," *Comput. Phys. Commun.* **124** (2000) 76–89, `arXiv:hep-ph/9812320`.

[85] G. Degrassi, S. Heinemeyer, W. Hollik, P. Slavich, and G. Weiglein, "Towards high-precision predictions for the MSSM Higgs sector," *Eur. Phys. J.* **C28** (2003) 133–143, `arXiv:hep-ph/0212020`.

[86] S. Heinemeyer, W. Hollik, H. Rzehak, and G. Weiglein, "The Higgs sector of the complex MSSM at two-loop order: QCD contributions," *Phys.Lett.* **B652** (2007) 300–309, `arXiv:0705.0746 [hep-ph]`.

[87] A. Lahanas, K. Tamvakis, and N. Tracas, "One loop corrections to the neutralino sector and radiative electroweak breaking in the MSSM," *Phys.Lett.* **B324** (1994) 387–396, `arXiv:hep-ph/9312251 [hep-ph]`.

[88] D. Pierce and A. Papadopoulos, "Radiative corrections to neutralino and chargino masses in the minimal supersymmetric model," *Phys.Rev.* **D50** (1994) 565–570, `arXiv:hep-ph/9312248 [hep-ph]`.

[89] T. Fritzsche and W. Hollik, "Complete one loop corrections to the mass spectrum of charginos and neutralinos in the MSSM," *Eur.Phys.J.* **C24** (2002) 619–629, `arXiv:hep-ph/0203159 [hep-ph]`.

[90] W. Oller, H. Eberl, and W. Majerotto, "Precise predictions for chargino and neutralino pair production in e+ e- annihilation," *Phys.Rev.* **D71** (2005) 115002, `arXiv:hep-ph/0504109 [hep-ph]`.

[91] A. Fowler and G. Weiglein, "Precise Predictions for Higgs Production in Neutralino Decays in the Complex MSSM," *JHEP* **1001** (2010) 108, `arXiv:0909.5165 [hep-ph]`.

[92] A. Bharucha, A. Fowler, G. Moortgat-Pick, and G. Weiglein, "Renormalisation in the Chargino and Neutralino sector of the complex MSSM." DESY 12-015.

[93] D. M. Pierce, J. A. Bagger, K. T. Matchev, and R.-J. Zhang, "Precision corrections in the minimal supersymmetric standard model," *Nucl.Phys.* **B491** (1997) 3–67, `arXiv:hep-ph/9606211 [hep-ph]`.

[94] H. Eberl, M. Kincel, W. Majerotto, and Y. Yamada, "One loop corrections to the chargino and neutralino mass matrices in the on-shell scheme," *Phys.Rev.* **D64** (2001) 115013, `arXiv:hep-ph/0104109 [hep-ph]`.

[95] A. Bharucha, "Renormalisation in the Chargino and Neutralino sector of the complex MSSM." Theory Seminar Bonn, May 30th 2011.

[96] A. Chatterjee, M. Drees, S. Kulkarni, and Q. Xu, "On the On-Shell Renormalization of the Chargino and Neutralino Masses in the MSSM," `arXiv:1107.5218 [hep-ph]`.

[97] J. Kublbeck, M. Bohm, and A. Denner, "FeynArts: Computer algebraic generation of Feynman graphs and amplitudes," *Comput.Phys.Commun.* **60** (1990) 165–180.

[98] A. Denner, H. Eck, O. Hahn, and J. Kublbeck, "Feynman rules for fermion number violating interactions," *Nucl.Phys.* **B387** (1992) 467–484.

[99] J. Kublbeck, H. Eck, and R. Mertig, "Computeralgebraic generation and calculation of Feynman graphs using FeynArts and FeynCalc," *Nucl.Phys.Proc.Suppl.* **29A** (1992) 204–208.

[100] T. Hahn, "Generating Feynman diagrams and amplitudes with FeynArts 3," *Comput. Phys. Commun.* **140** (2001) 418–431, `arXiv:hep-ph/0012260`.

[101] T. Hahn and C. Schappacher, "The implementation of the minimal supersymmetric standard model in FeynArts and FormCalc," *Comput. Phys. Commun.* **143** (2002) 54–68, `arXiv:hep-ph/0105349`.

[102] T. Hahn, "Generating and calculating one loop Feynman diagrams with FeynArts, FormCalc, and LoopTools," `arXiv:hep-ph/9905354 [hep-ph]`.

114

[103] T. Hahn, "Automatic loop calculations with FeynArts, FormCalc, and LoopTools," *Nucl.Phys.Proc.Suppl.* **89** (2000) 231–236, `arXiv:hep-ph/0005029`.

[104] T. Hahn and M. Rauch, "News from FormCalc and LoopTools," *Nucl. Phys. Proc. Suppl.* **157** (2006) 236–240, `arXiv:hep-ph/0601248`.

[105] T. Hahn, "A Mathematica interface for FormCalc-generated code," *Comput. Phys. Commun.* **178** (2008) 217–221, `arXiv:hep-ph/0611273`.

[106] T. Hahn, "Feynman Diagram Calculations with FeynArts, FormCalc, and LoopTools," *PoS* (2010) 078, `arXiv:1006.2231 [hep-ph]`.

[107] J. Vermaseren, "New features of FORM," `arXiv:math-ph/0010025 [math-ph]`.

[108] T. Hahn, "CUBA: A library for multidimensional numerical integration," *Comput. Phys. Commun.* **168** (2005) 78–95, `arXiv:hep-ph/0404043`.

[109] K. Gottfried and J. D. Jackson, "On the Connection between production mechanism and decay of resonances at high-energies," *Nuovo Cim.* **33** (1964) 309–330.

[110] The Particle Data Group, "Particle Data Booklet," 2010.

[111] E. Byckling and K. Kajantie, *Particle Kinematics.* WILEY, 1972.

[112] D. A. Dicus, E. Sudarshan, and X. Tata, "Factorization theorem for decaying spinning particles," *Phys.Lett.* **B154** (1985) 79.

[113] N. Kauer, "Narrow-width approximation limitations," *Phys. Lett.* **B649** (2007) 413–416, `arXiv:hep-ph/0703077`.

[114] N. Kauer, "A threshold-improved narrow-width approximation for BSM physics," *JHEP* **04** (2008) 055, `arXiv:0708.1161 [hep-ph]`.

[115] C. F. Uhlemann and N. Kauer, "Narrow-width approximation accuracy," *Nucl. Phys.* **B814** (2009) 195–211, `arXiv:0807.4112 [hep-ph]`.

[116] A. Denner, H. Eck, O. Hahn, and J. K "Compact Feynman rules for Majorana fermions," *Physics Letters B* **291** no. 3, (1992) 278 – 280.

[117] J. F. Gunion, H. E. Haber, G. L. Kane, and S. Dawson, "The Higgs Hunter's Guide," *Front.Phys.* **80** (2000) 1–448.

[118] H. E. Haber, "Spin formalism and applications to new physics searches," `arXiv:hep-ph/9405376 [hep-ph]`.

[119] G. Passarino and M. Veltman, "One Loop Corrections for e+ e- Annihilation Into mu+ mu- in the Weinberg Model," *Nucl.Phys.* **B160** (1979) 151.

[120] T. Hahn, "LoopTools 2.7 User's Guide," 2005.

Nomenclature

Table A.1.: Nomenclature of abbreviated expressions.

Symbol	Meaning
NWA	narrow-width approximation
sNWA	simple/ usual NWA (without interference term)
gNWA	generalised NWA (with interference term)
SM	Standard Model of Particle Physics
MSSM	Minimal Supersymmetric Standard Model
BW	Breit-Wigner
BR	branching ratio
dlips	differential Lorentz invariant phase space
R_i	interference factor
x_i	relation of matrix elements
I	integral over overlapping BW propagators
os	on-shell

List of Figures

List of Tables

Erklärung nach §18(8)der Prüfungsordnung für den Bachelor-Studiengang Physik und den Master-Studiengang Physik an der Universität Göttingen:

Hiermit erkläre ich, dass ich diese Abschlussarbeit selbständig verfasst habe, keine anderen als die angegebenen Quellen und Hilfsmittel benutzt habe und alle Stellen, die wörtlich oder sinngemäß aus veröffentlichten Schriften entnommen wurden, als solche kenntlich gemacht habe.
Darüberhinaus erkläre ich, dass diese Abschlussarbeit nicht, auch nicht auszugsweise, im Rahmen einer nichtbestandenen Prüfung an dieser oder einer anderen Hochschule eingereicht wurde.

Göttingen, den 20. März 2012

(Elina Fuchs (20677732))